**Human Skeletal Muscle Units for the Repair of Volumetric Muscle Loss**

by

Olga Maria Wroblewski

A dissertation submitted in partial fulfillment
of the requirements for the degree of
Doctor of Philosophy
(Biomedical Engineering)
in the University of Michigan
2022

Doctoral Committee:

Professor Lisa M. Larkin, Chair
Professor Susan Brooks Herzog
Professor Paul Cederna
Professor Jan Stegemann

Olga M. Wroblewski

olgamwro@umich.edu

ORCID iD:  0000-0002-4219-6043

**Dedication**

This dissertation is dedicated to my loving family. Without their endless love and encouragement, I would never have made it this far.

Special thanks to:

My Mother and Father, Tamara and Jack,

for instilling a love of learning in me from a young age,

My brother, sister-in-law, and nephew, Norbert, Arielle, and Bruno,

for never failing to put a smile on my face,

My husband, Thomas,

whose immeasurable faith and support helped me reach my dreams.

**Acknowledgements**

The research in this dissertation was supported by funding from the Department of Defense (W81XWH-16-1-0752), the National Institute of Arthritis and Musculoskeletal and Skin Diseases (1R01AR067744-01), and the University of Michigan's Rackham Merit Fellowship Program, Microfluidics in Biomedical Sciences Training Program (T32-EB005582-11), and Tissue Engineering and Regeneration Grant (T32-DE007057-39). I would also like to acknowledge the support by provided the Rackham Graduate School and the College of Engineering.

Extensive contributions to the experiments in this dissertation were made by the members, past and present, of the Skeletal Tissue Engineering Laboratory at the University of Michigan, under the mentorship of Dr. Lisa Larkin. I would also like to thank my collaborators at the University of Michigan's Department of Plastic Surgery, under the mentorship of Dr. Paul Cederna. I would also like to express my gratitude for the members of my dissertation committee for their mentorship during my thesis work and their contributions towards my dissertation, especially Dr. Lisa Larkin.

## Table of Contents

## List of Figures

## Abstract

Volumetric muscle loss (VML) is a common pathological condition caused by traumatic loss of skeletal muscle that exceeds the muscle's regenerative capabilities and results in functional impairment. Current standards-of-care fail to fully recover contractile function. To address these limitations, our laboratory has developed scaffold-free tissue engineered skeletal muscle units (SMUs) for the treatment of VML. Isolated skeletal muscle stem cells (satellite cells) and fibroblasts are cultured into a confluent cell monolayer before being rolled into a cylindrical 3D construct. SMUs are biocompatible, incorporate into surrounding muscle tissue upon implantation, and have shown efficacy to partially repair a 30% VML in rat and sheep models. Ideally, SMUs could be engineered from small autogenic muscle biopsies, alleviating the limitations of donor site morbidity and immune rejection seen in current VML treatments. There are two key challenges that must be resolved to successfully translate our technology to a human cell-sourced model. To date, it has been difficult to grow human cell-sourced SMUs with contractile function. Secondly, many satellite cells are required for SMU fabrication. Any methodology that can optimize the number of cells obtained in a human skeletal muscle biopsy and enhance the functional properties of the resultant muscle tissue will advance SMUs towards clinical use. The work described in this thesis addresses these challenges.

Human epidermal growth factor (hEGF) has shown promise enhancing myobundle formation and contractile function in vitro, but the impact of hEGF treatment on SMU fabrication had yet to be evaluated. We investigated the effects of hEGF on SMU

fabrication, structure, and biomechanical function. Our results indicated that hEGF treatment was an effective means to enhance contractile function in human cell-sourced SMUs as evidenced by the 30 times higher force generated by SMUs treated with 7.5nM hEGF. The higher force was primarily due to increases in SMU myosin content.

Due to the small numbers of satellite cells present in skeletal muscle, we also sought to optimize our methodologies so that fewer satellite cells are required for effective SMU fabrication. By altering the timing of our fabrication protocol and allowing cell cultures to reach >90% confluency in media that promotes proliferation, we found that we could lower starting cell-seeding density by 90% compared to ovine models to 1,000 cells/cm$^2$ with no detrimental impact to monolayer development or SMU function.

To further expand the capabilities of satellite cells from a single autogenic skeletal muscle biopsy, we evaluated the impact of in vitro cell proliferation (increasing cell number by cell passaging) on human primary skeletal muscle cells within an engineered skeletal muscle tissue environment. While cell passaging decreased the percentage of Pax7-positivecells in the total cell population from 17% to >10%, the size and contractile function of skeletal muscle constructs formed were not different from those created with unpassaged cells. With a cell-seeding density of 1,000 cells/cm$^2$, a single passage can increase the total cell yield from a human skeletal muscle biopsy fiftyfold compared to cells harvested without a passage.

Overall, this work significantly contributed to the field of skeletal muscle tissue engineering by advancing fabrication methodologies to develop SMUs of appropriate structure and function for human application. We addressed key limitations in human cell-sourced skeletal muscle tissue engineering by optimizing cell culture conditions to

increase the cell yield from a single skeletal muscle biopsy and also promoting SMU biomechanical function.

# Chapter 1 Introduction

## 1.1 Skeletal Muscle

### *1.1.1 Native Skeletal Muscle Structure and Mechanical Function*

Skeletal muscle is one of the largest organs of the body representing 40% of an average male's body weight [1]. Innervated by and receiving signals from the somatic nervous system, skeletal muscle serves as a motor by converting electrochemical signals into mechanical contractile forces [2, 3]. Due to skeletal muscle's connections to the skeleton via bundles of collagen known as tendon, these contractile forces allow the human body to move and interact with the external environment [3]. Skeletal muscle's mechanical function is directly influenced by its hierarchical structure [4].

Skeletal muscle is a highly organized, aligned tissue with anisotropic structural properties necessary for optimal functional properties (**Figure 1A-C** [5]). Skeletal muscle's hierarchical structure begins with the sarcomere, the muscle's smallest working contractile unit [5, 6]. During skeletal muscle development, mononucleated cells known as myoblasts fuse to form cylindrical, multinucleated myofibrils [2]. Myofibrils consist of between 1,000 to 2,000,000 linear sarcomeres arranged in series [5-7]. In turn, 500 to 10,000 myofibrils are arranged in parallel and ensheathed in a cell membrane known as the sarcolemma forming a myofiber [5-7]. Each myofiber is encased in a basement membrane and are bundled together to form a fascicle [6]. The basement membrane is

composed of the basal lamina and the reticular lamina [8]. Fascicles are arranged in parallel to create the muscle belly, completing the hierarchical structure [6].

The sarcomere consists of series of interdigitating myosin and actin filaments modulated by tropomyosin and troponin(**Figure 1C-D** [5]). Thick filaments contain myosin, while thin actin filaments are made up of two strings of globular actin molecules [9]. Each myosin molecule found in thick filaments consists of the following: two

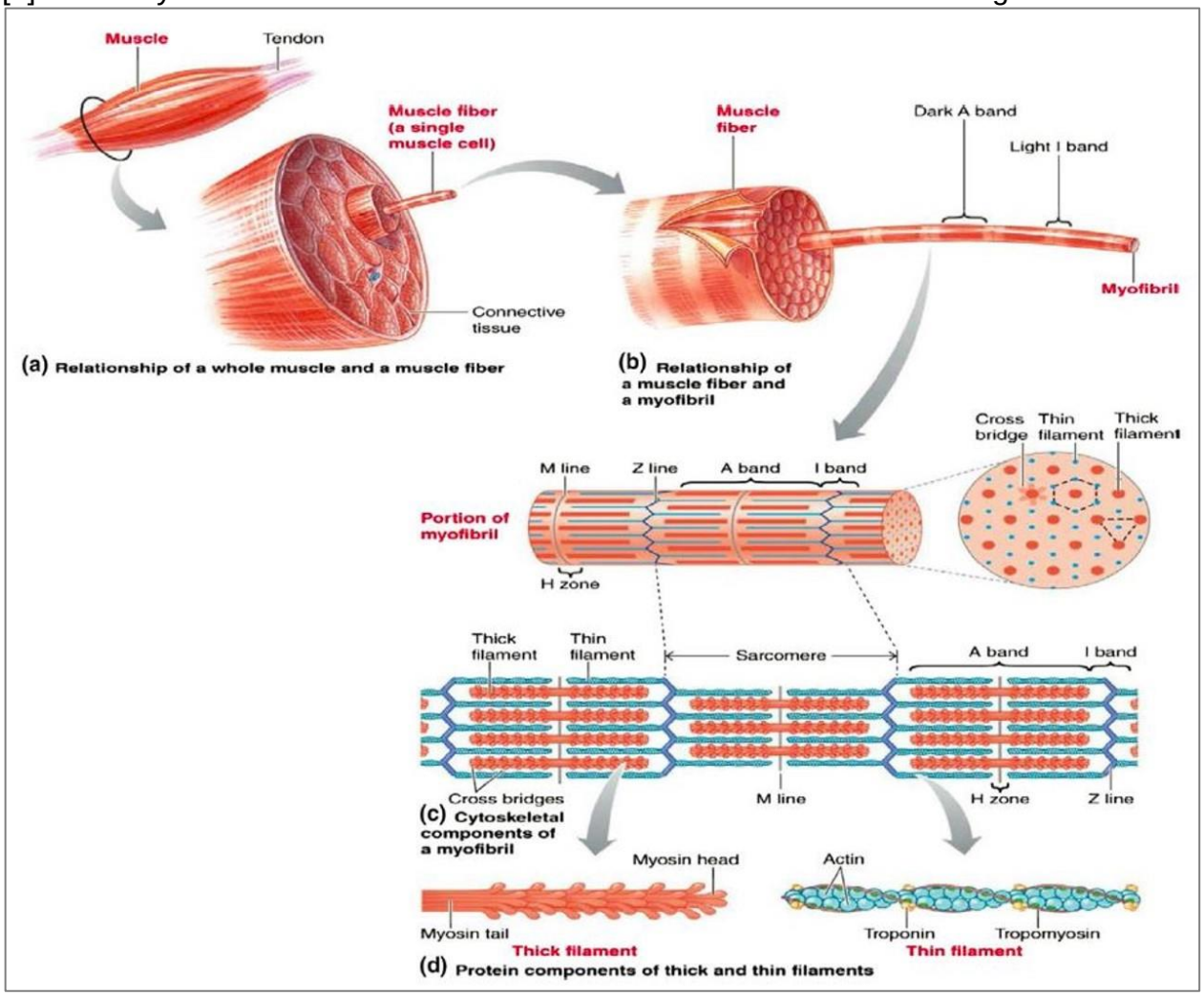


**Figure 1. The Structure of Skeletal Muscle.** Skeletal muscle is a highly organized tissue. The skeletal muscle belly consists of fascicles containing muscle fibers (also known as myofibers) bundled in connective tissue (**A**). In turn, myofibers consist of myofibrils bundled and arranged in parallel (**B**). Each myofibril contains linear series of sarcomeres, the muscle's smallest working contractile unit (**C**). Sarcomeres consist of interdigitating series of thin (myosin) and thick (actin, troponin, and tropomyosin) filaments that slide past each other during a cross-bridge cycle, leading to muscle contraction (**D**). Image adapted from Fronter and Ochela. Calcif Tissue Int, 2015 [5] and reproduced with permission from Springer.

intertwined heavy chains, two alkali light chains, and two regulatory light chains [10]. Under an electron microscope, a sarcomere is demarcated as the region between two Z-bands [10-12]. At a Z-band, thin filaments from adjacent sarcomeres are cross-linked by alpha-actinin [11]. The proteins titin and nebulin are both tethered to the Z-bands [13]. Titin runs alongside the thick filaments, while, similarly, nebulin runs along the thin filaments [13].

Starting from the sarcomere, the organized, hierarchical arrangement of cellular components, cells, and tissue in native skeletal muscle allow for microscopic mechanical forces to result in full skeletal muscle contractions [4]. On the sarcomeric level, muscle contraction occurs via a repetitive cross-bridge cycle that involves thick filaments' myosin heads binding and pulling on thin filaments' actin causing the filaments to slide past each other [10]. The myosin heads then disengage from the thin filament, bind to a new position on the actin molecule, and repeat the cycling process[10].

The synchronized movement of thick and thin filaments past each other results in the generation of force in myofibers [14]. In a skeletal muscle, myofibers can align along or at an angle to the force-producing axis [4]. In parallel muscles, muscle fibers run and generate force parallel to the long-axis of the skeletal muscle [14]. Parallel skeletal muscles contain long series of aligned sarcomeres, optimal for large and fast movements [4]. Alternatively, in pennate muscles, these myofibers are oriented at an angle to the force-producing axis which causes the muscles to produce two-dimensional (2D) force vectors [4]. Pennation increases the number of muscles fibers than can be arranged in parallel, creating muscle structures optimal for small and powerful movements [4]. A skeletal muscle's force generating capability can be used to generate

intramuscular tension which occurs during an isometric contraction, or to shorten the skeletal muscle which in turn creates movement [14].

### *1.1.2 Skeletal Muscle Regeneration: Key Cells and Regulatory Factors*

In uninjured skeletal muscle fibers, muscle progenitor cells, known as satellite cells, can be found quiescent between the sarcolemma and basal lamina [15]. In adult skeletal muscle, satellite cells commonly represent 2-7% of nuclei within skeletal muscle [16, 17]. The exact satellite cell number is dependent on age and muscle fiber type [18]. An increase in age results in a decrease in the total number of satellite cells [18]. Due to their proximity to capillaries, myonuclei, and motor neuron junctions, slow-twitch oxidative (Type I) muscle fibers have up to 6 times greater satellite cell content compared to fast-twitch (Type II) fibers [18-21].

Satellite cells are considered the key myogenic progenitors in adult skeletal muscle [22, 23]. During mitosis, satellite cells are capable of dividing into two unique daughter cells, known as asymmetric division [24]. One daughter cell serves to maintain the satellite population in the stem cell niche, while the other cell is destined to differentiate down the myogenic lineage [24].

During normal muscle growth and development, satellite cells are activated and donate nuclei to existing muscle fibers [25]. Upon traumatic injury or microinjury due to mechanical loading, satellite cells become activated and those destinated to differentiate migrate to the injury site, where they are induced to myoblasts that fuse and mature into myotubes (**Figure 2** [15, 26]). Skeletal muscle regeneration following injury is heavily dependent on expression patterns of various growth factors as well as chemical and mechanical cues present intracellularly. The transcription factor Pax7 is expressed in

quiescent satellite cells and regulates satellite cell proliferation [15, 22]. A spike in the expression of transcription factor MyoD signals the activation of satellite cells and the induction of satellite cells to myoblasts [23]. The myogenic regulatory factor Myf5 is also present in both quiescent and activated satellite cells [23]. A decline in Pax7 and MyF5 expression as well as the appearance of muscle-specific transcription factor myogenin marks a myoblast's commitment to myogenic differentiation into myotubes [22, 23]. The myoblasts proliferate and fuse resulting in multinucleated myotubes that eventually mature into organized and fully functional myofibers [15, 25-27]. It is predicted that proteins in myoblasts' semi-stable intercellular junction protein structure promote the alignment and fusion of myoblasts into myotubes [27]. Additionally, myotubes and myofibers express the skeletal muscle proteins desmin, vimentin, and nestin, all cytoplasmic intermediate filament proteins implicated in myoblast fusion [27].

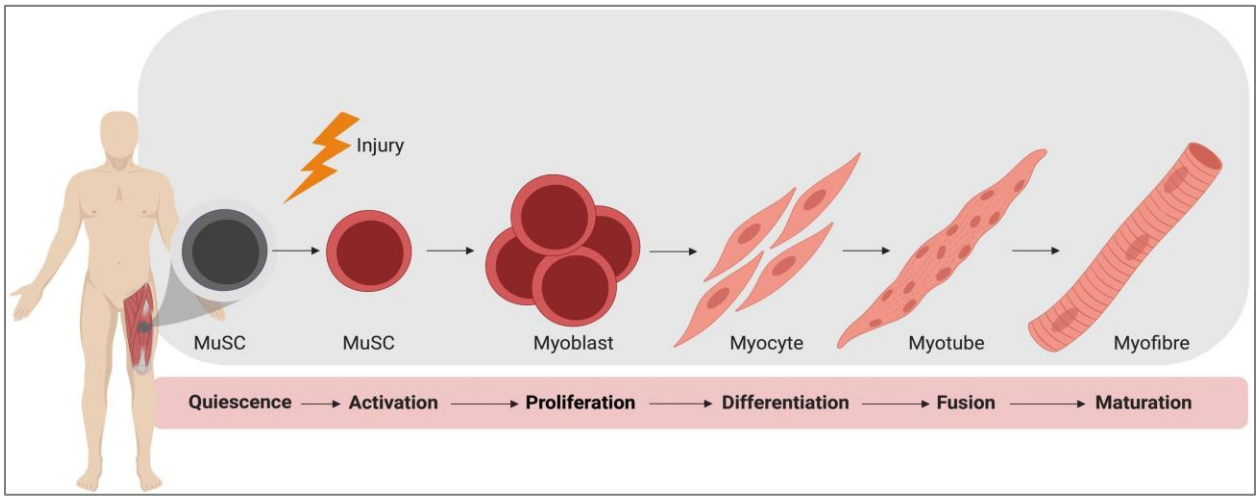


**Figure 2. Myogenic Differentiation upon Injury.** Muscle stem cells (MuSC), known as satellite cells, are considered the key myogenic progenitors in adult skeletal muscle. Upon injury to native skeletal muscle, satellite cells become activated and migrate to the injury site, before proliferating and differentiating into myoblasts. Myoblasts proliferate, align with existing myofibers and with each other before fusing into multinucleated myotubes that mature into organized myofibers. Figure adapted from Nguyen et al. Front. Cell. Dev. Biol. 2019 [26] with permission from the publisher, Frontiers Media SA.

Fibroblasts and the extracellular matrix (ECM) surrounding skeletal muscle cells in the muscle also play a significant role in modulating satellite cell behavior and myoblast differentiation [8, 28]. Both fibroblasts and satellite cells secrete proteins that maintain the surrounding ECM and take part in reciprocal signaling that prompts increased proliferation in both cell types [29]. Connective tissue fibroblasts also regulate the maturation of myotube myosin heavy chain isoforms by expressing the transcription factor Tcf4 which impacts β-catenin activation and the Wnt signaling pathway [30]. The basal lamina consists of abundant networks of collagen type IV and laminin-2, cross-linked by glycoprotein nidogen [8]. The cross-linked matrix also includes collagen type VI, and proteoglycans such as perlecan and decorin [8]. The reticular lamina and the sarcolemma link to the basal lamina via collagen type VI and dystroglycan complexes, respectively [8]. Satellite cells receive chemical and mechanical cues from the surrounding extracellular matrix via integrins, cell-surface receptors that bind to the basal lamina's laminin and collagen type VI to form focal adhesion complexes [8]. Upon skeletal muscle injury, matrix proteases degrade the basal lamina releasing signaling molecules that promote stem cell activation, migration, and proliferation [8]. Heparan sulfate proteoglycans (HSPGs) control the local concentrations of several growth factors known to bind to quiescent satellite cells receptors and promote satellite cell activation and proliferation, including fibroblast growth factor, insulin-like growth factor, transforming growth factor beta (TGFβ), and hepatocyte growth factor [31, 32]. Considering mechanical cues, skeletal muscle cells respond to changes in ECM composition, porosity, and stiffness during activation and differentiation [8, 33]. Mechanical stresses present in the ECM play a significant role

in differentiation, in myoblast and myotube actin cytoskeleton reorganization and the stimulation of stretch-activated ion channels [4, 8].

The inflammatory pathway also plays a key role in skeletal muscle regeneration. Upon injury and inflammation of a skeletal muscle, insulin-like growth factor 1 (IGF1) is expressed by muscle cells, in addition to being secreted by macrophages and endothelial cells [34]. IGF1 initiates a signaling pathway responsible for skeletal muscle protein synthesis, regeneration, and hypertrophy [31, 34]. Injury and inflammation also result in the recruitment of activated platelets and macrophages, which secrete platelet-derived growth factor (PDGF) [35, 36]. PDGF serves to promote myogenic proliferation and angiogenesis to the injury site [35, 36].

Epidermal growth factor (EGF) is a mitogenic polypeptide that has garnered interest due to its potential in tissue engineering methodologies [37-40]. EGF is a growth factor found in a number of sources *in vivo*, include platelets, duct cells in the submandibular gland, and in Brunner's gland cells in the duodenum [41, 42]. EGF is part of a family of molecules that binds to epidermal growth factor receptors (EGFRs) and stimulate mitogenesis in EGF-sensitive cells [43]. It is predicted that EGF is a key exogenous regulator of wound healing and tissue growth [42, 43]. EGF's role in native skeletal muscle has not been completely elucidated. EGF has been shown to activate epidermal growth factor receptors EGFRs localized on the basal surface of satellite cells and instigate satellite cell proliferation and asymmetric division [44]. Asymmetric division is promoted via the recruitment of Aurka, a protein responsible for the mitotic spindle assembly [44]. Along with TGFβ, EGF is predicted to regulate leukemia-inhibiting factor (LIK), a cytokine implicated in muscle hypertrophy and regeneration [36, 45]. When used

*in vitro*, EGF has been shown to enhance satellite cell proliferation by triggering cell division and metabolic processes in human myogenic cell cultures [38, 40]. In such cultures, EGF has also promoted sarcomeric maturation in myotubes when added to cell differentiation media [37-40].

## 1.2 Volumetric Muscle Loss

### *1.2.1 Definition and Prevalence*

Acute volumetric muscle loss (VML) is a common pathological condition caused by the traumatic loss of skeletal muscle that exceeds the muscle's regenerative capabilities and results in chronic functional impairment [46-49]. VML is commonly associated with high-energy trauma, including vehicular accidents and military combat injuries [46, 47, 50]. However, VML can result from any event that invokes a significant loss in a skeletal muscle's satellite cells and extracellular matrix, including collateral loss due to surgical operations [46, 47, 50]. Due to the complexity of VML injuries, they are not well tracked [49]. While the exact incidence of VML is unknown, the impact of VML on military is highlighted by the fact that the most common injury amongst soldiers in Operations Enduring Freedom and Iraqi Freedoms were soft-tissue extremity injuries [46, 47, 50-52]. An investigation studying orthopedic wounds in Iraq and Afghanistan deployed service members from 2005 to 2009 estimated the incidence of soft-tissue musculoskeletal injuries as 4.04 per 1000 deployed personnel per year [53]. Considering extremity injuries, a 2015 retrospective study of military veterans found that 65% of permanent disability cases in a type III open tibia fracture cohort were at least partially attributable to VML [46]. VML can result in lifelong complications and accounts for 60-65% of military disability patients resulting in an estimated lifetime disability cost of $340k-

440k per patient [46, 49]. Considering civilian injuries, the 2010 Cost and Injury Reports from the United States Centers for Disease Control and Prevention report $30 billion in medical and work loss cost due to hospitalizations from nonfatal vehicular accidents [51].

### *1.2.2 Current Standards of Care and Limitations*

VML results in functional impairment in skeletal muscle and necessitates medical intervention [46]. The current standards of care are muscle flap procedures, which involve the surgical replacement of damaged or lost muscle with healthy allogenic or autogenic skeletal muscle tissue from outside the zone of injury (**Figure 3** [15, 47]). In traditional muscle flap procedures, healthy muscle adjacent to the defect in rotated or advanced into the defect site [15]. During such a procedure, the donor muscle's blood and nerve supply does not need to be severed [15, 47]. The most common muscle flap procedure for VML extremity injuries is free functional muscle transfer (FFMT), which involves the complete excision and transplantation of a skeletal muscle and its accompanying nerve, artery, and vein from one location in the body to the injury site [54, 55]. Once the flap is transplanted to the injury site, the nerve, artery, and vein are sewn into the surrounding tissue to promote revascularization and reinnervation [15]. FFMT involves the use of autogenous tissue [15]. Composite tissue allotransplantation (CTA) also involves the transplantation of composite tissue but from an allogenic source [15].

The surgical standards-of-care for VML treatment have several limitations. The use of autogenic muscle sources can result in donor site morbidity, while allogenic sources can result in tissue rejection at the repair site or disease transmission from donor tissue [15, 46, 56]. Additionally, allogenic sources require chronic immunosuppression [46]. Donor muscle from either source must meet requirements regarding muscle size,

bulk, and orientation [14]. These procedures have limited success, frequently failing to significantly stimulate muscle regeneration or restore contractile function, even after extensive physical rehabilitation [15, 57]. Functional recovery is heavily impaired, resulting in suboptimal motor function and overall patient dissatisfaction [15, 57]. Additionally, size and shape mismatches between donor muscle flaps and VML sites can prevent repair of any cosmetic deformities caused by the original injury.

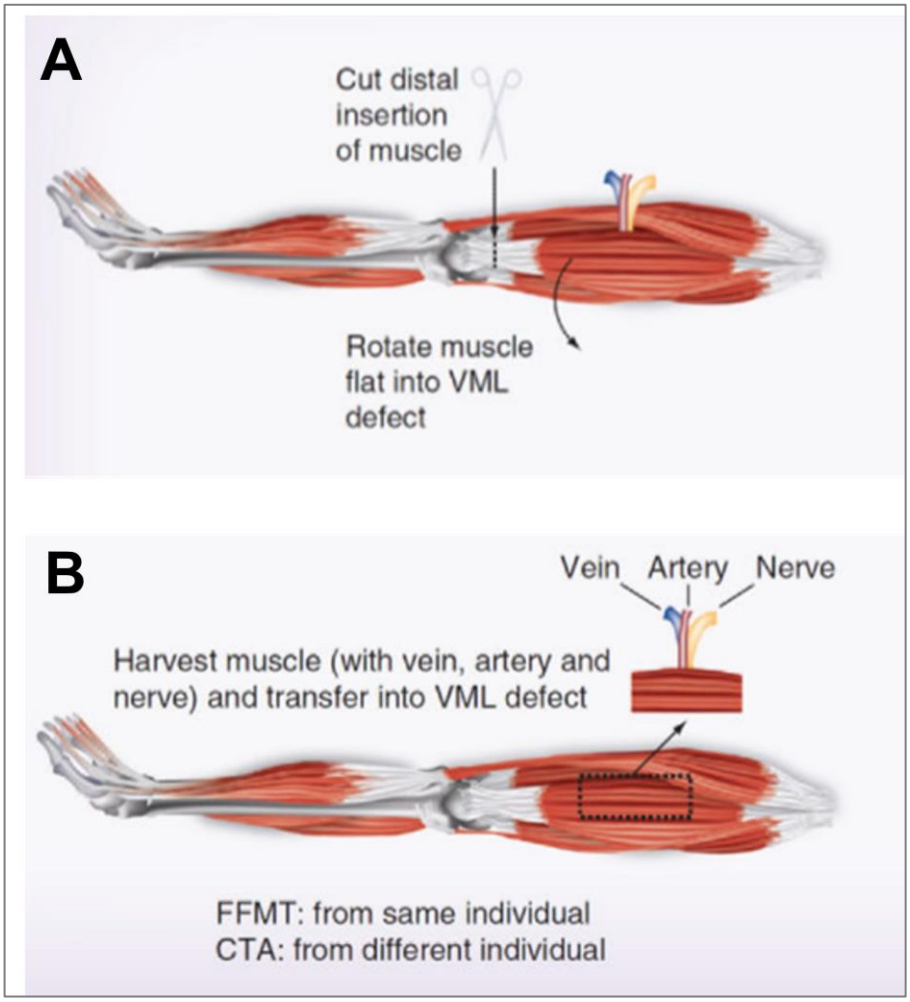


**Figure 3. Current Standards of Care for VML.** VML necessitates medical intervention and current standards of care are muscle flap procedures. In traditional muscle flap procedures, healthy skeletal muscle tissue adjacent to the injury is rotated into the VML defect (A). In autogenic free functional muscle transfer (FFMT) and allogenic composite tissue allotransplantation (CTA), healthy skeletal muscle along with its accompanying nerve, artery, and vein are completely excised and transplanted into the injury site (B). Image adapted from Mertens et al. Regen Med, 2014 [15] and reproduced with permission from the publisher, Future Medicine.

## 1.3 Skeletal Muscle Tissue Engineering

### *1.3.1 Benefits of Tissue Engineering Approaches for VML*

There is a clear clinical need for improved therapeutic options for VML and emerging musculoskeletal tissue engineering technologies have the potential of addressing the shortcomings of current surgical techniques by growing exogenous muscle tissue that can promote appropriate muscle regeneration *in vivo*. Such methodologies are compelling approaches since they can provide manipulatable and patient-specific grafts that not only replace lost skeletal muscle but also provide an environment that promotes infiltration of native cells, integration with local tissue, and regeneration of muscle in the injury site [40, 46, 47]. Using small, non-damaging, autogenic muscle biopsies as a cell source, engineered skeletal muscle could alleviate issues with donor site morbidity and immune response [46].

### *1.3.2 Tissue Engineering Methodologies*

For VML repair applications, engineered skeletal muscle tissue needs to effectively replicate the complex structure and function of native skeletal muscle after implantation. Since Vandenburgh's 1988 work culturing avian myotubes in collagen-coated tissue culture plates, skeletal muscle tissue engineering research has advanced significantly [58]. Skeletal muscle tissue engineering strategies use combinations of scaffolding, chemical cues, and mechanical forces in an attempt to promote myogenesis [15, 59, 60].

The most common approaches include directly injecting satellite cells expanded *in vitro* into the site of injury, seeding satellite cells on a synthetic or native ECM scaffold, or using cell monolayers to grow scaffold-free 3D skeletal muscle constructs [15, 37, 40, 61,

62]. While many original regenerative medicine techniques involved directly transplanting satellite cells into areas of injured muscle, such approaches result in a low number of viable engrafted cells [40]. Scaffold tissue engineering systems bring up concerns of biocompatibility and immune rejection *in vivo* and approaches frequently have issues providing adequate nutrient diffusion and cell infiltration and proliferation for large engineered constructs [15, 63-65]. For tissue-engineered skeletal muscle intended for transplantation, scaffold systems should degrade and replaced by extracellular matrix components secreted by the seeded cells [64, 66]. However, the rate of scaffold degradation is commonly nonlinear and unpredictable, resulting in challenges creating a scaffold system that provides cells with the structure needed to attach, proliferate, and differentiate without disrupting ECM secretion, tissue growth, and remodeling [63].

### *1.3.3 Scaffold-Free Tissue Engineering*

Scaffold-free methodologies involve co-cultures of satellite and fibroblast cells that, given the appropriate chemical and mechanical signals, secrete matrix proteins and self-assemble sarcomeres and myofibers into cohesive, 3D muscle constructs [15, 59, 67-69]. Our lab has developed a novel scaffold-free tissue engineering approach that fabricates skeletal muscle units (SMUs) that addresses several skeletal muscle tissue engineering challenges (**Figure 4** [59, 67-71]). Briefly, satellite and fibroblast cells harvested from a muscle biopsy are induced down a myogenic and fibroblastic lineage forming a monolayer of myotubes and ECM that will delaminate around pins inserted into the plate.

SMUs can be designed to be multiphasic through the fabrication of tissue-engineered bone-tendon anchors [67]. Bone marrow cells are isolated from harvested

bone marrow are cultured in bone proliferation and differentiation media [67]. During the culturing process, cell cultures reach confluence and bone monolayers began to delaminate from the plate and form 3D cylindrical bone-tendon constructs [67]. These constructs are cut and pinned into developing muscle monolayers [67]. When monolayers delaminate, they surround the bone-tendon tissue and fuse down, creating 3D skeletal muscle constructs held at length by engineered bone-tendon anchors [67].

*In vitro*, rat SMUs have been shown to possess neonatal muscles characteristics displayed extensive myotube fusion, sarcomere structure, and a comprehensive extracellular matrix, while also spontaneously contracting and displaying twitch and tetanus in response to electrical stimulus [67, 68, 71]. *In vivo*, SMUs have shown efficacy in partially repairing a 30% VML in rodent models, inducing the body to autonomously regenerate muscle while also vascularizing and innervating the VML injury site [67, 68, 71]. Moreover, the SMU technology results in the addition of new muscle fibers in the repair area and incorporation of the construct into surrounding tissue [67, 68].

The SMU construct can be fabricated from autogenic cell sources and the fabricated tissue can be directly engrafted, which reduces or even eliminates drawbacks

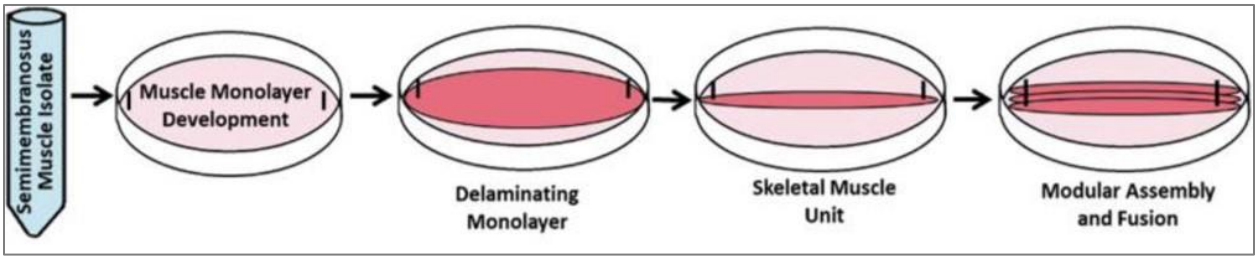


**Figure 4. Skeletal Muscle Unit Fabrication and Scale-Up.** To fabricate scaffold-free skeletal muscle units (SMUs), primary skeletal muscle cells are isolated from a muscle biopsy and seeded onto tissue culture plates. Isolated satellite cells are induced down a myogenic lineage forming a monolayer that will delaminate around pins inserted into the plate. After delamination, monolayer roll-up and fuse down into SMUs. To scale-up the thickness of engineered constructs, individual SMUs can be pinned side-to-side, resulting in fusion. Image adapted from Novakova et al. Tissue Eng Part A, 2020 [69] and reproduced with permission from the publisher, Mary Ann Liebert, Inc.

seen in the other approaches [15]. *In vivo*, the native skeletal muscle environment serves as a bioreactor and constructs quickly remodel and regenerate to form advanced muscle characteristics [15]. The SMU approach is appealing because all components of the construct occur naturally *in vivo* and native cells are used, both of which reduce the risk of immune rejection [15]. Furthermore, this multiphasic approach with its bone-tendon ends provides way of incorporating the engineering muscle into surrounding tissue.

To develop a translational tissue-engineered VML therapy, it is crucial to establish methods for growing larger tissue constructs that effectively accelerate the VML healing process for injuries of the magnitude seen in human limbs. One of the key issues preventing the scale-up of skeletal muscle tissue engineering technologies is limitations in nutrient diffusion. Nutrients and oxygen are unable to reach all cells in an engineered tissue due to its thickness. Small scale, scaffold-free approaches do not have the *in vitro* nutrient diffusion limitation seen in scaffold techniques. During the SMU fabrication process, cell cultures have ample access to media [15]. When 3D constructs are formed, one dimension of the SMU is maintained >1mm allowing nutrients to reach all cells in the SMU [15]. Additionally, our laboratory has developed a method for modularly scaling-up constructs, tested in both rat and ovine VML models (**Figure 4** [69, 71]). In this approach, individual SMUs are grown following the standard protocol [69, 71]. After formation of 3D constructs, individuals SMUs are pinned side-by-side and allowed to fuse, in order to create a single graft of the size necessary to fill a VML defect [69, 71]. By allowing fusion to occur immediately prior to graft implantation, SMUs can be scaled up to a clinically-relevant size without the formation of a necrotic core *in vitro.* Hence, the SMU approach addresses several of the most common skeletal muscle tissue engineering barriers.

### *1.3.4 Current Challenges in Tissue Engineering*

There are still several key limitations preventing the clinical adoption of tissue-engineered based therapies for VML. While there are many studies demonstrating measurable *in vitro* contractile forces from 3D engineered skeletal muscle models that use a rodent or ovine cell source, there are few reports of scaffold-free engineered human muscle with structure or contractile forces comparable to native adult human muscle [15, 37, 46, 61]. The lack of successful engineering of human muscle is partially due to differences in *in vitro* growth factor needs and the proliferation and differentiation rates of skeletal muscle cell types between species. For the purpose of tissue engineering scaffold-free skeletal muscle grafts for VML, the *in vitro* expansion of myogenic cells to sufficient numbers for the creation of a monolayer and a contractile SMU is critical. Scaffold-free skeletal muscle tissue engineering approaches rely on chemical cues to create *in vitro* environments that simulate *in vivo* myogenesis conditions [72, 73]. As a result, cell proliferation and differentiation during SMU fabrication is heavily dependent on the sera and growth factors in the cell culture medium. Myogenic cells and fibroblasts from different species have distinct optimal growth factor requirements [59, 71-74]. Thus, protocols used for rodent and ovine models do not translate to human muscle fabrication.

In addition to interspecies differences in growth factor requirements, the difference in both satellite cell and fibroblast proliferation and maturation rates between species can cause great differences in the initial satellite cell numbers (seeding densities) needed for skeletal muscle tissue engineering technologies [75, 76]. This is because scaffold-free tissue engineering relies on a careful balance between the satellite cell and fibroblast cell population. To grow a construct with skeletal muscle content, a high density of satellite

cells needs to mature into myoblasts, and then myotubes [76]. However, fibroblasts must be available to form extracellular matrix components and create the support structure for a robust construct [77]. Determining essential growth factors and optimal cell-seeding densities is critical for the successful translation of animal-model tissue engineering methodologies to a human cell source, but the number of technologies that have conducted such optimization testing are limited.

The greatest limitation among all current approaches is the inability to produce human cell-sourced biocompatible constructs at clinically relevant sizes [15]. In order for SMU technology to be biocompatible and translatable to a clinic, the engineered tissue must consist solely of human-derived cells. However, only 2-7% of the nuclei with native adult human skeletal muscle is from satellite cells and harvesting large biopsies from a VML patient increases the risk of creating additional muscular trauma or VML [78].The passaging of myoblasts is a common technique for engineered skeletal muscle systems that require large populations of cells for fabrication and scale-up, but the impact of the passaging on human primary skeletal muscle isolates used to fabricate tissue-engineered skeletal muscle constructs intended for use as grafts for VML remained, prior to this thesis, to be elucidated [37, 76, 79]. To successfully create a human autologous engineered skeletal muscle graft for a clinical setting, methodologies that increase the efficacy of isolated satellite cells and enhance the capabilities of fabricating constructs using low seeding densities need to be investigated.

### 1.4 Summary

In summary, volumetric muscle loss is a debilitating clinical condition that requires medical intervention. Current surgical standards-of-care are limited by tissue availability

and donor site morbidity and fail to appropriately regenerate muscle and restore contractile function. Using cells isolated from autologous skeletal muscle biopsies, skeletal muscle tissue engineering methodologies can fabricate grafts that promote muscle regeneration *in vivo*. Our laboratory has developed a scaffold-free method of fabricating scaled-up skeletal muscle units that are biocompatible, incorporate into surrounding muscle tissue upon implantation, and have shown efficacy to partially repair a 30% VML in rat and sheep models.

There are several key challenges that must be resolved for the successful translation of scaffold-free animal-model tissue engineering methodologies to a human cell source. To date, it has been difficult to grow human cell-sourced SMUs with any noteworthy contractile function. Secondly, large numbers of satellite cells are required for SMU fabrication, but a limited number of satellite cells can be extracted from a minimally-invasive autologous skeletal muscle biopsy.

The coming chapters will address our approaches to overcoming these limitations. Chapter II focuses on determining the essential growth factors necessary to promote contractile function in human cell-sourced SMUs. Specifically, this chapter evaluates the impact of human epidermal growth factors on SMU fabrication, structure, and biomechanical function. Chapter III addresses the high number of satellite cells required for SMU fabrication by optimizing the initial cell-seeding density parameters and methodology for construct development. Chapter IV addresses methodologies of expanding the capabilities of satellite cells from a single autogenic skeletal muscle biopsy in tissue engineering modalities. Overall, this work significantly contributes to the field of

skeletal muscle tissue engineering by advancing fabrication methodologies to develop SMUs of appropriate structure and function for human application.

# Chapter 2 Impact of Human Epidermal Growth Factor on Tissue-Engineered Skeletal Muscle Structure and Function

The entirety of this chapter was originally published with the following citation: Wroblewski, O.M., Vega-Soto, E.E., Nguyen, M.H., Cederna, P.S., & Larkin, L.M. (2020). Impact of Human Epidermal Growth Factor on Tissue-Engineered Skeletal Muscle Structure and Function. Tissue Eng Part A. doi: http://doi.org/10.1089/ten.tea.2020.0255 [80]. This article has been reproduced with permission from the publisher, Mary Ann Liebert, Inc. The figures have been reformatted and/or reproduced in color.

## 2.1 Introduction

Traumatic extremity injuries, surgical removal of skeletal muscle, and congenital defects can all result in a clinical condition known as volumetric muscle loss (VML) [57, 67]. VML is defined as skeletal muscle loss that exceeds the native regenerative capacity and results in permanent loss of muscle structure and function [46]. VML frequently necessitates surgical intervention involving muscle flap or graft transposition [46]. These techniques are limited by graft source availability, donor-site morbidity, and inability to appropriately regenerate muscle mass or effectively restore contractile function [47].

Skeletal muscle tissue engineering technologies aim to grow exogenous muscle tissue that can replace lost native skeletal muscle while also promoting graft integration and muscle regeneration *in vivo* [46, 47]. A significant obstacle hindering the translation of such technologies into medical therapies has been the limited success in developing

human cell-sourced engineered skeletal muscle with *in vitro* structure or contractile forces comparable to native adult human muscle [15, 37, 61].

Skeletal muscle tissue engineering methodologies share the fundamental approach of creating *in vitro* environments simulating *in vivo* conditions, which enhance myogenesis by inducing primary skeletal muscle precursor cells down a myogenic lineage through the use of scaffold systems, mechanical forces, and/or chemical cues [15]. Using these approaches, tissue engineers rely on different media and growth factor formulations during the *in vitro* culture of myogenic cells to control cell proliferation and differentiation [72, 73].

The expansion of myogenic cells to sufficient numbers for tissue engineering requires the cell culture growth medium to contain serum and growth factors, such as fibroblast growth factor (FGF) that modulate cell proliferation and delay the onset of terminal differentiation [68, 73, 74]. For the differentiation of myogenic cells and for myotube fusion, the medium contains significantly less serum [68, 73, 74]. The absence of mitogenic components and inclusion of differentiation stimulating growth factors, such as insulin, trigger and promote differentiation [73, 74]. Myogenic cell proliferation and differentiation behavior is highly sensitive to the concentrations and timing of serum and growth factor administration [73].

Furthermore, research suggests species-specific differences in myogenic cell response to certain growth factors and sera indicating that myogenic cells from different species have distinct growth factor requirements for optimal proliferation and differentiation [72, 73]. The sensitivity of myogenic cells to these environmental factors can make it challenging to determine the optimal medium formulation and growth factor

dosing strategy necessary for maximum cell performance in culture, especially when transitioning tissue engineering methodologies from animal to human cell culture models. Identifying essential growth factors, optimal concentration, and optimal exposure timing for human myogenic cell cultures is critical in enhancing the *in vitro* myogenesis of skeletal muscle precursors used in engineered skeletal muscle.

One growth factor of interest is human epidermal growth factor (hEGF), a mitogenic polypeptide found in platelets. hEGF is believed to be a key regulator of tissue growth and wound healing [41-43, 81]. The signaling pathway for hEGF in native skeletal muscle has not been completely elucidated, but it is thought that hEGF regulates leukemia-inhibiting factor, a multifunctional cytokine involved in the regeneration of injured muscle [36, 82]. Also, in human myogenic cell culture, hEGF has been shown to enhance proliferation by triggering cell division and metabolic processes [38-40]. The addition of hEGF to differentiation media has resulted in myotubes, which exhibit visible sarcomeric striations and spontaneous twitching [39, 40]. Thus, in the development of techniques to engineered skeletal muscle, hEGF has been primarily used in human myogenic cell growth media [37, 38].

Human myogenic cells expanded in medium treated with hEGF before being seeded in scaffolds have been shown to form myobundles, bundles of muscle fibers, with superior contractile function compared with cells expanded in untreated medium [37].[6] To date, hEGF has been shown to have profound effects on human myogenic cell cultures *in vitro*, but the quantitative impact hEGF-treated growth and differentiation media has on engineered skeletal muscle structure and contractile function has yet to be evaluated.

Our laboratory has fabricated scaffold-free tissue-engineered skeletal muscle units (SMUs) from primary myogenic cells and fibroblasts [67, 68, 71]. Our SMU fabrication process is well defined in rat and ovine models, but this is the first publication detailing the fabrication of a human SMU comprising human primary cells. The scaffold-free design provides a unique opportunity to investigate the impact of hEGF on primary myogenic cell behavior and extracellular matrix deposition without the confounding effects caused by the chemical and mechanical cues present in different scaffold materials.

We hypothesized that exposing primary myogenic cells to hEGF in the SMU fabrication process through hEGF-treated muscle growth media and hEGF-treated muscle differentiation media would allow us to determine the optimal time points and time spans for enhancing *in vitro* myogenesis and skeletal muscle development. Thus, the purpose of this study was to examine the effects of hEGF on the structure and function of our scaffold-free SMU graft.

## 2.2 Materials and Methods

### *2.2.1 Isolation of muscle cells*

Human soleus skeletal muscle surgical discards were obtained from two healthy males, 21 and 35 years of age. All experimental protocols involving the use of human skeletal muscle biopsies were approved by the University of Michigan Medical School Institutional Review Board (HUM00151617). Skeletal muscle biopsies underwent cell isolation procedures, as described previously [67, 68, 70, 71]. In brief, muscle biopsies were removed under aseptic conditions, sterilized in 70% ethanol, and finely minced before being placed under ultraviolet light for 15 minutes. Minced muscle was then

incubated in dissociation solution consisting of 2.3 mg/mL dispase (Cat. No. 17105-041; Thermo Fisher) and 0.3 mg/mL collagenase type IV (Cat. No. 17104-019; Thermo Fisher) for 2 hours.

The resulting suspension was then filtered through 100 µm (Cat. No. 22-363-549; Fisher Scientific) and 40 µm (Cat. No. 22-363-547; Fisher Scientific) mesh filters before undergoing centrifugation. The resulting cell pellet was either resuspended in muscle growth media (MGM) for immediate plating and SMU fabrication, or frozen down in freezing media for future use.

MGM contained 60% F-12 Kaighn's Medium (Cat. No. 21127-022; Gibco), 24% Dulbecco's modified Eagle's medium (DMEM; Cat. No. 11995-065; Gibco), 15% fetal bovine serum (FBS; Cat. No. 10437-028; Gibco), and 1% antibiotic/antimycotic (ABAM, Cat. No. 15240-062; Gibco). Additionally, MGM was supplemented with 2.4 ng/mL basic FGF (Cat. No. 100-18B; PeproTech) and 4.0 ng/mL dexamethasone (DEX; Cat. No. D8893; Sigma-Aldrich). Freezing media contained 20% horse serum (Cat. No. 16050122; Gibco), 10% dimethyl sulfoxide (Cat. No. BP231-100; Fisher Scientific), and 70% DMEM. The freezing medium was supplemented with 1% ABAM.

### *2.2.2 SMU fabrication and hEGF addition*

Muscle cell isolates were plated in MGM on 60-mm tissue culture-treated polystyrene plates (BD Falcon, Franklin Lakes, NJ) at a seeding density of 10,000 cells/cm$^2$. To allow for cell attachment to the plates, cells were left undisturbed for 3 days before being fed MGM every 2 days. Seven days post-seeding, after cells had become confluent and myotube networks had formed, the media was switched to muscle differentiation media (MDM). Cells were fed with MDM every 2 days for the duration of

cell culture and SMU fabrication. MDM consisted of 70% Medium 199 (Cat. No. 1150067; Gibco), 23% DMEM, 6% FBS, and 1% ABAM. Additionally, MDM was supplemented with 0.1% insulin/transferrin/selenium X (Cat. No. 51500056; Gibco), 14.5 ug/mL ascorbic acid 2-phosphate (Cat. No. A8960-5G; Sigma Life-Aldrich), and 4.0 ng/mL DEX.

After 7 days in MDM, monolayers were manually delaminated with cell scrapers and transferred to 60-mm Sylgard-coated plates. Minuten pins were inserted through the monolayers into the Sylgard 3 cm apart and used as anchors. Over the next 7 days, the monolayer fused into cylindrical muscle constructs, held at length by the minuten pins.

During this SMU fabrication process, summarized in **Figure 5**, the media was treated with 7.5 nM hEGF (Cat. No. CC-4107; Lonza) at three different time spans: 0 to 6 days post-seeding (MGM Only), 7 to 21 days post-seeding (MDM Only), and 0 to 21 days post-seeding (MGM/MDM). These time spans were selected to analyze the impact of hEGF on human primary muscle cell cultures during cell proliferation and differentiation phases. The 0- to 7-day time span aligned with the time period the cell cultures were in MGM and the 7- to 21-day time span aligned with the time period the cell cultures were in MDM. Untreated plates served as controls.

### *2.2.3 Late differentiation: myotube size and density analysis*

Myotube size and density were evaluated to investigate the impact of hEGF on late differentiation. Fourteen days after initial plating of isolated cells, immediately before manual delamination of monolayers, monolayers in each experimental group ($n = 15$) were imaged using light microscopy. Three to five representative images were taken for each 60-mm plate. Using the ImageJ software package, images were evaluated to determine average myotube diameter and myotube network density. Using the multipoint

tool on the ImageJ software package, the total number of myotubes in each representative image was quantified and normalized by total image area to determine myotube network density. Additionally, ImageJ's line tool was used to measure the diameter of each individual myotube in all representative images to determine average myotube diameter.

Seven to eight days after the SMUs formed three-dimensional (3D) cylinders, they underwent maximum tetanic isometric force measurements to evaluate contractile function, as described previously [67, 68, 70, 71]. In brief, the anchor pin on one end of the SMU was attached to an optical force transducer and released from the Sylgard. Throughout testing, SMUs were kept in MDM cell culture at 37°C. To provide a relatively

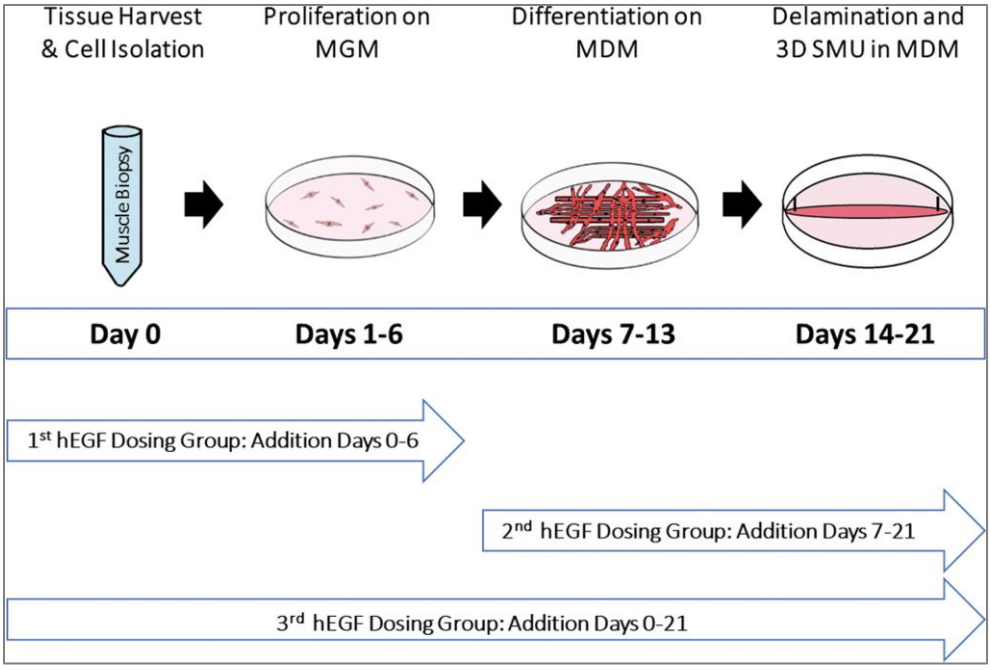


**Figure 5. Experimental Timeline**. To determine the effects of hEGF on the structure and function of SMUs, the media was treated with hEGF at three different time spans: 0 to 6 days to study effects on proliferation, 7 to 21 days to study effects on differentiation and structural maturation, and 0 to 21 days to investigate the combined effects of adding hEGF to both MGM and MDM.

uniform electrical field throughout the entire length of the construct, platinum wire electrodes were submerged in the MDM and placed on either side of the SMU.

Before the onset of each stimulation, the average baseline force of each SMU was measured to determine passive tension. Tetanic isometric forces were elicited using a stimulus of a 600 ms duration square wave train of 0.1 ms pulses at 1000 mA at 60, 90, and 129 Hz. Tetanic isometric force data were recorded and analyzed using LabVIEW 2012 (National Instruments). Maximum tetanic isometric force measurements were normalized by MF20-positive cross-sectional area (CSA) to determine the SMU-specific force.

### *2.2.4 Structure: immunohistochemical analysis*

Immunohistochemical staining (IHC) was conducted on SMU sections to qualitatively and quantitatively assess construct muscle structure. Immediately after force production measurements, SMUs were coated in Tissue Freezing Medium (Cat. No. 15-183-36; Fisher Scientific), frozen in liquid nitrogen-chilled isopentane, and stored at −80°C until sectioning. Ten micrometer-thick cross-sectional and longitudinal SMU cryosections were mounted on microscopy slides.

Before immunostaining, the slides were fixed in methanol chilled to −20°C. For immunostaining, slides were washed in 0.1% Triton X-100 (Cat. No. T8787; Sigma) in Dulbecco's phosphate-buffered saline (PBST). Slides were then blocked with 3% bovine serum albumin (Cat. No. A2153-10G; Sigma-Aldrich) in PBST for 30 min at room temperature. Following the blocking step, sections were covered in primary antibodies diluted in blocking medium and left to incubate overnight at 4°C.

To evaluate muscle content and overall construct CSA, SMU cross-sectional cryosections underwent IHC with primary antibodies for myosin heavy chain (MF20; mouse monoclonal antibody 1:200 dilution; Cat. No. MF 20-c; Developmental Studies Hybridoma Bank) and laminin (rabbit polyclonal antibody 1:200 dilution; Cat. No. 7463; Abcam). To evaluate sarcomeric structure, SMU longitudinal cryosections underwent IHC with a primary antibody for α-actinin (rabbit polyclonal antibody 1:300 dilution; Cat. No. ab18061; Abcam).

After incubation, samples were washed in PBST before incubation in 1:500 dilutions of Alexa Fluor anti-mouse or anti-rabbit (Life Technologies) for 3 h at room temperature. Following another set of washes in PBST, slides were preserved in ProLong Gold with 4′,6-diamidino-2-phenylindole (DAPI; Cat. No. P36935; Invitrogen). Slides were imaged using a ZEISS Apotome Microscope.

Using the ImageJ software package to analyze cross-sectional cryosections, the total CSA and MF20-positive CSA of each SMU was quantified. To measure total CSA, ImageJ's freehand selection tool was used to select the outer boundaries of the SMU. The total area was measured and converted from pixels to microns using ImageJ's “set scale” and “measure” features. To measure MF20-positive CSA, ImageJ's analyze particles tool was used to measure all areas of the section that display red MF20-positive fluorescence. Maximum tetanic isometric force measurements were normalized by MF20-positive CSA to determine the SMU-specific force.

### *2.2.5 Statistical analysis*

For all graphs, boxes and bars indicate mean ± standard error of the mean. Using GraphPad Prism software, statistical differences between experimental groups were

assessed through a one-way analysis of variance (ANOVA) with Tukey's multiple comparisons test. Differences were considered significant at a $p < 0.05$.

## 2.3 Results

### *2.3.1 Impact of hEGF on muscle cell differentiation and myotube fusion*

Light microscopy images of monolayers 14 days post-seeding were used to analyze muscle cell differentiation and myotube fusion. Images indicate monolayers fed hEGF have a denser myotube network, thicker myotube structures, and less fibroblast overgrowth compared with untreated control **(Fig. 6A–D)**.

Measurements of myotube size and density revealed that timing of hEGF dosing had a significant impact on monolayer development. Monolayers fed hEGF-treated MGM had a significantly greater average myotube diameter than untreated monolayer controls with averages of $24.1 \pm 0.5$ µm and $20.8 \pm 0.4$ µm, respectively ($p < 0.001$; **Fig. 6E**). Additionally, monolayers fed hEGF-treated MDM had an average myotube diameter of $23.2 \pm 0.6$ µm, significantly different from control monolayers ($p = 0.007$). Analysis of myotube network density (myotube/mm$^2$) also showed significant difference between groups ($p = 0.01$; **Fig. 6F**). Administration of hEGF in MGM+MDM led to a significant increase in myotube density when compared with control ($p = 0.02$) with means of $12.3 \pm 0.3$ myotubes/mm$^2$ versus $10.7 \pm 0.4$ myotubes/mm$^2$, respectively.

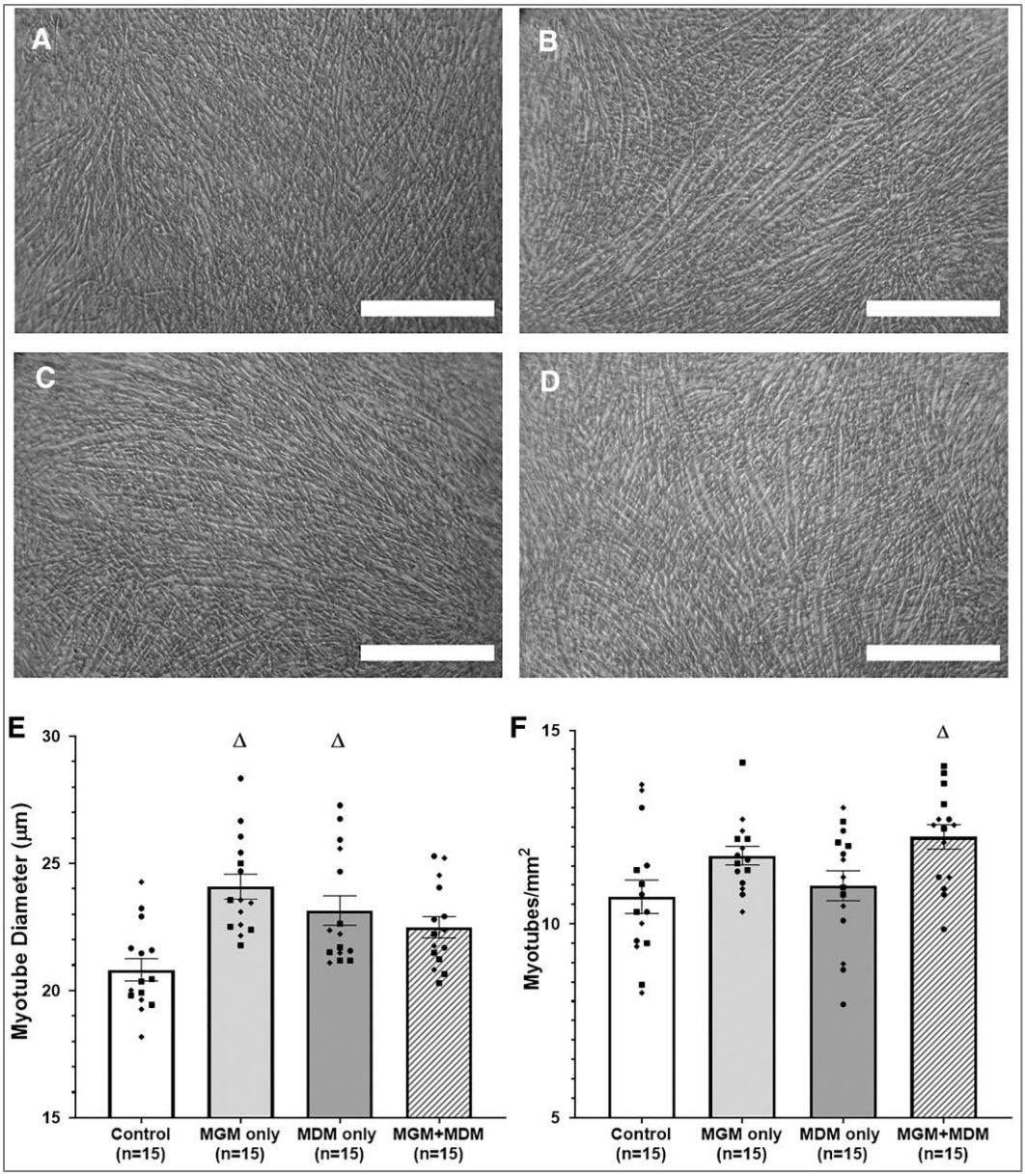


**Figure 6. Impact of hEGF on Muscle Cell Differentiation and Myotube Fusion.** Light microscopy images of the monolayer were taken just before delamination on day 14 post-seeding. Representative 10 × images are shown above for untreated control **(A)**, and monolayers exposed to hEGF-treated MGM **(B)**, hEGF-treated MDM **(C)**, and hEGF-treated MGM+MDM **(D)**. All monolayer images were used to evaluate myotube size **(E)** and myotube density **(F)**. Scale bars = 500 µm. Boxes and bars indicate mean ± standard error of the mean. Different data point formats are used to differentiate different cell sources: • for frozen cells from the soleus of a 21-year-old male, ♦ for fresh cells from the soleus of a 35-year-old male, and ▪ for frozen cells from the same 35-year-old male. Δ symbol above bars indicates statistically significant differences from control. One-way ANOVA indicated that hEGF had a significant impact on both myotube size and density ($p = 0.0001$ and $p = 0.0111$, respectively). Post hoc analysis demonstrated significant difference in myotube diameter between monolayers exposed to hEGF-treated MGM and untreated monolayer controls ($p < 0.0001$). There was also a significant difference in myotube diameters between monolayers exposed to hEGF-treated MDM and control monolayers ($p = 0.0065$). Additionally, monolayers fed hEGF-treated MGM+MDM had a significantly greater myotube density when compared with control ($p = 0.0151$). Monolayers fed hEGF-treated MGM+MDM displayed a denser myotube network and less fibroblast overgrowth compared with untreated control.

### *2.3.2 Effects of hEGF on SMU contractile force*

After 3D construct formation, SMUs underwent tetanic force production measurements to assess contractile function **(Fig. 7A)**. Average isometric tetanic forces were 2.6 ± 1.3 μN, 10.4 ± 1.2 μN, 54.2 ± 6.7 μN, and 90.4 ± 7.6 μN for control, hEGF-treated MGM only, hEGF-treated MDM only, and hEGF-treated MGM+MDM groups, respectively. A one-way ANOVA indicated that there was a significant difference in maximum tetanic force production between experimental groups ($p < 0.0001$, $n = 15$ for all experimental groups) signifying that treatment with hEGF and its dose timing increase SMU contractile force. A *post hoc* multiple comparisons test indicated no significant difference in force production between SMUs receiving hEGF-treated MGM and untreated control SMUs ($p = 0.07$).

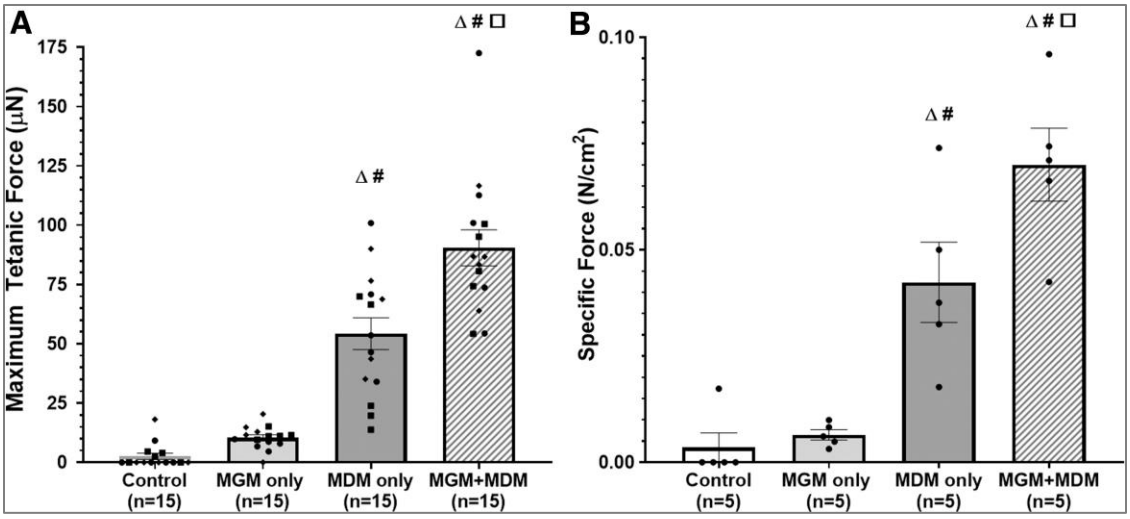


**Figure 7. Effects of hEGF on Maximum Isometric Force Production (A) and Specific Force (B).** Boxes and bars indicate mean ± standard error of the mean. Different data point formats are used to differentiate different cell sources: • for frozen cells from the soleus of a 21-year-old male, ♦ for fresh cells from the soleus of a 35-year-old male, and ▪ for frozen cells from the same 35-year-old male. Symbols above graphs indicate statistically significant differences: Δ from Control, # from MGM only, and □ from MDM only. Analysis of SMU maximum isometric force production in response to a tetanic electrical stimulus and SMU-specific force indicated a significant effect of hEGF timing ($p < 0.001$ for both). Compared with control, SMUs exposed to hEGF-treated MGM+MDM resulted in a 35-fold increase in force production and a 20-fold increase in specific force ($p < 0.001$ for both).

When compared with control, SMUs in hEGF-treated MDM and hEGF-treated MGM+MDM groups showed a significant 20-fold and 35-fold increase in average maximum tetanic force production respectively ($p < 0.0001$ for both). Additionally, average maximum tetanic force production between all hEGF-treated experimental groups were significantly different ($p < 0.0001$ for all). Overall, maximal force production was observed in SMUs in the hEGF-treated MGM+MDM group.

SMU maximum tetanic isometric force measurements were divided by MF20-positive CSA to assess SMU specific force **(Fig. 7B)**. Average specific forces were $(3.47 \pm 3.47) \times 10^{-3}$ N/cm$^2$, $(6.47 \pm 1.21) \times 10^{-3}$ N/cm$^2$, $(42.36 \pm 9.45) \times 10^{-3}$ N/cm$^2$, and $(70.04 \pm 8.58) \times 10^{-3}$ N/cm$^2$ for control, hEGF-treated MGM only, hEGF-treated MDM only, and hEGF-treated MGM+MDM groups respectively. A one-way ANOVA indicated that there was a significant difference in specific force between experimental groups ($p < 0.0001$, $n = 5$ for all experimental groups). A *post hoc* multiple comparisons test indicated significant increases in specific force in SMUs receiving hEGF-treated MDM and SMUs receiving hEGF-treated MGM+MDM when compared with untreated control SMUs ($p = 0.004$ and $p < 0.0001$), respectively.

There was no significant difference in specific force between SMUs receiving hEGF-treated MGM and untreated control SMUs ($p = 1.0$). SMUs receiving hEGF-treated MGM had significantly lower specific forces compared with SMUs receiving hEGF-treated MDM ($p = 0.007$) and SMUs receiving hEGF-treated MGM+MDM ($p < 0.0001$). Additionally, there was a significant increase in specific force in hEGF-treated MGM+MDM SMUs compared with hEGF-treated MDM SMUs ($p = 0.04$). SMUs in hEGF-

treated MGM+MDM groups showed the largest average specific force, 20 times larger than the average specific force of the control group.

### *2.3.3 Role of hEGF in SMU structural maturation*

IHC analysis of SMU cross-sections were used to determine SMU composition and CSA. In all experimental groups, DAPI, MF20, and laminin co-stains indicated the presence of large multinucleated myotubes surrounded by laminin sheaths **(Fig. 8A–D)**. Furthermore, IHC analysis indicated cell viability throughout the entire SMU cross-section in all groups, suggesting there were no limitations in nutrient diffusion during the SMU fabrication process.

A one-way ANOVA indicated that there was significant difference in CSA between experimental groups ($p = 0.0003$; **Fig. 8E**). SMUs exposed to hEGF-treated MDM had significantly greater whole construct CSAs compared with untreated control SMUs ($p = 0.0028$) with mean CSAs of $3.2 \pm 0.1\ mm^2$ versus $2.3 \pm 0.1\ mm^2$, respectively. Additionally, SMUs exposed to hEGF-treated MGM had mean CSAs of $2.1 \pm 0.1\ mm^2$, significantly smaller than the mean CSAs of SMUs exposed to hEGF-treated MDM ($p = 0.0004$) and hEGF-treated MGM+MDM ($2.8 \pm 0.2\ mm^2$; $p = 0.02$).

The MF20-positive CSA was also measured to quantify the amount of myosin heavy chain content in each SMU. A one-way ANOVA revealed that there was a statistically significant difference in MF20-positive CSA between groups ($p = 0.002$; **Fig. 8F**). A *post hoc* multiple comparisons test indicated all experimental groups exposed to hEGF showed a significant increase in myosin heavy chain content compared with control ($p = 0.04$ for hEGF-treated MGM, $p = 0.003$ for hEGF-treated MDM, $p = 0.006$ for hEGF-treated MGM+MDM).

SMUs receiving hEGF-treated MGM, hEGF-treated MDM, and hEGF-treated MGM+MDM had mean MF20-positive CSAs of $0.126 \pm 0.02\ mm^2$, $0.151 \pm 0.01\ mm^2$, and $0.144 \pm 0.01\ mm^2$, respectively. Mean MF20-positive CSAs for hEGF-treated MGM and MGM+MDM SMUs are over two times greater than the untreated control mean CSA of $0.070 \pm 0.01\ mm^2$.

Staining of longitudinal sections of 3D constructs with DAPI and α-actinin revealed myofilament alignment, the development of sarcomeric structure, and the maturing of Z-lines in hEGF-treated SMUs, a sarcomeric organization similar to adult skeletal muscle *in situ* **(Fig. 9)**. While myofilament alignment was present in untreated control SMUs, the development of organized sarcomeric structure was not observed. The improved structural maturation of 3D SMUs treated with hEGF is likely correlated with the SMU's enhanced force production compared with untreated controls.

### *2.3.4 Discussion*

Overall, this study used scaffold-free SMUs to investigate the impact of hEGF on the *in vitro* myogenesis and extracellular matrix deposition of human skeletal muscle stem cells in skeletal muscle tissue engineering models. We hypothesized that exposing myogenic cell cultures to 7.5 nM hEGF at different time spans during the fabrication process would determine the most favorable dosing strategy for enhancing human SMU structure and function.

The hEGF time periods examined aligned with periods of myogenic cell proliferation and differentiation in culture. Cell cultures exposed to hEGF-treated MGM

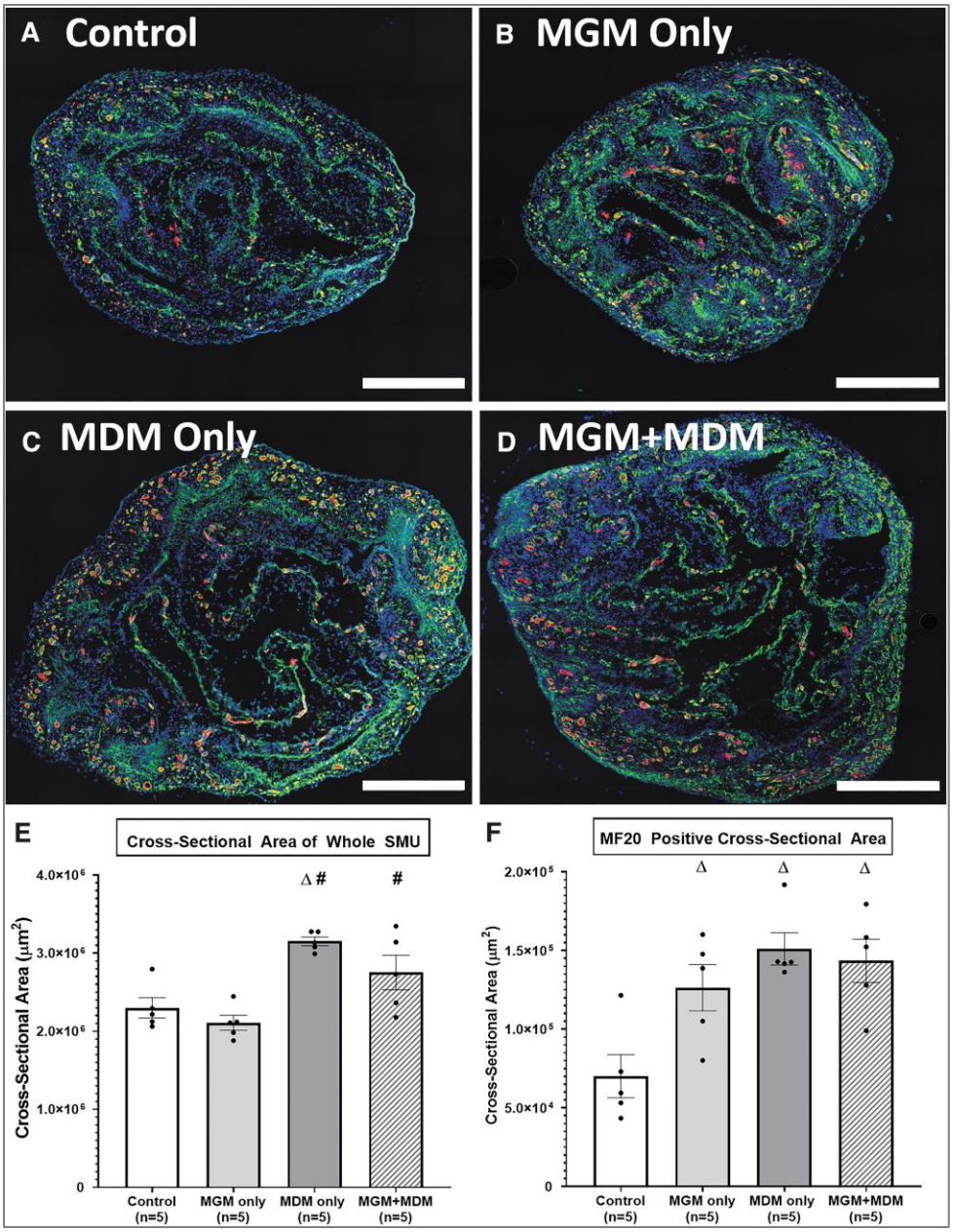


**Figure 8. Role of hEGF in SMU Structural Maturation.** Role of hEGF in SMU structural maturation. IHC of 3D SMU cross-sections was conducted to visualize cell viability (DAPI, blue), myosin heavy chain (MF20, red), and laminin protein (green). The images depicted are representative images of SMUs fed untreated media **(A)**, hEGF-treated MGM **(B)**, hEGF-treated MDM **(C)**, and hEGF-treated MGM+MDM **(D)**. The total CSA **(E)** and MF20-positive CSA **(F)** were quantified for each SMU cross-section that underwent staining (n = 5 per experimental group). Scale bars = 500 μm. Boxes and bars indicate mean ± standard error of the mean. Symbols above graphs indicate statistically significant differences: Δ from Control, and # from MGM only. Nucleated MF20-positive myotubes surrounded by laminin were present in all experimental groups. A one-way ANOVA indicated there was significant difference in CSA between groups ($p = 0.0003$). SMUs exposed to hEGF-treated MDM had significantly greater CSAs when compared with controls ($p = 0.0028$) and SMUs exposed to hEGF-treated MGM ($p = 0.0004$). SMUs fed hEGF-treated MGM+MDM had significantly greater CSAs compared with SMUs exposed to SMUs fed hEGF-treated MGM ($p = 0.0230$). There was also significant difference in myosin heavy chain content between experimental groups ($p = 0.0022$). SMUs exposed to hEGF showed significantly greater myosin heavy chain content compared with untreated controls ($p = 0.0378$ for hEGF-treated MGM, $p = 0.0027$ for hEGF-treated MDM, $p = 0.0060$ for hEGF-treated MGM+MDM).

were introduced to the growth factor during the key myogenic cell proliferation phase, 0 to 6 days post-seeding. Monolayers fed with hEGF-treated MDM were stimulated by the growth factor during periods of myogenic cell differentiation and maturation in both monolayer (two-dimensional [2D]) and SMU (3D) form, 7 to 21 days post-seeding. The addition of hEGF during the myogenic proliferation phase (MGM only) or during myocyte differentiation (MDM only) led to myotube hypertrophy and structural maturation during late differentiation in monolayers, indicated by the increased myotube sizes compared with control.

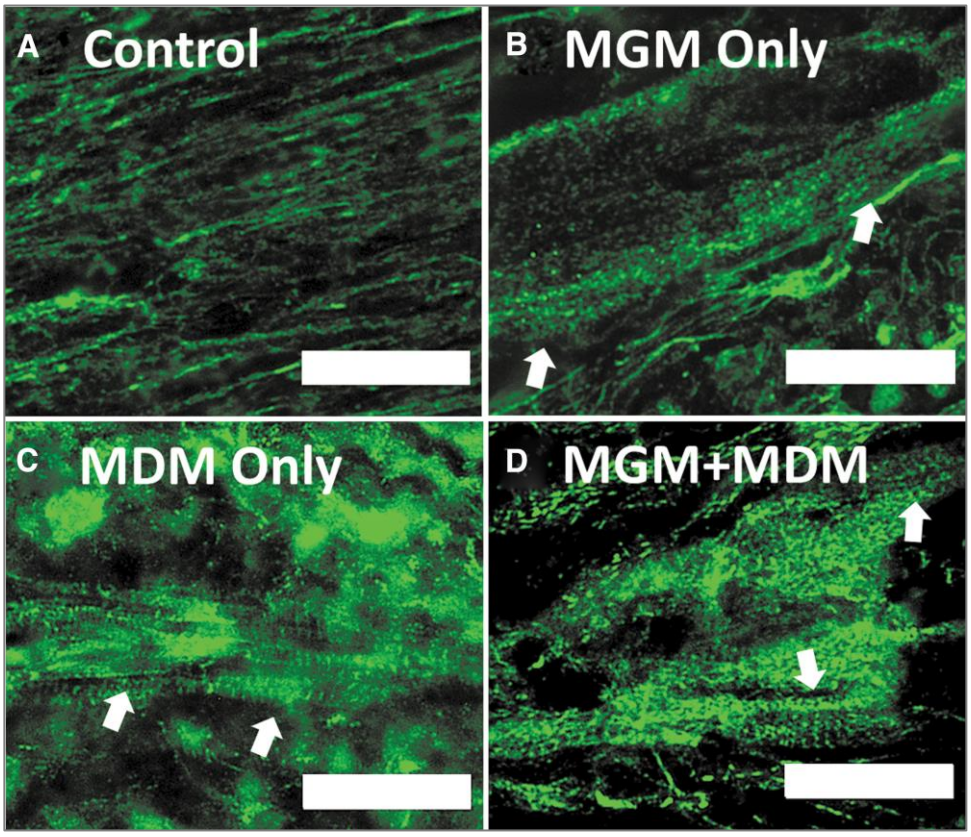


**Figure 9. Impact of hEGF on Sarcomeric Structure.** IHC of 3D SMU longitudinal sections was conducted to visualize sarcomeric structure (α-actinin, green). The images depicted are representative images of SMUs fed untreated media **(A)**, hEGF-treated MGM **(B)**, hEGF-treated MDM **(C)**, and hEGF-treated MGM+MDM **(D)**. Examples of sarcomeric striations are indicated by white arrows. Scale bars = 20 µm. Staining revealed the presence of organized sarcomeric structure and myofilament alignment in hEGF-treated SMUs, whereas organized sarcomeric structure was mostly absent from untreated controls.

Interestingly, hEGF-treated MGM+MDM cultures did not display an increase in myotube size, whereas hEGF-treated MGM only and hEGF-treated MDM only cultures did not show a significant increase in myotube density. Previous literature indicates that hEGF promotes myoblast proliferation but inhibits myoblast differentiation, providing a potential explanation for such results [83, 84]. The sustained administration of hEGF in hEGF-treated MGM+MDM cultures could have inhibited the fusion of myofibers to each other, diminishing overall myotube size. Periods of no hEGF administration in hEGF-treated MGM and hEGF-treated MDM experimental groups would have allowed for the fusion of myofibers to each other, increasing myotube size but decreasing myotube density.

Further analysis is necessary to determine which steps in the differentiation process are inhibited by hEGF. In total, these myotube diameter and myotube density results indicate that hEGF enhances human muscle cell differentiation and myotube fusion in 2D monolayers.

The addition of hEGF to cell culture also greatly impacted 3D SMU structure. All experimental groups treated with hEGF resulted in SMUs with advanced structural maturation compared with control, as indicated by the presence of organized sarcomeric structures. Additionally, the multinucleated myofibers surrounded by laminin sheaths observed in SMU cross-sections are physiologically similar to the individual muscle fibers surrounded by basal lamina sheaths in native muscle tissue.

The increase in myosin content indicates that the SMUs treated with hEGF had significantly increased myofibril content compared with control. hEGF additionally led to hEGF-treated MDM only SMUs and hEGF-treated MGM+MDM SMUs having significantly

larger CSAs compared with hEGF-treated MGM only SMUs, suggesting an increase in extracellular matrix proteins and other cellular material in addition to the increase in myosin content. The significant increase in myosin heavy chain and organized sarcomeric structure likely contributed to the increased force production and specific force of SMUs in hEGF-treated MDM and hEGF-treated MGM+MDM groups.

Our data suggest that starting time point and duration of treatment of hEGF play a significant role in SMU contractile function. The structural development induced by hEGF in 2D monolayers and 3D SMUs contributed to greater SMU force production, most notably in hEGF-treated MGM+MDM SMUs. While hEGF may have inhibited overall myotube size in monolayers, the extracellular matrix deposition and organization induced by hEGF supported the muscle networks present in SMUs allowing for efficient and unified force transmission. Overall, sustained administration of 7.5 nM hEGF during myogenic cell proliferation, differentiation, and maturation phases resulted in SMUs capable of producing the greatest specific forces. Initial studies examining 1.5, 7.5, and 10 nM hEGF in MGM+MDM suggest that hEGF continues to enhance SMU contractile function within that range of concentrations.

Using our scaffold-free tissue engineering model, we demonstrated that the supplementation of hEGF to human primary myogenic cell cultures improved tissue-engineered skeletal muscle structural and functional characteristics with the most promising advancements occurring in cultures exposed to hEGF during the entire fabrication process. Our results suggest that hEGF serves as a critical growth factor in advancing human skeletal muscle-engineered tissue models and developing skeletal muscle with adult phenotypes.

# Chapter 3 Impact of Cell-Seeding Density and Cell Confluence on Human Tissue Engineered Skeletal Muscle

The entirety of this chapter was originally published with the following citation: Wroblewski, O.M., Nguyen, M.H., Cederna, P.S., & Larkin, L.M. (2021). Impact of Cell-Seeding Density and Cell Confluence on Human Tissue Engineered Skeletal Muscle. Tissue Eng Part A. doi: http://doi.org/10.1089/ten.TEA.2021.0132 [85] . This article has been reproduced with permission from the publisher, Mary Ann Liebert, Inc. The figures have been reformatted and/or reproduced in color.

## 3.1 Introduction

Volumetric muscle loss (VML) is a clinical condition resulting from a volume loss of 30% or more in a single muscle [46]. A potential outcome of traumatic injuries, postoperative damage, and congenital defects, VML exceeds native skeletal muscle's self-repair mechanisms and results in impaired muscle function [46, 57, 86]. Current standards-of-care for VML rely on the use of allogenic or autogenic grafts for muscle flap or graft transposition procedures which have shown limited success in restoring skeletal muscle function [15, 47, 56]. Such treatments are additionally limited by issues with graft source availability and donor site morbidity [47]. Allogenic skeletal muscle transplants also risk additional patient complications due to tissue rejection at the repair site and the adverse effects of immunosuppression [47].

Skeletal muscle tissue engineering methodologies have the potential of resolving the shortcomings of current surgical techniques by recapitulating native myogenesis *in*

*vitro* and growing biocompatible and adaptable exogenous muscle tissue [15, 40, 46]. Ideally, skeletal muscle could be engineered from small autogenous muscle biopsies, alleviating or eliminating the limitations seen in current standards-of-care [46]. Techniques in the field have included the use of scaffold materials and chemical and mechanical stimuli to support the growth and maturation of engineered muscles *in vitro* [65, 87, 88]. Importantly, scaffold-free approaches have created engineered skeletal muscle capable of restoring skeletal muscle structure and function in a 30% VML in the peroneus tertius muscle of an ovine animal model [69]. The capability of creating scaled-up engineered skeletal muscle constructs is a promising advancement for the treatment of VML in humans.

Due to their essential role in native skeletal muscle regeneration and their presence throughout adult skeletal muscle, skeletal muscle stem cells, known as satellite cells, are a popular cell source for skeletal muscle regeneration technologies [89, 90]. Satellite cells are isolated via enzymatic digestion of skeletal muscle biopsies [91-93]. A significant obstacle preventing the widespread use of engineered skeletal muscle grafts in a clinical setting is the high number of satellite cells required for fabrication of human-sized skeletal muscle tissue [79, 94, 95]. Native adult skeletal muscle has a low incidence of satellite cells, which make up only 2%-7% of nuclei within skeletal muscle [96]. Furthermore, satellite cells have low expansion potential, showing a significant decrease in myogenic potential during extended *in vitro* cell culture or cell passaging [94, 97]. As a result, large muscle biopsies are required for the fabrication of engineered muscle, especially the scaled-up grafts needed for the treatment of human extremity VML injuries. However, collecting such large muscle biopsies increases donor site morbidity or

functional deficits in the site of muscle harvest, potentially creating a new VML injury to treat an existing VML injury.

Enzymatically digested skeletal muscle biopsies lead to a cell suspension that primarily contains myogenic cells and connective tissue fibroblasts. Several studies have used cells isolated from rodent or ovine skeletal muscle to fabricate engineered muscle grafts [67, 70, 78, 98]. These grafts have shown measurable contractile forces *in vitro* and success in partially repairing VML in animal models [67, 70, 78, 98]. In these studies, myogenic cells undergo proliferation and differentiation while fibroblasts regulate satellite cell expansion and secrete important extracellular matrix components [29, 77, 80]. However, the number of studies adapting these technologies into skeletal muscle engineered from a primary human skeletal muscle cell source are very limited [80]. A difference in cell source can have a significant impact on an engineered skeletal muscle technology, since there are interspecies differences between both fibroblast and satellite cell proliferation and differentiation behaviors and rates [75, 76]. While the presence of fibroblasts promotes skeletal muscle maturation in scaffold-free engineered constructs, large fibroblast numbers can inhibit regeneration, especially since fibroblasts proliferate more rapidly than satellite cells [99]. For the successful fabrication of skeletal muscle tissue engineering technologies from a primary human skeletal muscle cell source, the impact of human skeletal muscle isolate cell-seeding density on the structure and function of engineered tissue needs to be clearly defined.

Our laboratory has developed a method of fabricating scaffold-free tissue engineered skeletal muscle units (SMUs) [67]. The SMU fabrication process is well-defined in ovine and rat models, and constructs have shown the ability to fully or partially

repair 30% VML injuries when implanted *in vivo* [67, 69, 100]. Recent research from our lab has focused on optimizing the SMUs for satellite cells and fibroblasts isolated from human skeletal muscle biopsies, but we have yet to elucidate the ideal starting cell-seeding density that maximizes SMU structure and function while minimizing the quantity of cells required [80]. Additionally, our scaffold-free approach allows us to clearly investigate the impact of primary skeletal muscle cell seeding density on engineered skeletal muscle growth and maturation without the confounding effects of a scaffold's physical and chemical properties. Thus, the purpose of this study was to determine the impact of cell seeding density on the ability to fabricate functional human SMUs. We hypothesized that fabricating SMUs at different cell-seeding densities would determine a cell-seeding density parameter that minimizes scaffold-free tissue engineering cell requirements while maintaining SMU muscle-like content and tetanic force production *in vitro*.

## 3.2 Methodology

### *3.2.1 Experimental design- Cell-seeding Density Experiments*

To elucidate the impact of cell-seeding density on scaffold-free skeletal muscle tissue engineering, human skeletal muscle isolates were cultured into SMUs at 5 different starting cell-seeding densities: 1,000 cells/cm$^2$, 2,500 cells/cm$^2$, 5,000 cells/cm$^2$, 10,000 cells/cm$^2$, and 25,000 cells/cm$^2$. The densities of 25,000 cells/cm$^2$ and 10,000 cells/cm$^2$ were of interest because these starting densities previously led to successful SMU fabrication from rat and human cell sources, respectively [67, 80]. Due to previous human SMU work, cell cultures and SMUs prepared at a starting cell-seeding density of 10,000

cells/cm$^2$ served as controls. Additionally, lower cell seeding densities were examined to determine the potential for decreasing the required starting cell number necessary for SMU fabrication.

During SMU fabrication, human skeletal muscle isolates seeded on tissue culture plates underwent phases of cell proliferation and cell differentiation before monolayers fused into cylindrical 3D skeletal muscle constructs. To enhance cell proliferation, cells were fed muscle growth medium (MGM). To promote cell differentiation, cells were fed muscle differentiation medium (MDM). All five tested cell-seeding densities followed the established human cell source SMU fabrication timeline with monolayers being provided MGM for 7 days followed by MDM for 11 days [80]. During cell culture, it was observed that plates at seeding densities of 10,000 cells/cm$^2$ and 25,000 cells/cm$^2$ were overconfluent by the day of medium switch from MGM to MDM, as indicated by the presence of overgrown layers of cells on the cell culture plates. Plates seeded at densities of 5,000 cells/cm$^2$ or lower were underconfluent, as indicated by areas of no cell growth on the cell culture plates. Previous rat and sheep SMU work suggests that the ideal time to switch cell culture from MGM to MDM is when cells cover 90-100% of the cell culture surface [67, 69, 70, 80, 100]. At that point in time, monolayers are described as between 90-100% confluent [67, 69, 70, 80, 100].

### *3.2.2 Experimental design- Time-to-confluency Experiments*

To determine whether monolayer confluency prior to stimulated differentiation via MDM had any impact on the outcome of human cell-source SMU fabrication, additional time-to-confluency experiments were conducted. Two confluency experimental groups were examined. Monolayers at a starting cell seeding density of 1,000 cells/cm$^2$ and 10,000

cells/cm$^2$ were fed MGM until 90-100% confluency was achieved, after which monolayers were provided MDM for 7 days prior to being pinned as 3D constructs. For comparison, additional 1,000 cells/cm$^2$ and 10,000 cells/cm$^2$ cultures underwent the standardized SMU fabrication timeline, with cultures being switched from MGM to MDM 7 days post-seeding. The 1,000 cells/cm$^2$ confluency experimental group achieved 90-100% confluency after 9 days in MGM, while the 10,000 cells/cm$^2$ confluency group achieved 90-100% confluency after only 6 days in MGM. Cell cultures seeded at 1,000 cells/cm$^2$ that underwent the standardized SMU fabrication timeline were underconfluent (<90%) on the day of switch to MDM, defined as less than 90% of the cell culture area being covered by cells. Hence, during the time-to-confluency study, this experimental group was labelled "1,000 cells/cm$^2$ underconfluent". Cell cultures seeded at 10,000 cells/cm$^2$ that underwent the standardized SMU fabrication timeline were overconfluent (>100%) on the day of switch to MDM, and for the time-to-confluency study were labelled "10,000 cells/cm$^2$ overconfluent". Overconfluence was defined qualitatively as the visible presence of additional delaminating cell layers beyond the initial confluent monolayer upon inspection of the cell culture dish under a microscope. The SMU fabrication timeline and the experimental groups are summarized in **Figure 10**.

### *3.2.3 SMU Fabrication*

All tissue engineering studies involving the use of human skeletal muscle biopsies were approved by the University of Michigan Medical School Institutional Review Board (HUM00151617). Cells were isolated from a human soleus skeletal muscle discard obtained from a healthy 35-year-old male during a below-the-knee amputation, following previously described procedures.[26] Briefly, in an aseptic environment, the biopsy was

minced and subsequently added to an enzymatic digestion solution containing 2.3mg/mL dispase (Cat. No. 17105-041; Thermo Fisher) and 0.3mg/mL collagenase type IV (Cat. No. 17104-019; Thermo Fisher). After 2 hours of incubation in enzymatic solution, the resulting suspension was filtered through 40µm mesh filters (Cat. No. 22-363-547; Fisher Scientific) and then centrifuged. The resulting cell pellet was then frozen down in freezing media containing 70% Dulbecco's modified Eagle's medium (DMEM; Cat. No. 11995-065; Gibco), 20% horse serum (Cat. No. 16050122; Gibco), 10% dimethyl sulfoxide (Cat. No. BP231-100; Fisher Scientific), and a supplementary 1% antibiotic/antimycotic (ABAM, Cat. No. 15240-062; Gibco).

**A**

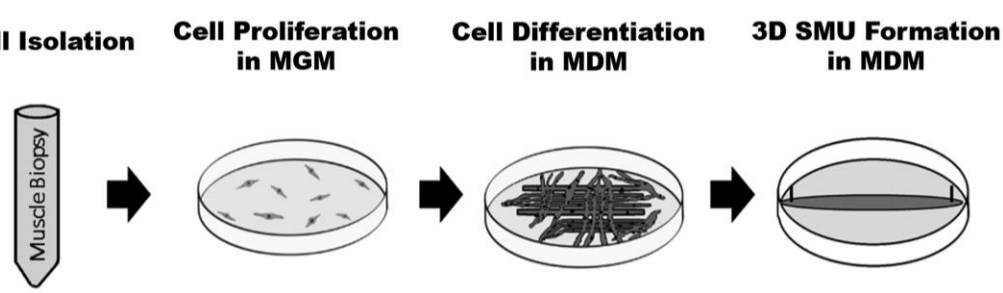


**B**

| Cell Seeding Density (cells/cm$^2$) | Days in MGM | Days in MDM | Monolayer Confluence during First MDM Feeding |
|---|---|---|---|
| 1,000 | 7 | 7 | Underconfluent |
| 2,500 | 7 | 7 | Underconfluent |
| 5,000 | 7 | 7 | Underconfluent |
| 10,000 | 7 | 7 | Overconfluent |
| 25,000 | 7 | 7 | Overconfluent |
| 1,000 | 9 | 7 | Confluent |
| 10,000 | 6 | 7 | Confluent |

**Figure 10. Experiment Design and Timeline.** To determine the impact of cell-seeding density on the engineering of skeletal muscle tissue, SMUs underwent cell-seeding density experiments. SMUs were fabricated with 5 different initial cell-seeding densities: 1,000 cells/cm$^2$, 2,500 cells/cm$^2$, 5,000 cells/cm$^2$, 10,000 cells/cm$^2$ (control), and 25,000 cells/cm$^2$. To investigate the impact of monolayer confluence on engineered skeletal muscle outcome in time-to-confluency experiments, additional experimental groups at starting cell-seeding densities of 1,000 cells/cm$^2$ and 10,000 cells/cm$^2$ were allowed to reach confluence prior to stimulated differentiation in MDM.

To initiate SMU fabrication, cells were thawed, centrifuged, and resuspended in MGM. Following the cell-seeding densities selected for the experimental design, isolated cells were seeded on 60 mm tissue culture-treated polystyrene plates (BD Falcon, Franklin Lakes, NJ) and left undisturbed for 3 days to allow for cell attachment. MGM contained 60% F-12 Kaighn's Medium (Cat. No. 21127-022; Gibco), 24% DMEM, 15% fetal bovine serum (FBS; Cat. No. 10437-028; Gibco), and 1% ABAM with a growth factor supplementation of 9.1 ng/mL human epidermal growth factor (hEGF; Cat. No. CC-4107; Lonza), 4.0 ng/mL dexamethasone (DEX; Cat. No. D8893; Sigma-Aldrich), and 2.4 ng/mL basic fibroblast growth factor (Cat. No. 100-18B; PeproTech).

After cell attachment, cell cultures were fed MGM every 2 days, until the medium switch to MDM, determined by the experimental design timeline. Following the switch, monolayers were fed MDM every 2 days for the duration of SMU fabrication. MDM contained 70% Medium 199 (Cat. No. 1150067; Gibco), 23% DMEM, 6% FBS, and 1% ABAM with a growth factor supplementation of 0.1% insulin/transferrin/selenium X (Cat. No. 51500056; Gibco), 14.5 ug/mL ascorbic acid 2-phosphate (Cat. No. A8960-5G; Sigma Life-Aldrich), 9.1 ng/mL hEGF and 4.0 ng/mL DEX.

After 7 days in MDM, each monolayer was manually delaminated from its polystyrene plate and transferred to a 60 mm plate coated with a soft silicone elastomer (Sylgard 184; Cat. No. 24236-10, Electron Microscopy Sciences). Two stainless steel pins spaced 3cm apart were used to pin the monolayer to the silicone elastomer plate. Over the course of 4 days in MDM, the monolayers fused down in 3D cylindrical SMUs using the pins as anchor points.

### *3.2.4 Monolayer Differentiation: Myotube Density and Size*

To investigate the impact of cell-seeding density on monolayer differentiation and myotube maturation, myotube density and size were investigated. Immediately prior to manual delamination, 5 representative light microscopy images were taken at randomly chosen locations on each monolayer. To determine the myotube density of each monolayer, ImageJ/Fiji was used to quantify the total number of myotubes amongst all 5 images. The number of myotubes was normalized by total image area. Additionally, the diameter of each individual myotube was measured to determine average myotube size. All monolayer images were analyzed by one researcher.

### *3.2.5 SMU Function: Contractile Measurements*

Four days after manual delamination, SMU maximum tetanic isometric force production was measured to evaluate the contractile function of the engineered skeletal muscle constructs, as described previously [67, 70, 80]. Briefly, the anchor pin on one end of the SMU was released from the silicone elastomer and attached to an optical force transducer. Platinum wire electrodes were placed on either side of the SMU to provide a uniform electric field stimulation along the SMU length. During testing, SMUs and electrodes were submerged in MDM maintained at a temperature of 37°C. Tetanic contractions were elicited via a 600ms train of 2.5ms pulses at currents of 900 mA and 1000 mA, and frequencies of 30 Hz, 60 Hz, 90 Hz, 100 Hz, 120 Hz, and 130 Hz to create a force frequency curve. LabVIEW 2012 was used to record and analyze tetanic isometric force data.

### *3.2.6 SMU Structure: Immunohistochemical Analysis*

SMU sections were immunohistochemically stained for the qualitative and quantitative structural analysis of engineered skeletal muscle structure. Immediately after force testing, SMUs were coated in Tissue Freezing Medium (Cat. No. 15-183-36; Fisher Scientific) and flash-frozen in liquid nitrogen-chilled isopentane. Constructs were stored at -80°C until sectioning. SMU cryosections were fixed in -20°C methanol prior to immunostaining.

To investigate SMU total CSA, skeletal muscle content, and extracellular matrix (laminin) deposition, 10µm thick SMU mid-belly cross-sections were stained for nuclei with 4',6-diamidino-2-phenylindole (DAPI, Cat. No. P36935; Invitrogen) and antibodies for myosin heavy chain (MF20; mouse monoclonal antibody 1:200 dilution; Cat. No. MF 20-c; Developmental Studies Hybridoma Bank) and laminin (rabbit polyclonal antibody 1:200 dilution; Cat. No. 7463; Abcam). To evaluate SMU sarcomeric structure, 10 µm thick SMU cross-sections were stained for an α-actinin antibody (rabbit polyclonal antibody 1:300 dilution; Cat. No. ab18061; Abcam).

All stained sections were imaged using a Zeiss Apotome microscope. ImageJ/Fiji's freehand selection and analyze particle tools were used to quantify the total CSA, MF20-positive CSA, and laminin-positive CSA of each stained SMU section. All image data was analyzed by one researcher. To determine an engineered construct's specific force, the maximum tetanic isometric force measurement for each SMU was normalized by the SMU's MF20-positive CSA. The SMU's MF20-positive CSA was used in order to directly examine the force production capabilities of the SMU's skeletal muscle-like content. Maximum tetanic isometric force measurements for each SMU were also normalized by

the SMU's total CSA in order to further investigate the contractile capabilities of the engineered constructs. This measurement is referred to as the normalized force.

### *3.2.7 Statistical Analysis*

All values are presented as mean ± standard error of the mean. Statistical analysis was performed using GraphPad Prism software. Significant differences between experimental groups in the cell-seeding density experiments were determined through the comparison of means via one-way analysis of variance (ANOVA) with Tukey post hoc comparisons. In time-to-confluency experiments, experimental groups with the same seeding densities were categorized and compared via student t-test. Differences were considered significant at $p < 0.05$.

## 3.3 Results

### *3.3.1 Effect of cell-seeding density on muscle cell differentiation and myotube fusion*

Light microscopy images of monolayers taken immediately prior to delamination indicated the presence of thick, elongated myotubes and dense myotube networks in all experimental groups (**Fig. 11A-G**). Even when cell cultures were switched to MDM prior to reaching 90-100% confluence, lower starting cell-seeding densities did not negatively impact a cell culture's ability to form a cohesive and structurally durable monolayer and all experimental groups resulted in monolayers capable of being delaminated and converted into 3D cylindrical constructs.

In cell-seeding density experiments, there was a significant difference in myotube diameter between experimental groups ($p < 0.0001$; **Fig. 11H**). Monolayers in the 25,000 cells/cm$^2$ experimental group had a significantly smaller average myotube diameter compared to the 1,000 cells/cm$^2$ ($p=.0002$), 2,500 cells/cm$^2$ ($p=.0005$), and 5,000 cells/cm$^2$ ($p=.0009$) experimental groups with a mean of 15.4 µm versus means of 19.6 µm, 19.3 µm, and 18.8 µm, respectively. The same trend was seen with the 10,000 cells/cm$^2$ control group, which, with a mean of 16.6 µm, had a significantly smaller average myotube diameter compared to the 1,000 cells/cm$^2$ ($p=.003$), 2,500 cells/cm$^2$ ($p=.008$), and 5,000 cells/cm$^2$ ($p=.02$) experimental groups. The 10,000 cells/cm$^2$ control group did not have a significant difference in myotube diameter when compared to the 25,000 cells/cm$^2$ experimental group. Interestingly, in time-to-confluency experiments, there was a significant difference in myotube diameter ($p=0.0005$) between the 10,000 cells/cm$^2$ overconfluent experimental group (mean of 16.50 µm) and the 10,000 cells/cm$^2$ confluent experimental group (mean of 18.12 µm; **Fig. 11I**). There was no significant difference in myotube diameter between monolayers in the 1,000 cells/cm$^2$ underconfluent experimental group and the 1,000 cells/cm$^2$ confluent experimental group.

Monolayer images were also used to analyze myotube density, measured by myotubes/mm$^2$ (**Fig. 11J-K**). In both cell-seeding density and time-to-confluency experiments, there was no statistically significant difference in myotube density between experimental groups with average values ranging from 15.2 myotubes/mm$^2$ to 17.7 myotubes/mm$^2$. While some experimental groups had significant differences in myotube diameter, these differences in diameter were not large enough to impact the myotube density over the analyzed area.

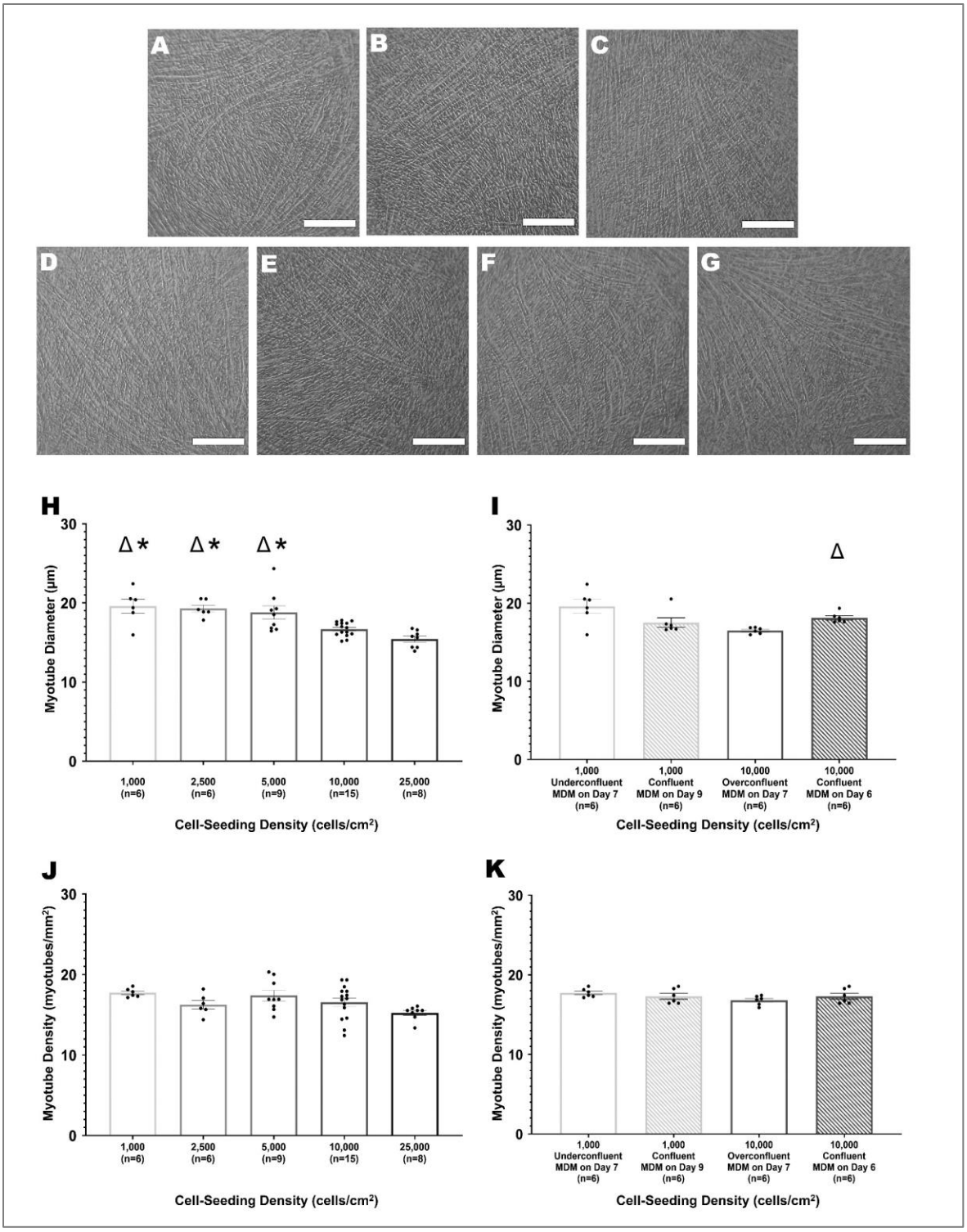
A
B
C
D
E
F
G
H
Myotube Diameter (μm)
Δ*
Δ*
Δ*
1,000 (n=6)
2,500 (n=6)
5,000 (n=9)
10,000 (n=15)
25,000 (n=8)
Cell-Seeding Density (cells/cm²)
I
Myotube Diameter (μm)
Δ
1,000 Underconfluent MDM on Day 7 (n=6)
1,000 Confluent MDM on Day 9 (n=6)
10,000 Overconfluent MDM on Day 7 (n=6)
10,000 Confluent MDM on Day 6 (n=6)
Cell-Seeding Density (cells/cm²)
J
Myotube Density (myotubes/mm²)
1,000 (n=6)
2,500 (n=6)
5,000 (n=9)
10,000 (n=15)
25,000 (n=8)
Cell-Seeding Density (cells/cm²)
K
Myotube Density (myotubes/mm²)
1,000 Underconfluent MDM on Day 7 (n=6)
1,000 Confluent MDM on Day 9 (n=6)
10,000 Overconfluent MDM on Day 7 (n=6)
10,000 Confluent MDM on Day 6 (n=6)
Cell-Seeding Density (cells/cm²)

**Figure 11 Effect of cell-seeding density on muscle cell differentiation and myotube fusion.** Image on preceding page. After 7 Days in MDM, monolayers were imaged under a light microscope at 10x magnification immediately prior to delamination. Scale bars = 250 µm. Images shown are representative of monolayers with a starting cell seeding density of 1,000 cells/cm$^2$ (**A**), 2,500 cells/cm$^2$ (**B**), 5,000 cells/cm$^2$ (**C**), 10,000 cells/cm$^2$ (control, **D**), and 25,000 cells/cm$^2$ (**E**). Monolayers seeded at 1,000 cells/cm$^2$ and 10,000 cells/cm$^2$ and allowed to reach confluence prior to being switched from MGM to MGM were also imaged (**F** &**G**, respectively). Using monolayer images, myotube size and density were evaluated for both cell-seeding density (**H, J**) and timing-to-confluency (**I,K**) experiments. For time-to-confluency experiments, cell-seeding density, monolayer confluency, and culture day of initial MDM feeding is listed for each experimental group. Boxes and bars indicate mean ± standard error of the mean. Δ indicates significant difference from the 10,000 cells/cm$^2$ control group. * above bars indicate significant difference from the 25,000 cells/cm$^2$ experimental group. For cell-seeding density experiments, one-way ANOVA indicated that starting cell-seeding density had a significant effect on myotube diameter ($p<0.0001$). Post hoc analysis indicated a significant difference in myotube diameters between monolayers initially seeded at 10,000 cells/cm$^2$ (control) and monolayers initially seeded at 1,000 cells/cm$^2$ ($p=.003$) , 2,500 cells/cm$^2$ ($p=.008$), and 5,000 cells/cm$^2$ ($p=.02$). The 25,000 cells/cm$^2$ experimental group had significant lower myotube diameters compared to the 1,000 cells/cm$^2$ ($p=.0002$) , 2,500 cells/cm$^2$ ($p=.0005$), and 5,000 cells/cm$^2$ ($p=.0009$) experimental groups. A Student's t-test indicated a significant increase in the myotube diameters in 10,000 cells/cm$^2$ confluent monolayers compared to 10,000 cells/cm$^2$ overconfluent monolayers ($p=0.005$). No significant difference in myotube density between experimental groups was noted.

### *3.3.2 Impact of cell-seeding density on SMU contractile function*

After 3D construct formation, SMU contractile function was assessed via tetanic force production measurements (**Fig. 12A-B**). Regarding cell-seeding density

experiments, an ordinary one-way ANOVA indicated significant difference in maximum tetanic force production between experimental groups ($p= 0.0008$). SMUs in the 25,000 cells/cm$^2$ group had an average maximum tetanic force of 165.6 µN. A post hoc multiple comparisons test indicated that the 25,000 cells/cm$^2$ SMUs had significantly weaker contractile function compared to SMUs in the 2,500 cells/cm$^2$ ($p=.004$), 5,000 cells/cm$^2$ ($p=.002$), and 10,000 cells/cm$^2$ control ($p=.006$) experimental groups, which had average maximum tetanic forces of 323.9, µN, 319.2 µN, and 289.9 µN, respectively. There was no statistically significant difference in contractile functions between SMUs in the 25,000 cells/cm$^2$ and the 1,000 cells/cm$^2$ group. Additionally, there was no significant difference in maximum tetanic force between the 1,000 cells/cm$^2$, 2,500 cells/cm$^2$, 5,000 cells/cm$^2$ , and 10,000 cells/cm$^2$ control experimental groups. Tetanic

force production measurements from time-to-confluency experiments indicated that the confluency of a monolayer on the day cell culture is switched from muscle growth media to muscle differentiation media has an impact on SMU contractile function. With an average of 331.0 μN, SMUs from the 1,000 cells/cm$^2$ confluent experimental group had significantly greater maximum tetanic forces compared to 1,000 cells/cm$^2$ underconfluent SMUs (mean of 235.6 μN, p=0.002). These results signify that introducing a cell culture to MDM while the monolayer is underconfluent is detrimental to the contractile properties of the resulting SMU. There was no significant difference in tetanic force production measurements between 10,000 cells/cm$^2$ overconfluent (mean of 300.5 uN) and 10,000 cells/cm$^2$ confluent (mean of 320.2 uN) experimental groups.

To further investigate construct contractile properties, SMU specific force was assessed (**Fig. 12C-D**). The specific force of individual SMUs was determined by normalizing each SMUs maximum tetanic isometric force by the SMUs MF20-positive CSA. A one-way ANOVA combined with Tukey post hoc comparisons indicated no significant difference between cell-seeding density study experimental groups, suggesting no difference in the amount of contractile force capability per area of SMU muscle-like content. Student's t-tests indicated no significant difference in specific force between time-to-confluency study experimental groups. SMU maximum tetanic force production was also normalized by SMU total cross-sectional area. With an average of 0.0041 N/cm$^2$, SMUs from the 25,000 cells/cm$^2$ experimental group had significantly lower normalized tetanic forces compared to the 1,000 cells/cm$^2$ (mean of 0.014 N/cm$^2$, p=0.002), 2,500 cells/cm$^2$ (mean 0.016 N/cm$^2$, p=0.003), and 5,000 cells/cm$^2$ SMUs (mean 0.016 N/cm$^2$, p=0.002). There was no other significant difference in normalized

tetanic forces between experimental groups in the cell-seeding density study. Regarding the time-to-confluency study, SMUs from the 1,000 cells/cm$^2$ confluent experimental group had significantly lower normalized tetanic forces compared to SMUs from 1,000 cells/cm$^2$ underconfluent experimental group with an average of 0.00023 N/cm$^2$ versus

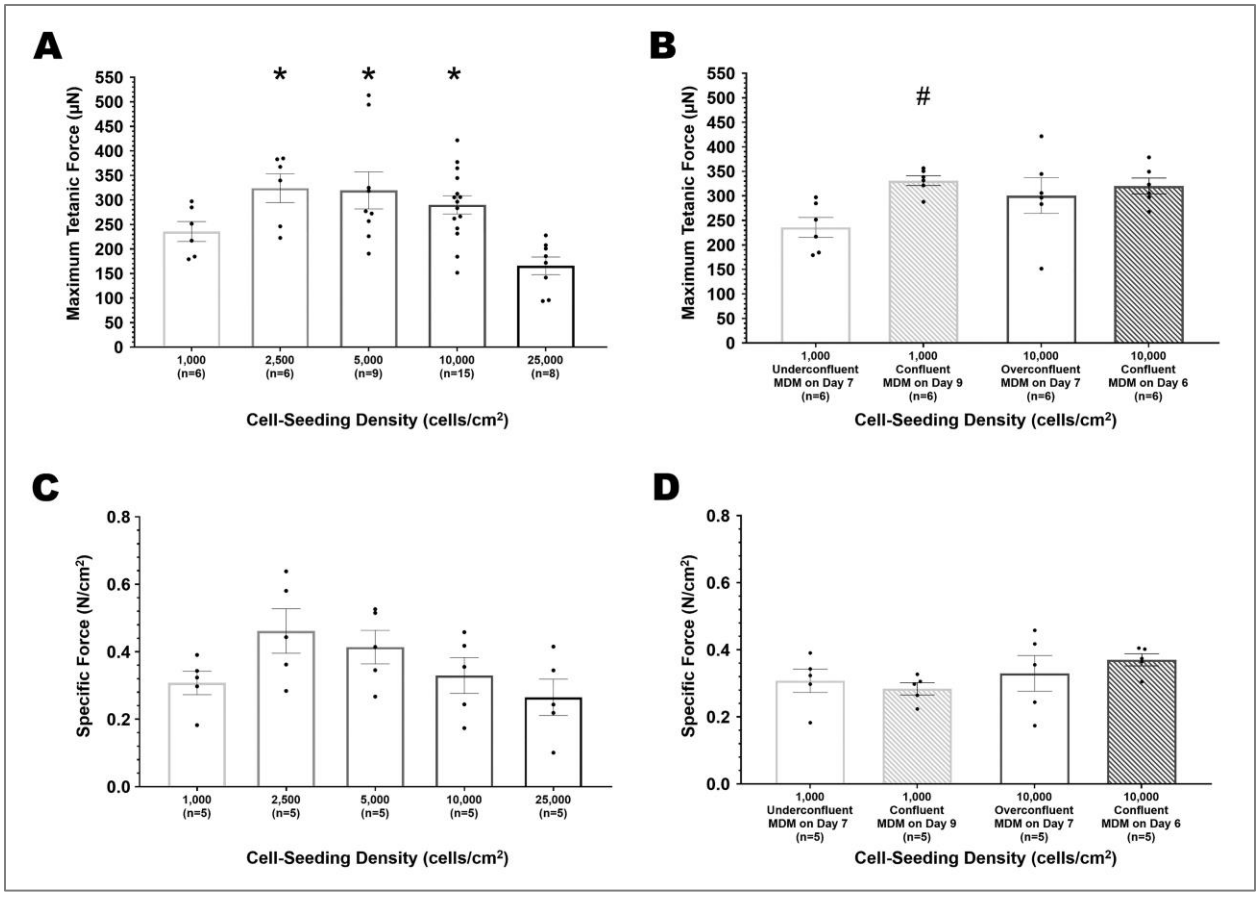


**Figure 12 Impact of cell-seeding density on SMU maximum tetanic force production and specific force in cell-seeding density (A, C) and time-to-confluency (B,D) experiments**. For time-to-confluency experiments, cell-seeding density, monolayer confluency, and culture day of initial MDM feeding are listed for each experimental group. Boxes and bars indicate mean ± standard error of the mean. * above bars indicate significant difference from the 25,000 cells/cm$^2$ experimental group. # indicates significant different from the 1,000 cells/cm$^2$ experimental group. For cell-seeding density experiments, measurement of SMU contractile properties indicated significant difference in maximum tetanic force production between experimental groups (p= 0.0008). SMUs fabricated from an initial cell-seeding density of 25,000 cells/cm$^2$ had significantly lower maximum tetanic force production compared to SMUs fabricated from an initial cell-seeding density of 2,500 cells/cm$^2$ (p=0.004), 5,000 cells/cm$^2$ (p=0.002), and 10,000 cells/cm$^2$ (control, p=0.006). Considering SMUs fabricated from monolayers that reached confluence prior to being fed MDM, the 1,000 cells/cm$^2$ confluent experimental group had significantly larger maximum tetanic forces compared to the 1,000 cells/cm$^2$ underconfluent experimental group (p=0.002). The maximum tetanic force of representative SMUs from each experimental group was normalized by the SMUs MF20-positive cross-sectional area to determine specific force. There was no significant difference in specific force between experimental groups.

0.014 N/cm$^2$ (p= 0.0002). Additionally, 10,000 cells/cm$^2$ confluent SMUs had an average normalized tetanic force significantly lower than 10,000 cells/cm$^2$ overconfluent SMUs (mean of 0.00022 N/cm$^2$ versus 0.010 N/cm$^2$ , p=0.005).

### *3.3.3 Structural maturation of SMUs at different starting cell-seeding densities*

IHC staining of SMU cross-sections elucidated details about construct structure and composition (**Fig. 13**). For all experimental groups, DAPI stains indicated the presence of cells throughout the entire area of the construct. These results suggest that starting cell-seeding density did not impact nutrient diffusion during SMU formation. SMUs in all experimental groups also had abundant laminin deposition, important for construct structural integrity and cohesiveness. Myosin heavy chain was present in all stained SMUs. Furthermore, all stained SMUs contained multinucleated myotubes surrounded by laminin sheaths.

Quantitatively, a one-way ANOVA indicated that the cell-seeding density study experimental groups had significantly different total cross-sectional areas (p <0.0001, **Fig. 14A**). SMUs in the 25,000 cells/cm$^2$ experimental group had significantly greater total CSAs compared to SMUs in the 1,000 cells/cm$^2$, 2,500 cells/cm$^2$, 5,000 cells/cm$^2$, and 10,000 cells/cm$^2$ control experimental groups with a mean of 3.9 mm$^2$ versus 1.7 mm$^2$, 2.0 mm$^2$, 2.1 mm$^2$, and 2.7 mm$^2$, respectively (p<0.001 for 1,000 cells/cm$^2$, 2,500 cells/cm$^2$, and 5,000 cells/cm$^2$, p=0.005 for 10,000 cells/cm$^2$). SMUs in the 1,000 cell/cm$^2$ group had significantly lower total CSAs compared SMUs in the 10,000 cells/cm$^2$ control group (p=0.02) but were not significantly different from SMUs in the 2,500 cells/cm$^2$ and 5,000 cells/cm$^2$ groups. SMUs in the 2,500 cells/cm$^2$, 5,000 cells/cm$^2$, and 10,000 cells/cm$^2$ control groups showed no significant difference in total CSAs. In the time-to-

confluency study, 1,000 cells/cm$^2$ confluent SMUs had a mean total CSA of 2.3 mm$^2$, significantly greater than 1,000 cells/cm$^2$ underconfluent SMUs, which had a mean total CSA of 1.7 mm$^2$ (p=0.048). There was no significant difference in mean total CSA measurements between 10,000 cells/cm$^2$ overconfluent (mean of 2.7 mm$^2$) and 10,000

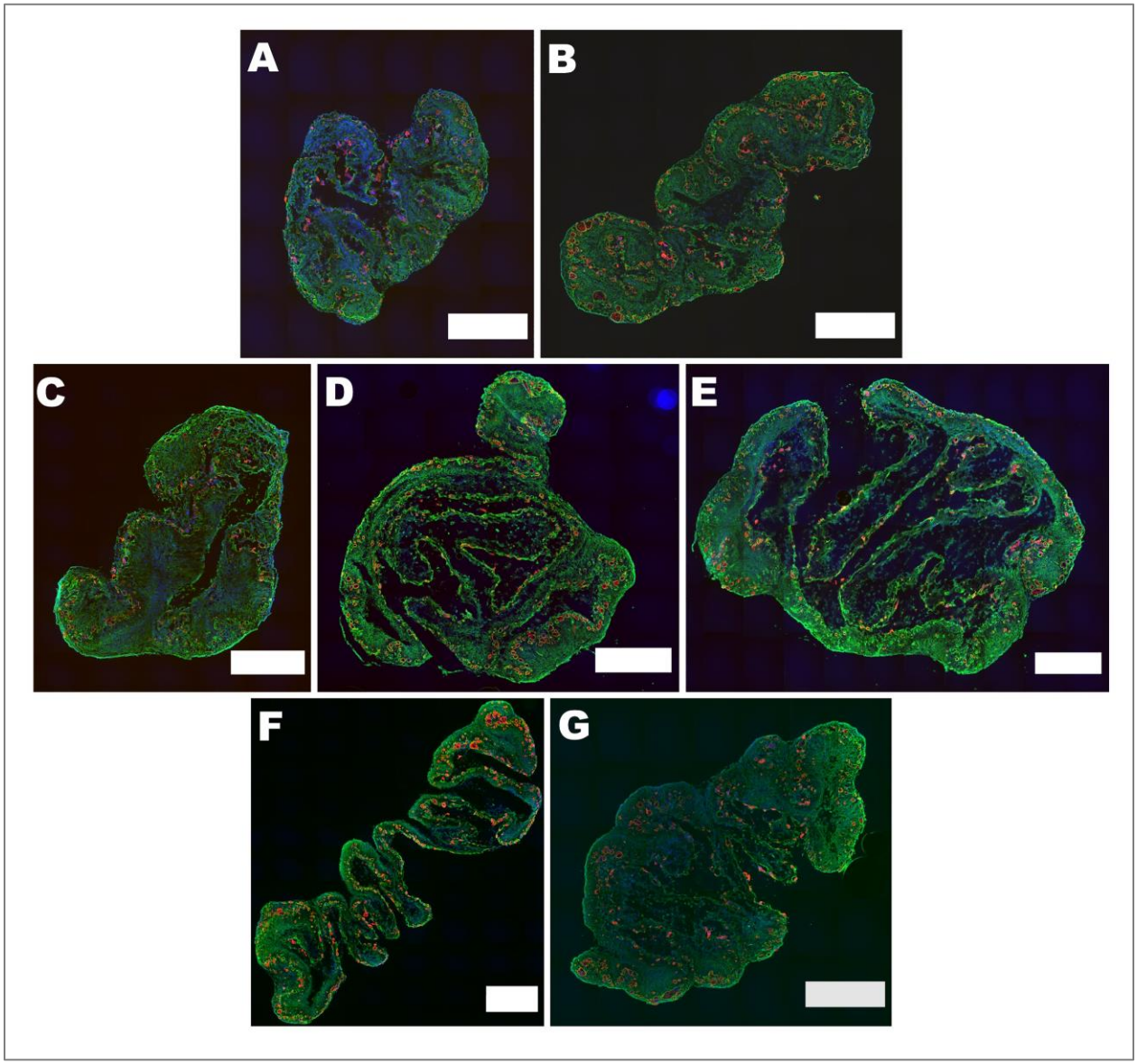


**Figure 13. SMU Myosin Heavy Chain and Laminin Content.** SMU cross-sections underwent IHC staining for cell viability (**DAPI, blue**), myosin heavy chain (**MF20, red**), and laminin protein (**green**). Scale bars = 500 µm. The images depicted are representative cross-sections of SMUs with initial cell seeding densities of 1,000 cells/cm$^2$ (**A**), 2,500 cells/cm$^2$ (**B**), 5,000 cells/cm$^2$ (**C**), 10,000 cells/cm$^2$ (control, **D**), and 25,000 cells/cm$^2$ (**E**). From the time-to-confluency experiments, images **F** and **G** depict SMUs formed from monolayers seeded at 1,000 cells/cm$^2$ and 10,000 cells/cm$^2$, respectively, and grown to confluence prior to being switched from MGM to MDM.

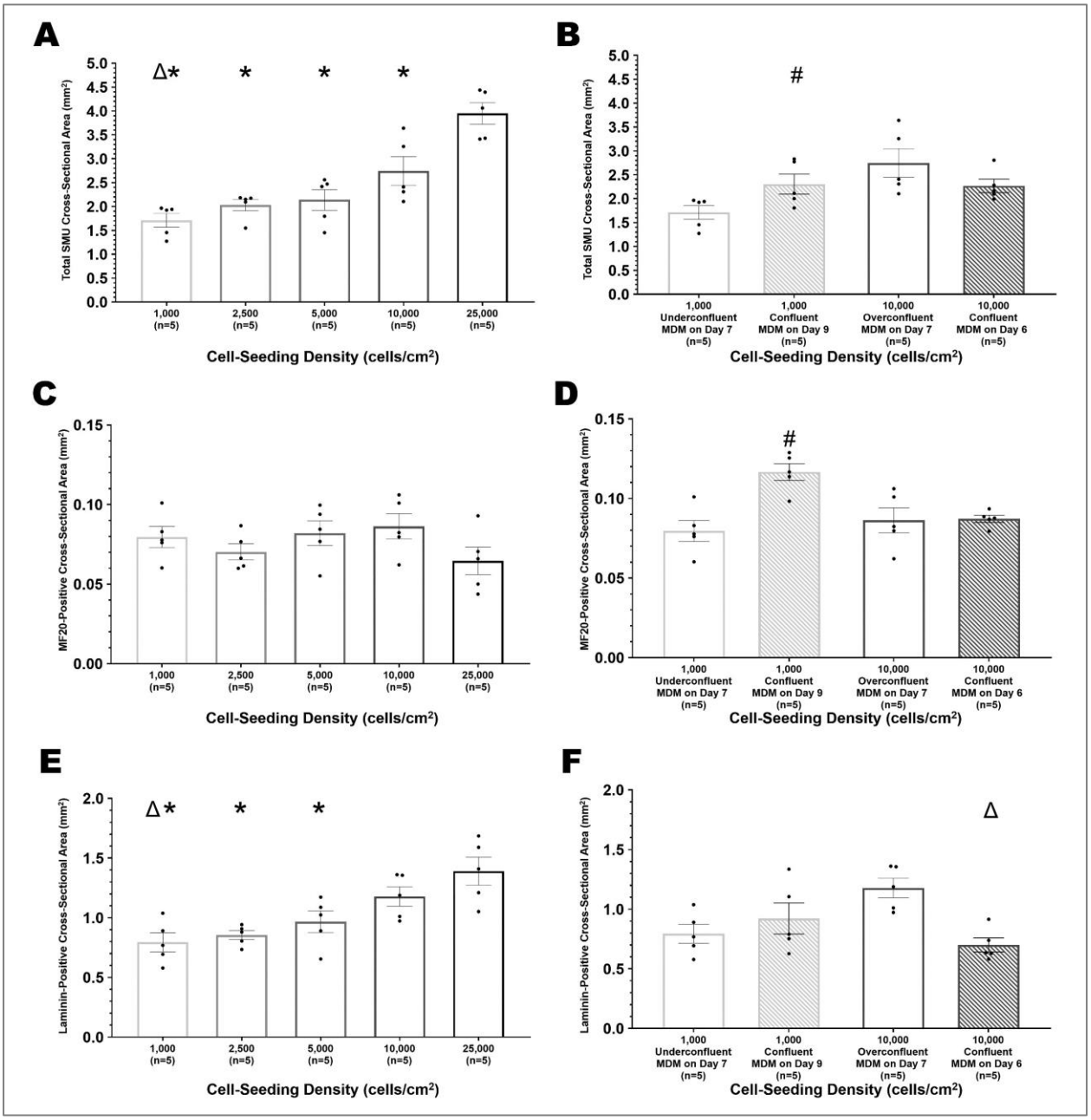
A
Total SMU Cross-Sectional Area (mm²)
Δ*
*
*
*
1,000 (n=5)
2,500 (n=5)
5,000 (n=5)
10,000 (n=5)
25,000 (n=5)
Cell-Seeding Density (cells/cm²)
B
Total SMU Cross-Sectional Area (mm²)
#
1,000 Underconfluent MDM on Day 7 (n=5)
1,000 Confluent MDM on Day 9 (n=5)
10,000 Overconfluent MDM on Day 7 (n=5)
10,000 Confluent MDM on Day 6 (n=5)
Cell-Seeding Density (cells/cm²)
C
MF20-Positive Cross-Sectional Area (mm²)
1,000 (n=5)
2,500 (n=5)
5,000 (n=5)
10,000 (n=5)
25,000 (n=5)
Cell-Seeding Density (cells/cm²)
D
MF20-Positive Cross-Sectional Area (mm²)
#
1,000 Underconfluent MDM on Day 7 (n=5)
1,000 Confluent MDM on Day 9 (n=5)
10,000 Overconfluent MDM on Day 7 (n=5)
10,000 Confluent MDM on Day 6 (n=5)
Cell-Seeding Density (cells/cm²)
E
Laminin-Positive Cross-Sectional Area (mm²)
Δ*
*
*
1,000 (n=5)
2,500 (n=5)
5,000 (n=5)
10,000 (n=5)
25,000 (n=5)
Cell-Seeding Density (cells/cm²)
F
Laminin-Positive Cross-Sectional Area (mm²)
Δ
1,000 Underconfluent MDM on Day 7 (n=5)
1,000 Confluent MDM on Day 9 (n=5)
10,000 Overconfluent MDM on Day 7 (n=5)
10,000 Confluent MDM on Day 6 (n=5)
Cell-Seeding Density (cells/cm²)

**Figure 14 Impact of cell-seeding density on SMU Composition**. Image on preceding page. Using cross-sections stained for DAPI, myosin heavy chain, and laminin, the total CSA (**A-B**), MF20-positive CSA (**C-D**), and laminin-positive CSA (**E-F**) were quantified for representative SMUs cell-seeding density (**A,C,E**) and time-to-confluency (**B,D,F**) experiments. For time-to-confluency experiments, cell-seeding density, monolayer confluency, and culture day of initial MDM feeding is listed for each experimental group. Boxes and bars indicate mean ± standard error of the mean. Δ above bars indicates significant difference from the 10,000 cells/cm$^2$ control group. * indicates significant difference from the 25,000 cells/cm$^2$ experimental group. # indicates significant difference from the 1,000 cells/cm$^2$ confluence experimental group. For cell-seeding density experiments, a one-way ANOVA indicated there was significant difference in total CSA ($p < 0.0001$) and laminin positive CSA ($p=0.0004$). SMUs in the 25,000 cells/cm$^2$ experimental group had significantly larger total CSAs compared to SMUs in all other experimental groups ($p<0.001$ for 1,000 cells/ cm$^2$, 2,500 cells/ cm$^2$, and 5,000 cells/ cm$^2$, $p=0.005$ for 10,000 cells/ cm$^2$ ). Additionally, SMUs in the 10,000 cells/cm$^2$ control group had significantly larger total CSAs to SMUs in the 1,000 cells/cm$^2$ experimental group ($p=0.02$). 25,000 cells/ cm$^2$ SMUs had significantly larger laminin-positive CSAs compared to SMUs in the 1,000 cells/cm$^2$ ($p=0.0007$), 2,500 cells/cm$^2$ ($p=0.002$), and 5,000 cells/cm$^2$ ($p=0.02$) experimental groups . In time-to-confluency experiments, 1,000 cells/ cm$^2$ confluent SMUs displayed significantly greater total and MF20-positive CSAs compared to the 1000 cells/cm$^2$ underconfluent experimental group ($p=0.048$ and $p=0.002$, respectively). 10,000 cells/cm$^2$ confluent SMUs also had significantly smaller laminin-positive CSAs compared to 10,000 cells/cm$^2$ overconfluent SMUs ($p=0.002$).

cells/cm$^2$ confluent (mean of 2.3 mm$^2$) experimental groups. Focusing on myosin heavy chain content, there was no significant difference in MF20-positive CSA between experimental groups in the cell-seeding density study ($p=0.0002$, **Fig. 14C**). However, in the time-to-confluency study, 1,000 cells/cm$^2$ confluent SMUs displayed significantly greater MF20-positive CSAs compared to 1,000 cells/cm$^2$ underconfluent SMUs with an average of 0.12 mm$^2$ versus 0.08 mm$^2$ ($p=0.002$, **Fig. 14D**).SMU MF20-positive CSA measurements were also normalized by SMU total CSA measurements to determine the percentage of skeletal muscle-like content in SMU cross-sections. In the cell-seeding density study, SMUs in the 25,000 cells/cm$^2$ experimental group had significantly lower percentages of MF20-positive content compared to SMUs in the 1,000 cells/cm$^2$, 2,500 cells/cm$^2$, 5,000 cells/cm$^2$, and 10,000 cells/cm$^2$ control experimental groups with a mean of 1.6% versus 4.8%, 3.5%, 4.0%, and 3.2%, respectively ($p<0.0001$ for 1,000 cells/cm$^2$, $p=0.01$ for 2,500 cells/cm$^2$, $p= 0.001$ for 5,000 cells/cm$^2$, and $p=0.04$ for 10,000 cells/cm$^2$). 1,000 cells/cm$^2$ and 10,000 cells/cm$^2$ control SMUs also had significantly different

percentages of MF20-positive content (p=0.04). In time-to-confluency studies, 10,000 cells/cm$^2$ confluent SMUs had significantly greater percentages of MF20-positive content compared to 10,000 cells/cm$^2$ overconfluent SMUs (3.9% versus 3.2%, p=0.03). There was no significant difference in total percentage of MF20-positive content between 1,000 cells/cm$^2$ underconfluent and 1,000 cells/cm$^2$ confluent SMUs.

To determine the impact of starting cell-seeding density on extracellular matrix deposition, laminin-positive CSA was measured in SMU cross-sections (**Fig. 14E-F**). In the cell-seeding density study, statistical analysis indicated a significant difference in laminin-positive CSA between groups (p=0.0004). SMUs in the 25,000 cells/cm$^2$ experimental group with a mean laminin-positive CSA of 1.4 mm$^2$ had significantly greater CSAs compared to SMUs in the 1,000 cells/cm$^2$ (p=0.007), 2,500 cells/cm$^2$ (p=0.002), and 5,000 cells/cm$^2$ (p=0.02) experimental groups (means of 0.79 mm$^2$, 0.85 mm$^2$, and 0.97 mm$^2$ respectively). Additionally, SMUs in the 10,000 cells/cm$^2$ control experimental group had a mean laminin positive-CSA of 1.2 mm$^2$ significantly greater than SMUs in the 1,000 cells/cm$^2$ experimental group (p=0.03). In the time-to-confluency study, the 10,000 cells/cm$^2$ confluent experimental group SMUs had a significantly smaller mean laminin-positive CSA compared to the 10,000 cells/cm$^2$ overconfluent experimental group, with a mean of 0.7 mm$^2$ versus 1.2 mm$^2$ (p=0.002). To determine the percentage of extracellular matrix content in SMUs, SMU laminin-positive CSA measurements were normalized by SMU total CSA measurements. In the cell-seeding density study, experimental groups saw no significant difference in percentage of laminin-positive content with averages of 46.6%, 42.9%, 44.3%, and 35.7% for 1,000 cells/cm$^2$, 2,500 cells/cm$^2$, 5,000 cells/cm$^2$, 10,000 cells/cm$^2$ control, and 25,000 cells/cm$^2$ SMUs, respectively. In the time-to-

confluency study, there was no significant difference in total percentage of laminin-positive content between 1,000 cells/cm$^2$ underconfluent and 1,000 cells/cm$^2$ confluent SMUs. With a mean of 30.8%, 10,000 cells/cm$^2$ confluent SMUs had significantly lower percentages of laminin-positive content compared to 10,000 cells/cm$^2$ overconfluent SMUs (mean of 44.4%, p=0.01).

Longitudinal sections of SMUs in each experimental group were stained for DAPI and α-actinin to assess the maturity of myotubes. These stains revealed the presence of aligned and striated sarcomeric structures in all experimental groups (**Fig. 15**). These results indicated that SMUs fabricated at all tested starting cell-seeding densities were capable of developing mature muscle-like content with sarcomeric organization similar to the aligned structures seen in adult skeletal muscle *in situ*.

### 3.4 Discussion

For this study, we fabricated scaffold-free skeletal muscle units to characterize the role of cell-seeding density on the outcome of skeletal muscle engineered from human skeletal muscle stem cells and to optimize a protocol for the fabrication of human cell-sourced SMUs. We aimed to decrease the skeletal muscle biopsy size required to fabricate human cell-sourced SMUs. These experiments served to determine whether the skeletal muscle cell isolate seeding density could be decreased from a standard control of 10,000 cells/cm$^2$ without impacting SMU structure and contractile function.

Previous work in our laboratory has determined that the ideal starting cell-seeding densities for rat and ovine SMUs are 25,000 cells/cm$^2$ and 10,000 cells/cm$^2$, respectively [67, 69, 70, 80, 100]. Highlighting the impact of species cell-source on the *in vitro* growth of engineered skeletal muscle, the high starting cell-seeding density used in rat models

was detrimental to the contractile function of the human cell-sourced SMUs fabricated in this study. Lower cell-seeding densities had an average maximum tetanic force production of up-to 2 times greater than SMUs fabricated with a starting cell-seeding density of 25,000 cells/cm$^2$. Analysis of monolayers, SMU cross-sections, and SMU

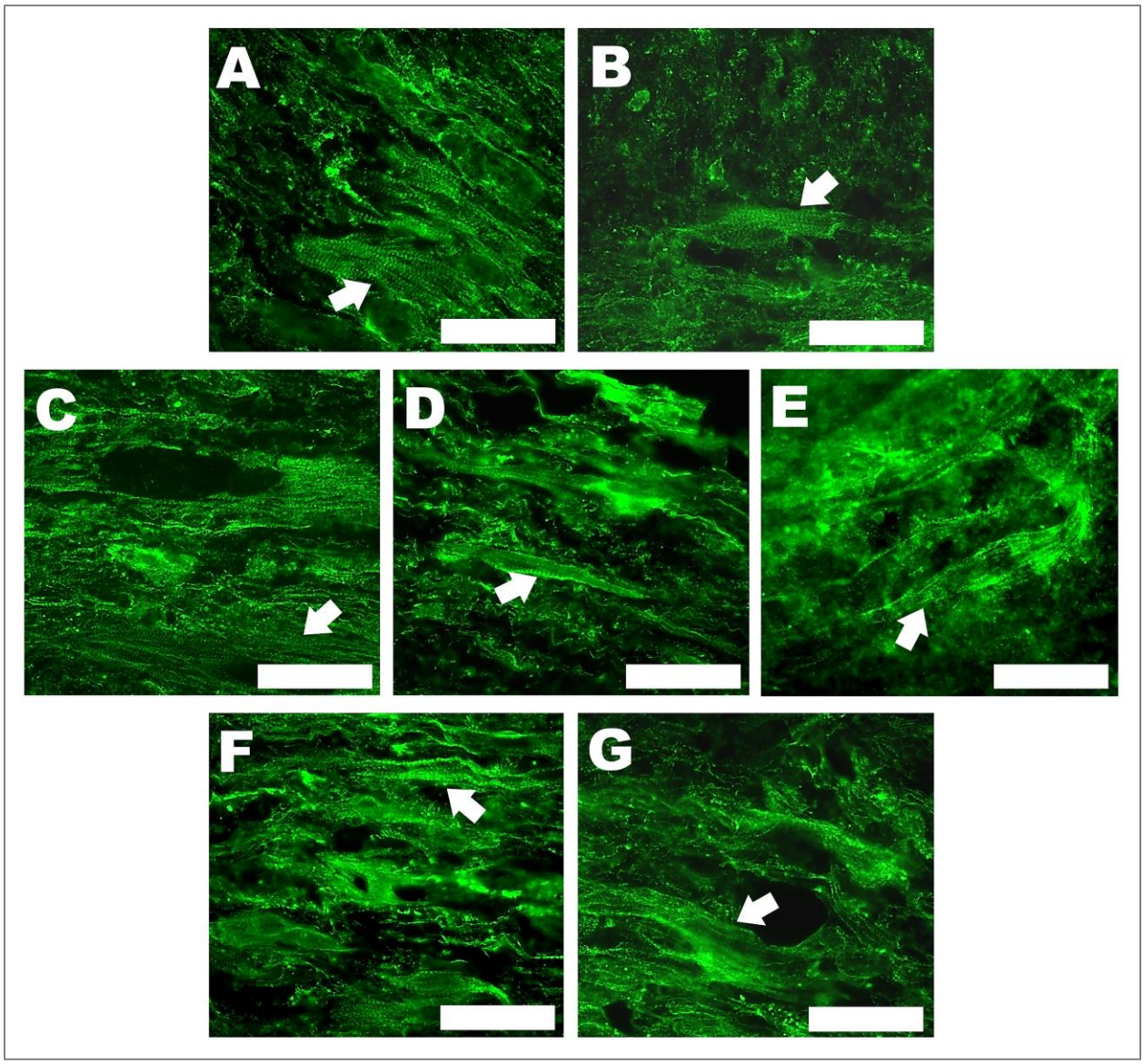


**Figure 15. Impact of Cell Seeding Density on SMU Structural Maturation.** SMU longitudinal sections underwent IHC staining to visualize sarcomeric structure (**α-actinin, green**). Scale bars = 50 µm. The images depicted are representative of SMUs fabricated with initial cell seeding densities of 1,000 cells/cm$^2$ (**A**), 2,500 cells/cm$^2$ (**B**), 5,000 cells/cm$^2$ (**C**), 10,000 cells/cm$^2$ (control, **D**), and 25,000 cells/cm$^2$ (**E**). SMUs formed from monolayers seeded at 1,000 cells/cm$^2$ and 10,000 cells/cm$^2$ and grown to confluence prior to being switched from MGM to MDM were also imaged (**F** and **G**, respectively). Aligned and striated sarcomeric structures were founded in each experimental group with examples indicated by white arrows.

normalized force provides a possible explanation for the decrease in contractile function. Higher cell-seeding densities result in excessive non-myogenic cell populations and extracellular matrix deposition that impedes myotube hypertrophy in monolayers and SMU 3D fusion after delamination. Overall, the outcomes of this study suggest that, when transitioning engineered skeletal muscle technologies from a rat or ovine cell-source to a human cell-source, the initial cell-seeding density should be decreased for optimal results.

Investigations into the low initial cell-seeding densities of 1,000 cells/cm$^2$, 2,500 cells/cm$^2$, and 5,000 cells/cm$^2$ yielded exciting results. Despite the significant decrease in initial cell total compared to the 10,000 cells/cm$^2$ control, cells in all lower density experimental groups were able to proliferate, form extensive myotube networks, and secrete extracellular matrix leading to robust monolayers. Moreover, these monolayers were capable of forming 3D structures that could withstand prolonged periods of *in vitro* culture and mechanical force testing. Furthermore, as indicated by MF20 and α-actinin staining, lower cell-seeding densities did not negatively impact SMU muscle-like content or sarcomeric maturity. Historical rat and ovine SMU data has indicated that, at minimum, SMUs grown in 60 mm plates must produce a maximum tetanic force of 100 uN *in vitro* to promote successful skeletal muscle regeneration and restoration of skeletal muscle function upon *in vivo* implantation in animal VML models [69]. Importantly, all tested SMUs with initial seeding densities from 1,000 cells/cm$^2$ to 10,000 cells/cm$^2$ surpassed this parameter with maximum tetanic forces ranging from 151 µN to 513 µN. These promising results indicate that, even when fabricated from initial cell-seeding densities 1/10$^{th}$ the amount standardly used, human cell-sourced SMUs display *in vitro* structure and

contractile function that suggest huge potential for success upon implantation as skeletal muscle grafts for VML treatment.

Time-to-confluency studies provided an opportunity to investigate the impact of monolayer confluency prior to stimulated differentiation with MDM on overall SMU structure and contractile function. Interestingly, it appeared that monolayer overconfluence and underconfluence had different impacts on SMU outcome. The changes in the structure and function of 1,000 cells/cm$^2$ confluent SMUs when compared to 1,000 cells/cm$^2$ underconfluent SMUs did not show the same trends as between the 10,000 cells/cm$^2$ confluent experimental group SMUs and the 10,000 cells/cm$^2$ overconfluent experimental group. In the case of plates initially seeded at 1,000 cells/cm$^2$, it took 9 days of growth in MGM before plates achieved 90-100% confluence. As a result, cells were in MGM for two days longer compared to the standard SMU fabrication protocol. This extra culture time in MGM provided ample opportunity for myogenic cells to proliferate, significantly increasing the amount of myosin heavy chain content seen in SMUs, as well as the total SMU cross-sectional area. This increase in myosin heavy chain content could be the reason the 1,000 cells/cm$^2$ confluent experimental group had SMUs with maximum tetanic forces significantly greater than SMUs in the 1,000 cells/cm$^2$ underconfluent experimental group. Cell culture plates initially seeded at 10,000 cells/cm$^2$ reached 90-100% confluence at 6 days, with plates following the standard SMU fabrication protocol being overconfluent on the initial MDM feeding day (day 7). Even with only a one day difference in MGM cell culture time, the impact of over-confluence was apparent with SMUs in the 10,000 cells/cm$^2$ overconfluent experimental group having greater ECM deposition compared to SMUs in the 10,000 cells/cm$^2$ confluent

experimental group. The results suggest that timing the switch from MGM to MDM during monolayer culture is critical in optimizing SMU structure and contractile function. If monolayers are switched before they reach at least 90% confluency, myogenic cells miss critical time to proliferate. If monolayers are switched after they surpass 100% confluency, SMUs can have excessive ECM deposition that could potentially obstruct contractile function.

It is interesting to note that in both the cell-seeding studies and the time-to-confluency studies, there was no significant difference in specific force between experimental groups, Additionally, IHC analysis indicated that most experimental groups had similar MF20-positive cross-sectional areas. When considered collectively, these results suggest that the differences in average maximum tetanic forces between experimental groups are not only influenced by the MF20-positive cross-sectional area, but additional factors. Such factors include the maturity and sarcomeric alignment of a SMU's skeletal muscle content, as well as the cohesiveness and organization of a SMU's extracellular matrix components.

While there is no significant difference in specific force, there are significant differences in normalized force. In the cell-seeding density study, SMUs fabricated from a high cell-seeding density (25,000 cells/$cm^2$) has lower normalized forces compared to 1,000 cells/$cm^2$, 2,500 cells/$cm^2$ and 5,000 cells/$cm^2$ experimental group SMUs. Higher cell-seeding densities result in excessive extracellular matrix deposition, which increase the total SMU CSA without improving SMU contractile function. Interestingly, confluency studies indicate that underconfluency and overconfluency in monolayers can increase SMU normalized force, while having minimal or negative impact on SMU maximum

tetanic force or specific force. These results support the theory that confluency impacts extracellular matrix deposition and organization in monolayers and SMUs.

In terms of SMU fabrication, results suggest that initial cell-seeding density can be decreased to as low as 1,000 cells/cm$^2$ without negatively impacting SMU muscle-like structure and function if monolayers are 90-100% confluent prior to being switched to MDM. Even if monolayers are given time to reach confluency, this decrease in initial cell-seeding density only increases the cell culture period by two days compared to standard SMU protocol. A decrease in initial cell seeding density from 10,000 cells/cm$^2$ to 1,000 cells/cm$^2$ with minimal change in overall SMU fabrication time has serious implications for the development of clinically-relevant engineered skeletal muscle tissue. In previous work, our laboratory used sheep cells at a seeding density of 10,000 cells/cm$^2$ to create SMUs 14 cm long and 2 cm in diameter, a size close to the parameters needed to fill a 30% VML in a human tibialis anterior limb muscle [69]. For this sheep study, 20 million cells were required to generate a single implantable construct. From the results of this study, we now know we could create a human cell-sourced scaled-up SMU of the same size and diameter with only 2 million cells. With current human skeletal muscle precursor cell isolation techniques, 2 million cells could be harvested from a standard 200 mg (a sample size around 20mm$^3$) skeletal muscle biopsy during a minimally-invasive procedure and a scaled-up SMU could be fabricated without the risk of morbidity at the biopsy donor site [101, 102].

Using our SMU model, we demonstrated that the initial starting cell-seeding density for human scaffold-free engineered skeletal muscle fabrication can be significantly lower than the cell-seeding density used for rat and ovine models without

negatively impacting engineered skeletal muscle growth, maturation, or contractile function. These results are a key advancement regarding the fabrication of clinically-relevant engineered skeletal muscle from autologous muscle biopsies and the translation of skeletal muscle tissue engineering technologies into medical therapies.

# Chapter 4 Impact of Passaging of Primary Skeletal Muscle Cell Isolates on the Engineering of Skeletal Muscle

## 4.1 Introduction

A potential outcome of extreme skeletal muscle trauma is volumetric muscle loss (VML) [46, 57, 67]. VML is a clinical condition resulting from skeletal muscle tissue loss exceeding native skeletal muscle's self-repair mechanisms [46, 57, 67]. Such a loss permanently impairs skeletal muscle structure and function, and necessitates medical intervention [46]. The current standard-of-care for VML treatment relies on the transplantation of autogenic or allogenic skeletal muscle grafts via muscle flap or graft transposition [46]. Such surgical procedures have several limitations including potential for donor site morbidity from the use of autogenic skeletal muscle grafts, risk of disease transmission or tissue rejection from the use of allogenic muscle sources, and donor muscle to VML site differences in muscle composition and graft source availability for both types of grafts [56, 57]. Furthermore, such procedures have shown only limited success in stimulating muscle regeneration or restoring native contractile function [47].

Emerging musculoskeletal tissue engineering technologies have the potential to address the shortcomings of current surgical techniques by growing biocompatible and adaptable muscle tissue *in vitro* that can promote appropriate graft integration and muscle regeneration *in vivo* [15, 40, 46]. These tissue engineering methodologies all share a fundamental approach of creating tissues using environments that activate *in vitro* myogenesis via some combination of scaffolding, mechanical forces, or chemical cues

[15]. In a promising advancement towards the development of a tissue engineered graft for the treatment of VML in humans, it has been found that scaffold-free approaches for fabricating engineered skeletal muscle grafts are capable of being scaled-up to sizes relevant for a 30% VML limb injury.[8] Such grafts have been shown to effectively restore muscle structure and function in ovine VML models [69].

To alleviate concerns of donor site morbidity, tissue rejection, and muscle composition mismatch seen in current treatment, human engineered skeletal muscle grafts should ideally be fabricated from small autogenous muscle biopsies [46, 56, 57]. Skeletal muscle stem cells, known as satellite cells, can be isolated from muscle biopsies and used in skeletal muscle tissue engineering due to their critical role in native skeletal muscle wound healing and regeneration [89-93]. Enzymatic digestion is used on muscle biopsy specimens to release cells, resulting in a suspension of primarily myogenic cells and connective tissue fibroblasts [70, 78, 98]. Simulating myogenesis in native skeletal muscle, satellite cells can be induced to proliferate and differentiate down a myogenic lineage [15]. Satellite cells differentiate into myoblasts, which will fuse to form myotubes and mature into myofibers [15]. However, satellite cells only make up around 5% of nuclei within native adult human skeletal muscle [96]. Due to their essential role in muscle tissue engineering methodologies, the low incidence of satellite cells in native adult skeletal muscle is a significant obstacle impeding the translation of skeletal muscle tissue engineering technologies into clinical therapies [79, 94, 95]. Increasing the size of the skeletal muscle biopsy harvested in order to increase the number of satellite cells increases the risk of additional trauma to the VML patient. Thus, methodologies that can

increase the number of cells harvested or amplify the cells isolated during harvest would be a significant advancement to skeletal muscle tissue engineering.

Recent research suggests that the number of human satellite cells required for successful fabrication of human-sized skeletal muscle tissue is significantly lower than previously believed, partially addressing this obstacle [85] To successfully create a human autologous engineered skeletal muscle graft for a clinical setting, methodologies that further increase the efficacy of isolated satellite cells need to be investigated. In the field of tissue engineering, passaging of myoblasts is a technique that has been used for engineered skeletal muscle systems in rodent models that require large populations of cells for fabrication and scale-up [37, 76, 79]. However, satellite cells are known to have a low expansion potential *in vitro* [94, 97]. Studies culturing rat skeletal muscle isolates *in vitro* indicate that myogenic potential decreases 35% by the third passage [103]. The impact of passaging human primary skeletal muscle isolates on tissue engineered constructs intended for use as grafts for VML remains to be elucidated.

Our laboratory has developed a method of fabricating scaffold-free tissue engineered skeletal muscle units (SMUs) from human skeletal muscle biopsies [80, 85]. This fabrication methodology provides us the opportunity to investigate the impact of cell passaging on skeletal muscle cell isolate monolayers and on engineered skeletal muscle tissue growth and maturation without the potential confounding effects of scaffolded tissue engineering systems. The purpose of this study was to evaluate the impact of cell passaging on human primary skeletal muscle cells isolated from biopsies on the ability to engineered skeletal muscle tissue. We hypothesized that such a passaging study would determine a passage number that optimizes the number of cells that can be gained from

a single human skeletal muscle biopsy while maintaining the capability to grow a SMU with sufficient muscle structure and contractile function for use in repairing a VML site.

## 4.2 Methodology

### *4.2.1 Experimental Design*

For this study, passaging is defined as “the transfer of an inoculum of cells from an existing culture to fresh growth media in another vessel”, the standard used by the American Type Culture Collection [104] To investigate the impact of cell passage number on the capacity to engineered skeletal muscle, human skeletal muscle cells were freshly isolated cells (P0) or passaged once (P1), twice (P2), or thrice (P3) before being used to fabricate SMUs. As described in **Figure 16**, freshly isolated cells were seeded on tissue culture plates and allowed to proliferate. Once cell cultures reached >60% confluence, a subset of plates underwent passaging. Passaged cells were then seeded on tissue culture plates, setting up the P1 experimental group. The remaining skeletal muscle cells were cultured to 100% confluent monolayers and differentiated to form a three-dimensional (3D) SMUs. Cell cultures in the P1 experimental group were also either passaged or used to form SMUs. This process was repeated, and SMUs were created from each passage through P3.

*Cell Isolation*

The University of Michigan Medical School Institutional Review Board approved all experimental protocols involving the use of human skeletal muscle biopsies (HUM00151617). Following previously established procedures, skeletal muscle cells were isolated from a healthy gracilis muscle biopsy from a 41-year-old female patient [67,

69, 70, 80, 85]. Briefly, the muscle biopsy was finely minced in aseptic conditions before being incubated in dissociation solution consisting of 2.3mg/mL dispase (Cat. No. 17105-041; Thermo Fisher) and 0.3mg/mL collagenase type IV (Cat. No. 17104-019; Thermo Fisher). After two hours of enzymatic dissociation, the resulting cell solution was filtered through 100 µm (Cat. No. 22-363-549; Fisher Scientific) and 40 µm (Cat. No. 22-363-547; Fisher Scientific) mesh filters prior to being centrifuged. Following centrifugation, the resulting cell pellet was resuspended in Muscle Growth Media (MGM) and representative samples of cell solution were taken to determine the total number of cells. Samples of cell isolates were stained with acridine orange and propidium iodide (Cat. No. LGBD10012; Vita Scientific) before undergoing automated fluorescence counting via the Luna Automated Cell Counter (Cat. No. L1001; Logos Biosystems). The live cell count was

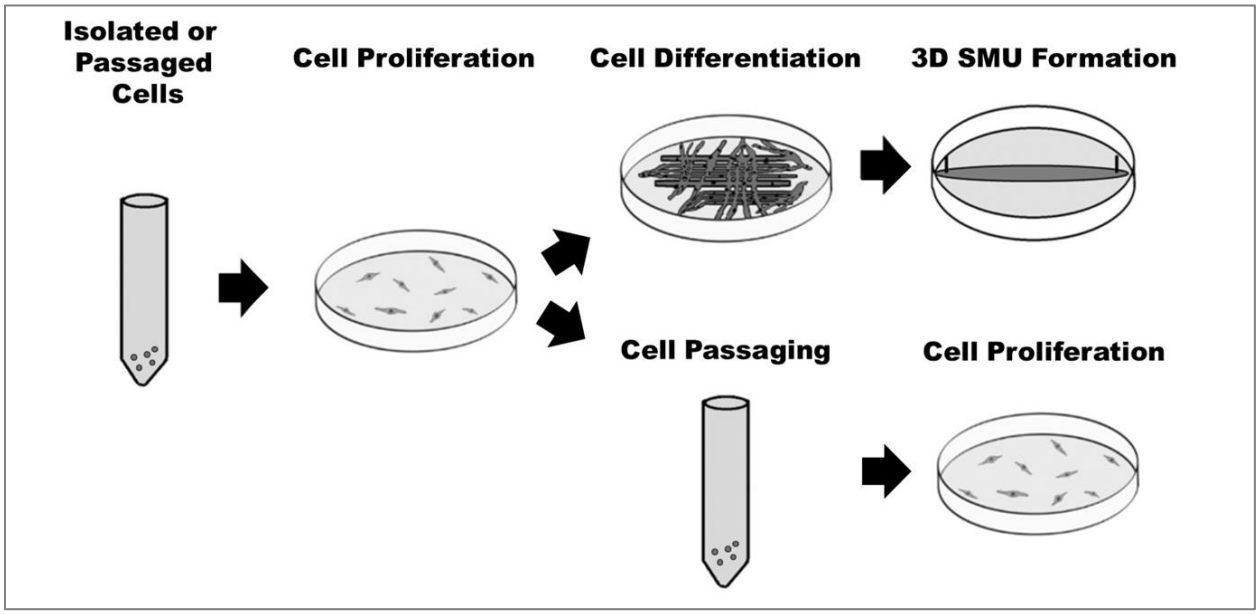


**Figure 16. Experimental Design.** To determine the impact of cell passaging on the engineering of skeletal muscle tissue, freshly isolated cells were seeded on tissue culture plates. After cell monolayers reached greater than 60% confluency, a subset of plates was passaged. The remaining plates underwent SMU fabrication (P0). This process was repeated until cells were passaged 3 times with SMUs being fabricated at each passage (P1, P2, and P3).

used to seed isolated cells in MGM onto tissue culture-treated polystyrene plates at a seeding density of 1,000 cells/cm$^2$.

MGM consisted of 60% F-12 Kaighn's Medium (Cat. No. 21127-022; Gibco), 24% DMEM, 15% fetal bovine serum (FBS; Cat. No. 10437-028; Gibco), and 1% ABAM, and was supplemented with 9.1 ng/mL human epidermal growth factor (hEGF; Cat. No. CC-4107; Lonza), 4.0 ng/mL dexamethasone (DEX; Cat. No. D8893; Sigma-Aldrich), and 2.4 ng/mL basic fibroblast growth factor (Cat. No. 100-18B; PeproTech). MDM consisted of 70% Medium 199 (Cat. No. 1150067; Gibco), 23% DMEM, 6% FBS, and 1% antibiotic/antimycotic (ABAM, Cat. No. 15240-062; Gibco) and was supplemented with 0.1% insulin/transferrin/selenium X (Cat. No. 51500056; Gibco), 14.5 ug/mL ascorbic acid 2-phosphate (Cat. No. A8960-5G; Sigma Life-Aldrich), 9.1 ng/mL hEGF and 4.0 ng/mL DEX.

### *4.2.2 SMU Fabrication*

To allow for cell attachment, tissue culture plates were left undisturbed for 3 days post-seeding. Afterwards, cell cultures were fed MGM every 2 days. At every cell feeding, monolayer confluence was monitored and recorded using a light microscope. Once monolayers reached greater than 90% confluence and myotube network had begun forming, the media was switched to Muscle Differentiation Media (MDM). Cultures were fed fresh MDM every two days for the duration of SMU fabrication.

After 7 days in MDM, monolayers were imaged under the light microscope to investigate monolayer differentiation. Afterwards, cell scrapers were used to manually delaminate monolayers from the polystyrene plates. Each monolayer was transferred and pinned to a polystyrene plate coated with soft silicone elastomer (Sylgard 184; Cat. No.

24236-10, Electron Microscopy Sciences) by two stainless steel pins spaced 3cm apart. Over the next 3 days, monolayers fused down into 3D cylindrical SMUs. 72 hours after fusion, SMUs underwent force testing and immunohistochemical analysis (IHC).

### *4.2.3 Cell Passaging*

As summarized in **Figure 16**, once cell cultures achieved greater than 60% confluence, a subset of plates underwent cell passaging. To enzymatically remove adherent skeletal muscle cells, each selected plate was treated with 0.25% trypsin-ethylenediaminetetraacetic acid solution (Trypsin-EDTA, Cat. No. 25200056, Gibco). During treatment, plates were inspected under light microscope to verify that all cells detached. Once all cells had detached, the Trypsin-EDTA was neutralized with MGM, and the resulting solution was harvested and centrifuged. After centrifugation, the supernatant was aspirated, and the cell pellet was resuspended in MGM.

For each passaging plate, representative samples of cell solution were stained with acridine orange and propidium iodide to determine the total number of cells per plate and the cell population doubling time. Cell solutions were then combined, and another cell count was conducted. Using this combined solution, tissue culture-treated polystyrene plates were seeded at a density of 1,000 cells/cm$^2$, beginning the next experimental group's cell culture. Additionally, representative samples of cell solution underwent immunocytochemical staining.

### *4.2.4 Cell Population Doubling Time: Proliferative Potential*

To analyze the impact of passage number on the proliferative potential of skeletal muscle isolate cells, the cell population doubling time was calculated for each passage cell culture. Doubling time was calculated using the standard growth rate equation:

$$T_d = t(ln(2))(ln\frac{D_f}{D_0})$$

with $T_d$ representing doubling time, *t* representing the elapsed time from seeding a plate to passaging a monolayer, *ln* representing the natural logarithm of a number, $D_0$ representing the initial number of live cells at seeding, and $D_f$ representing the total number of cells at passaging [105]. For this calculation, we assumed a constant relative growth rate from cell seeding to monolayer passaging.

### *4.2.5 Immunocytochemistry: Myogenic Characterization of Cell Populations*

To understand the role of passaging on the myogenicity of a skeletal muscle cell population, we characterized and compared freshly isolated skeletal muscle cells and cells from each passage tested via immunocytochemistry using techniques previously described [70]. Briefly, at each cell isolation or passaging, samples of the final cell solution were taken and diluted to a concentration of 5 x $10^5$ cells/mL (Pax7) or 1.5 x $10^5$ cells/mL (MyoD and Vimentin). Using a volume of 300 µL, aliquots were adhered to a glass microscope slide via the cytospin technique and fixed in 4% paraformaldehyde [70]. Cytospin slides were stained with 4',6-diamidino-2-phenylindole (DAPI; Cat. No. P36935, Thermo Fisher) to determine total cell nuclei with Pax7 (mouse monoclonal antibody; 1:100 dilution; Cat. No. Pax7c, DHSB) and MyoD (rabbit monoclonal antibody; 1:250 dilution; Cat. No. ab133627, Abcam) to identify myogenic cells, and with vimentin (rabbit

monoclonal antibody; 1:250 dilution; Cat. No. EPR3776, Abcam). To stain Pax7, both antigen retrieval and tyramide signal amplification techniques were used.[16] Tyramide signal amplification was provided through a tyramide SuperBoost kit (Cat. No. CB40913, Thermo Fisher).

All cytospin samples were imaged using a Zeiss Apotome Microscope. Images were analyzed via the Fiji image processing package to determine both the total number of myogenic cells and fibroblastic cells relative to the total number of cells in each cytospin. To enumerate the total number of cells in each cytospin, Fiji's Find Maxima and Binary Options functions were used to create an outline around each DAPI-stained nucleus in the cytospin, which were counted via Fiji's Analyze Particles function. To determine the total number of Pax7, MyoD, and Vimentin-positive cells, image of each stain were measured for Max Gray Value (MGV). Using Microsoft Office's Excel, the threshold of the MGV was adjusted for each stain to determine the positive cell count.

*Cell Monolayer Analysis: Myotube Size and Density*

Myotube size and density were evaluated to investigate the impact of cell passaging on monolayer differentiation and myotube maturation. Monolayers cultured for SMU fabrication were imaged using light microscopy immediately prior to manual delamination. Three to five representative images were taken for each monolayer. Images were analyzed via the ImageJ/FIJI software package to determine each monolayer's average myotube diameter and myotube network density. Myotube diameter was measured using ImageJ's Line function. To determine myotube network density, the number of myotubes in a monolayer's images were quantified using ImageJ's Multipoint function and normalized by the total image area.

### *4.2.6 Force Testing: SMU Contractile Function*

Three days after manual delamination and pinning, SMUs underwent force testing to measure maximum tetanic isometric force produce as an assessment of contractile function. The force testing procedure has been described previously [80, 85]. Briefly, the SMU was attached to an optical force transducer at one end and was anchored to the plate by a minutien pin at the opposite end. Over the course of force testing, SMUs were maintained at 37°C in MDM. To stimulate a uniform electric field, two platinum wire electrodes were submerged and placed along the length of the SMU. To elicit tetanic contractions, SMUs were stimulated via a 600ms square wave trains of 2.5 ms pulses at frequencies of 60 Hz, 90 Hz, 100 Hz, 120 Hz, and 130 Hz, and currents of 700 mA, 800 mA, 900mA, and 1000 mA. Force frequency curves were recorded and analyzed using LabVIEW 2012 (National Instruments).

### *4.2.7 Immunohistochemical Analysis: SMU Structure*

SMUs underwent immunohistochemical staining (IHC) to qualitatively and quantitatively assess the impact of cell passaging on engineered skeletal muscle structure. Immediately after force-testing, SMU constructs were coated in Tissue Freezing Medium (Cat. No. 15-183-36; Fisher Scientific), flash-frozen in liquid nitrogen-chilled isopentane, and stored at -80°C until sectioning. Prior to IHC, 10 micrometer-thick cross-sectional and 5 micrometer-thick longitudinal SMU cryosections were fixed in -20°C methanol.

To measure SMU total cross-sectional area (CSA), skeletal muscle content (myosin heavy chain), and extracellular matrix (laminin), cross-sectional cryosections of

the SMU mid-belly were stained for DAPI and antibodies for myosin heavy chain (MF20; mouse monoclonal antibody 1:200 dilution; Cat. No. MF 20-c; Developmental Studies Hybridoma Bank) and laminin (rabbit polyclonal antibody 1:200 dilution; Cat. No. 7463; Abcam). Stained sections were imaged using a Zeiss Apotome microscope, and total CSA, MF20-positive CSA, and laminin-positive CSA of each stained SMU section was quantified using ImageJ's Analyze Particle Function. To analyze the force production capabilities of the SMU's skeletal muscle content, the maximum tetanic isometric force measurement for each IHC-stained SMU was normalized by the SMU's MF20-positive CSA as a measure of specific force.

### *4.2.8 Statistical Analysis*

For all figures, boxes and bars indicate mean ± standard error of the mean. Using GraphPad Prism Software, statistical difference between experimental groups were assessed through the comparison of means via one-way analysis of variance (ANOVA) with Tukey post hoc comparisons. Differences were considered significant at $p < 0.05$.

## 4.3 Results

### *4.3.1 Effect of passage number on cell proliferation rate and myogenicity.*

The average cell population doubling time was calculated for each passaged cell culture to investigate how cell passaging effected the proliferative potential of skeletal muscle isolate cells (**Fig. 17**). Results indicated a statistically significant difference between experimental groups ($p<0.0001$). With an average doubling time of 1.41±0.03 days, cells being passaged from P0→P1 had a significantly slower proliferation rate than cells being passagings from P1→P2 (0.84±0.01 days), and from P2→P3 (0.88±0.04

days) ($p<0.0001$ for all). Interestingly, the P3 cell population had a significantly faster proliferation rate compared to P1 ($p=0.01$) and P2 ($p<0.0001$) cells. Cell proliferation rates for skeletal muscle isolate cell populations from the P1 and P2 experimental groups were not significantly different.

To further investigate the skeletal muscle cell isolate population, aliquots from both freshly isolated and passaged skeletal muscle cell isolates were monitored using immunocytochemistry to determine the impact of passage number on the percentage of

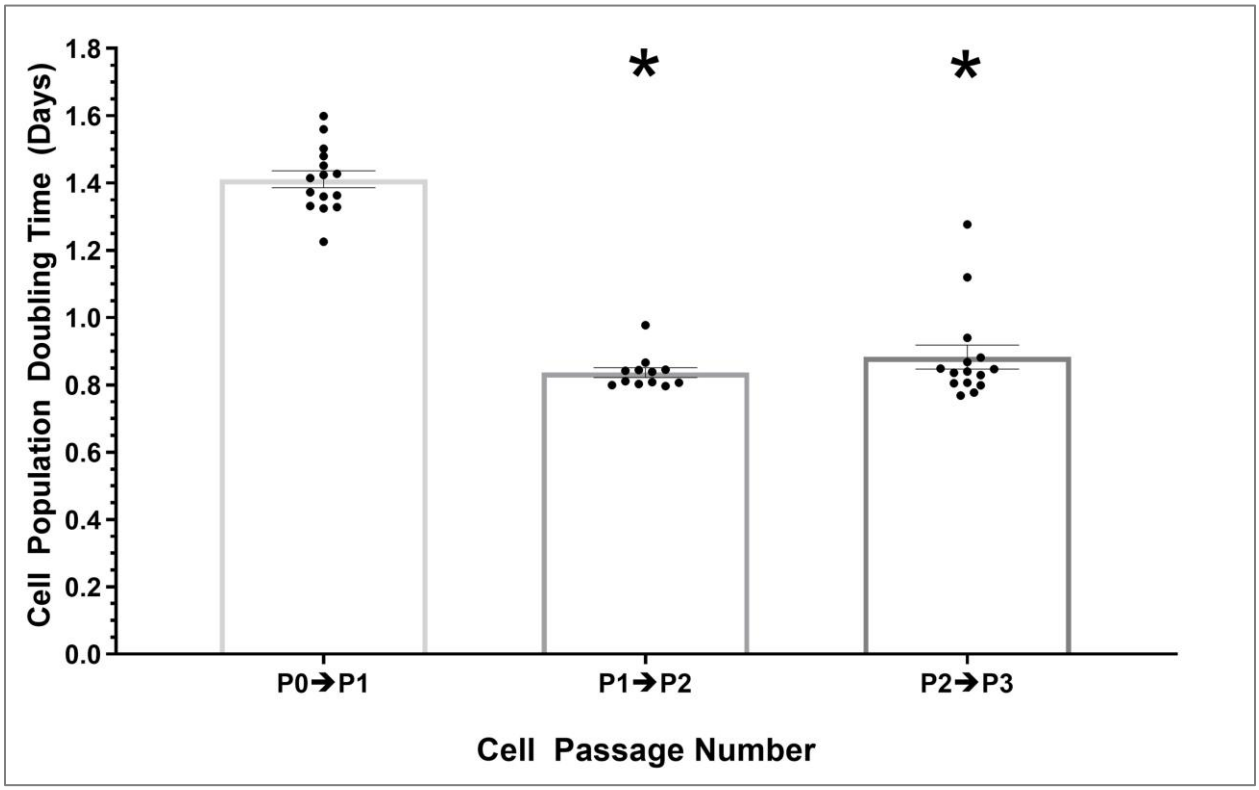


**Figure 17. Effects of Cell Passage Number on Cell Population Doubling Time.** At each cell passage, the total number of cells harvested from each tissue culture plate was determined via an acridine orange and propidium iodide stain. These values, the number of cells seeded on each plate, the number of cells harvested from each plate and the time between seeding and passaging were used to calculate the rate of cell-doubling. Boxes and bars indicate mean ± standard error of the mean. * symbol above bars indicates statistically significant differences: from cells being passaged from P0→P1. As the cell passage number increased, there was a statistically significant decline in population doubling time in cell populations ($p<0.0001$). P0→P1 cell populations had an average population doubling time of 1.4±0.03 days, significantly greater than P1 →P2, and P2→P3 cell populations which had doubling times of 0.84±0.01 and 0.88±0.04 days, respectively ($p<0.0001$ for both).

myogenic cells and fibroblastic cells in the total cell population (**Fig. 18**).One-way ANOVAs indicated that passaging had a significant impact on the average Pax7, MyoD, and Vimentin-positive cell population ($p<0.0001$ for all antibodies). The average percentage of Pax7-positive cells for P0, P1, P2, and P3 cell cultures was 17.4±2.7%, 9.7±0.7%, 1.0±0.2%, and 1.4±0.4%, respectively. A post-hoc multiple comparisons test indicated that P0 cell cultures had significantly higher percentages of Pax-7 positive cells compared to all other experimental groups ($p<0.0001$ for all comparisons).There was also a significant decrease in Pax7 positive cells after the first passage, with P1 cells having

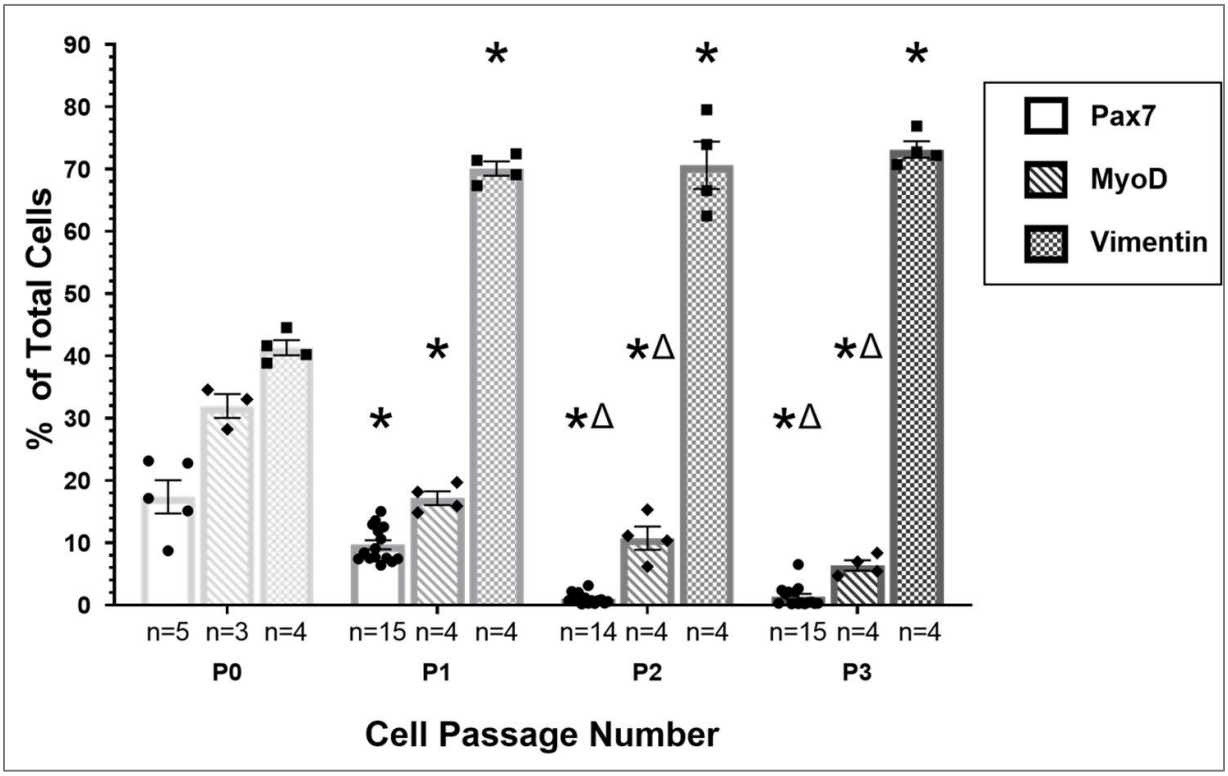


**Figure 18. Characterization of freshly isolated and passaged cell populations.** Cell samples at each passage underwent immunocytochemical assays to characterize the percentage of cells that expressed Pax7, MyoD, and Vimentin. Boxes and bars indicate mean ± standard error of the mean. Symbols above graphs indicate statistically significant differences between experimental groups: * from P0 (Control), and Δ from P1. One-way ANOVAs indicated a significant difference in the percent of myogenic and fibroblastic cells between all experimental groups ($p<0.0001$ for all tested antibodies). Post-hoc analyses indicated P0 cell populations had significantly greater percentages of Pax7-positive and MyoD-positive cells compared to P1, P2, and P3 cell cultures ($p\leq0.0001$ for all). Additionally, P1 cell populations had lower vimentin-positive percentages compared to P1, P2, and P3 cells ($p<0.0001$ for all). P1 cell populations have greater Pax7-positive percentages than P2 and P3 cell cultures ($p<0.0001$ for both) as well as greater MyoD-positive percentages ($p=0.03$ for P2, and $p=0.001$ for P3).

a significantly higher average Pax7 positive cell population comparedP2, and P3 cells cultures ($p<0.0001$ for both). There was no difference in the percentages of Pax7 positive cells between the P2, and P3 experimental groups.

A post-hoc multiple comparisons tested indicated that P0 cell cultures also had a mean MyoD-positive percentage of 32.0±1.9%, significantly greater than experimental groups P1 (mean: 17.2±1.1%,$p=0.0001$), P2 (mean: 10.8±1.1%, $p<0.0001$) and P3 (mean: 6.4±0.8%, $p<0.0001$). P1 cell populations also had significantly greater MyoD-positive cells compared to P2 ($p=0.03$) and P3 ($p=0.001$) cell cultures. P2 and P3 cell cultures were not significantly different from each other.

The P0 cell population had an average Vimentin-positive percentage of 41.3±1.2%, a percentage significantly lower than experimental groups P1 (mean: 70.1±1.1, $p<0.0001$), P2 (mean: 70.6±3.8, $p<0.0001$) and P3 (mean:73.2±1.3, $p<0.0001$). Regarding Vimentin-positive percentage, P1, P2, and P3 cell populations were not significantly different from each other.

### *4.3.2 Impact of cell passaging on muscle cell differentiation*

Analysis of light microscopy images of the monolayers after 7 days in MDM and immediately prior to delamination revealed that cell passaging had a statistically significant impact on myotube differentiation. A one-way ANOVA indicated significant difference in myotube diameters between the experimental groups ($p<0.0001$, **Fig. 19A**). Average myotube diameters were 15.3±0.2 µm, 16.0±0.3 µm, 14.3±0.2 µm, and 13.5±0.2 µm for P0, P1, P2, and P3 monolayers, respectively. According to a post-hoc multiple comparisons test, P1 monolayers were found to have significantly larger myotubes compared to P2 ($p=0.0006$) and P3 ($p<0.0001$) monolayers. Additionally, P0 myotubes were significantly larger than P3 myotubes ($p=0.0001$). Monolayers also underwent an

analysis of myotube density (myotube/mm$^2$) with results indicating no significant differences between experimental groups (**Fig. 19B**).

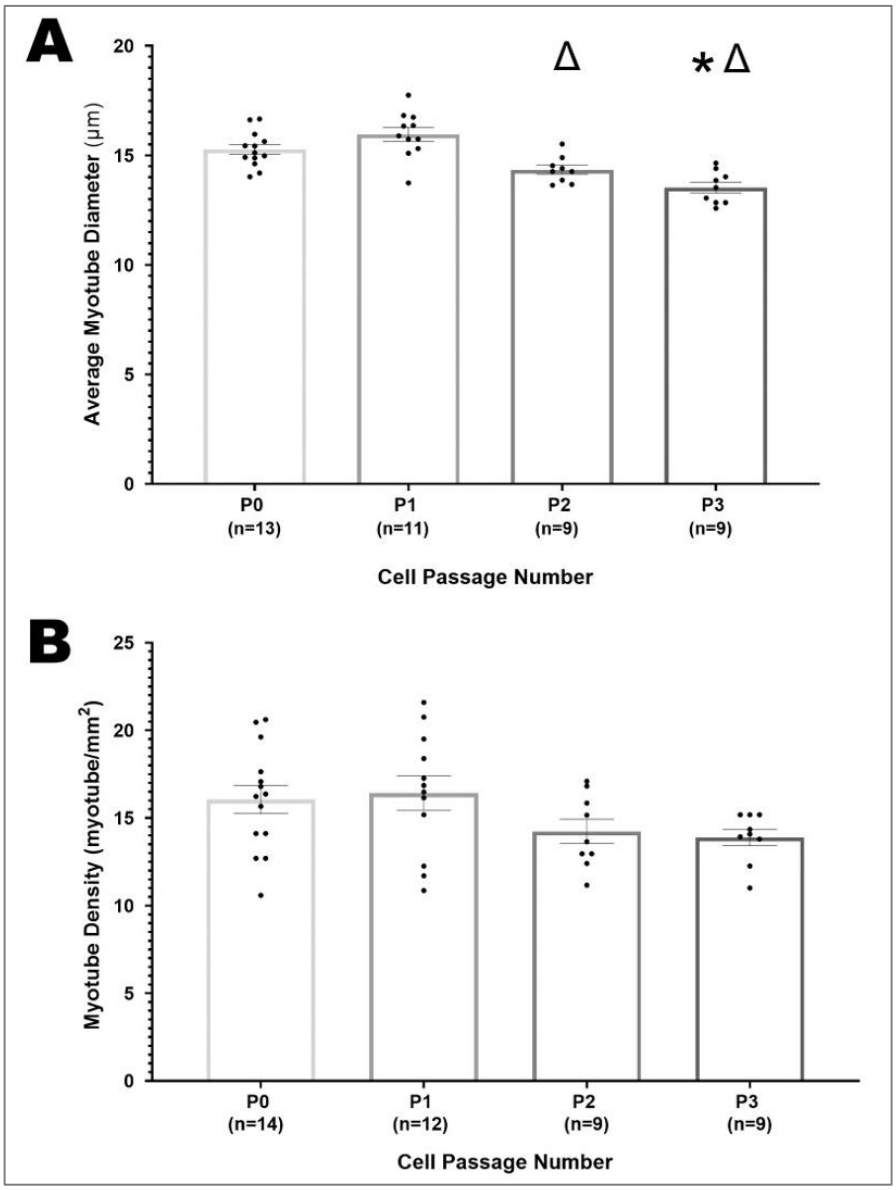


**Figure 19. Impact of cell passaging number on monolayer myotube size (A) and density (B).** Boxes and bars indicate mean ± standard error of the mean. Symbols above graphs indicate statistically significant differences: * from P0 and Δ from P1. Post-hoc comparison testing performed using Tukey's post-test analysis following one-way ANOVA indicated a significant difference in myotube diameters between P0 (control) and P3 experimental groups (p=.0001). The P1 experimental group had significantly higher myotube diameters compared to the P2 (p=.0006) and P3 (<.0001) experimental groups. No significant difference in myotube density between experimental groups was observed.

### *4.3.3 The significance of cell passage number on SMU contractile function*

SMUs fabricated from cells harvested at each passage underwent tetanic force production testing to assess contractile function (**Fig. 20A**). A one-way ANOVA indicated significant differences between experiment groups ($p<0.0001$). With an average maximum isometric tetanic force of 68.7±3.3 μN, P1 SMUs had significantly greater contractile force than P0 (mean of 50.0±2.3 μN) and P3 (mean of 39.4±2.2 μN) experimental groups ($p<0.0001$ for both). Maximum isometric tetanic forces were not significantly different between P1 and P2 SMUs, nor between P0 and P2 SMUs. Additionally, P3 SMUs averaged a maximum isometric tetanic force of 39.8±2.2 μN with force values significantly lower than both P0 SMUs ($p=0.0497$) and P2 SMUs ($p<0.0001$). These results suggest a parabolic pattern with SMUs reaching maximum force production capabilities at P1 and decreasing after subsequent passages.

SMU maximum tetanic isometric force measurements were normalized by MF20-positive CSA to assess SMU specific force (**Fig. 20B**). SMU specific forces were significantly different between experimental groups ($p=0.0002$) with average specific forces of 0.051±0.007 $N/cm^2$, 0.072±0.011 $N/cm^2$, 0.123±0.011 $N/cm^2$, and 0.081±0.008 $N/cm^2$ for P0, P1, P2, and P3 SMUs, respectively. Specifically, P2 SMUs had significantly larger specific forces compared to all other experimental groups ($p=0.0001$ for P0, $p=0.005$ for P1, and $p=0.02$ for P3). There were no significant differences between other experimental groups.

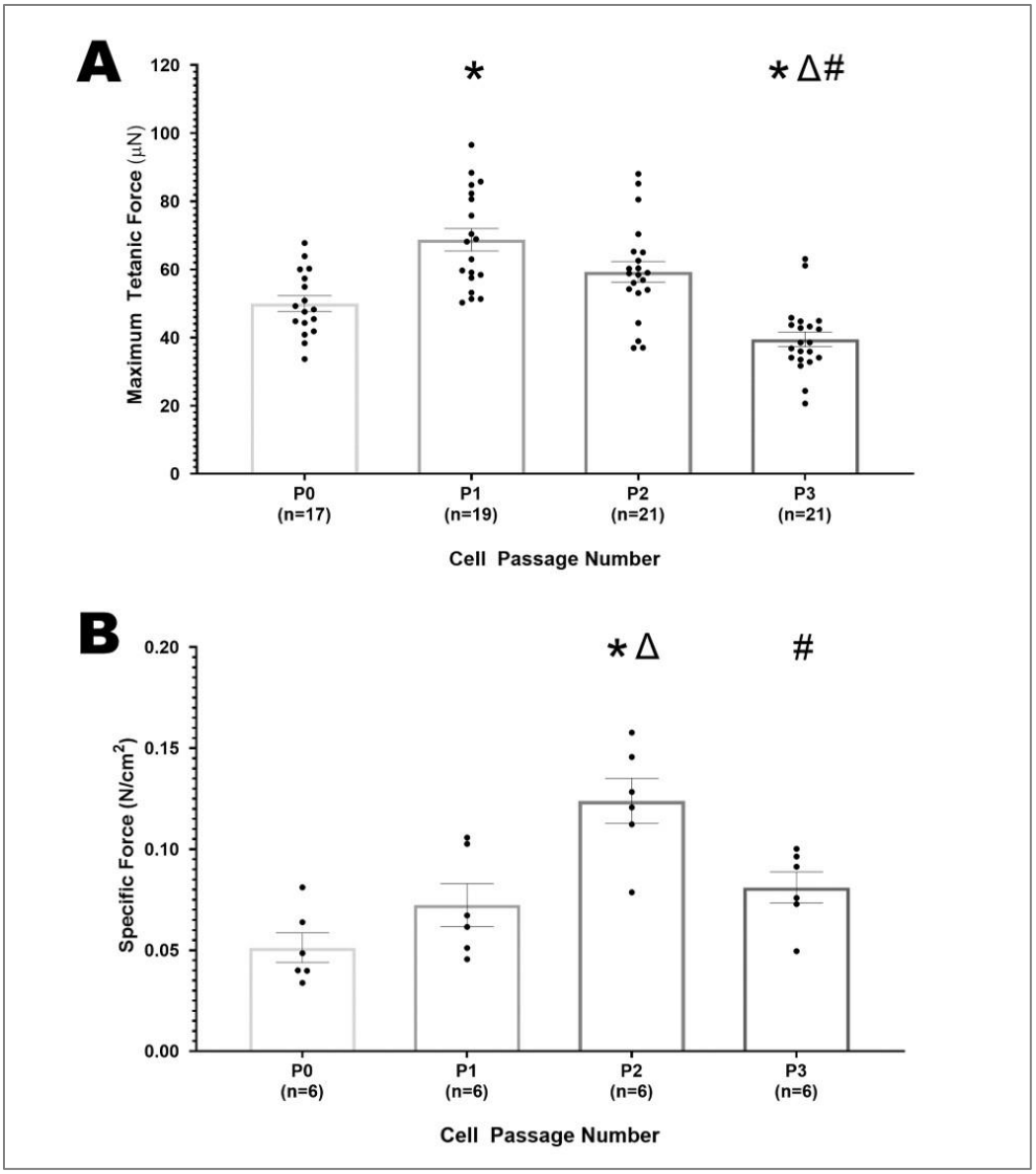


**Figure 20. Impact of cell passaging number on SMU maximum tetanic force production (A) and specific force (B).** Boxes and bars indicate mean ± standard error of the mean. Symbols above graphs indicate statistically significant differences: * from P0 (Control), Δ from P1, and # from P2. Cell passage number had a statistically significant impact on both SMU maximum isometric force production ($p<0.001$) and SMU specific force ($p=0.002$) . Compared to P0 Control SMUs, SMUs fabricated from P1 cells resulted in a significant 38% increase in maximum tetanic force production ($p<0.0001$). SMUs fabricated from P3 cells showed significant decreases in maximum isometric tetanic forces compared to all other experimental groups ($p=0.0497$ for P0, $p<0.0001$ for P1 and P2). SMUs fabricated from P2 cells had significantly greater specific forces compared to all other experimental groups ($p=0.0001$ for P0, $p=0.005$ for P1, and $p=0.02$ for P2).

### *4.3.4 Changes in SMU structure due to cell passaging*

IHC analysis of SMU cross-sections was conducted to investigate the impact of cell passaging on SMU composition and CSA (**Fig. 21**). For all passage numbers, DAPI stains revealed cell viability throughout the entirety of the SMU cross-sections, indicating appropriate nutrient diffusion throughout the construct during SMU formation. Myosin heavy chain was present in all examined SMUs. The laminin stain showed abundant extracellular matrix deposition throughout all SMUs, critical for the structural integrity of the constructs. Additionally, DAPI, MF20, and laminin co-stains revealed that all examined SMUs had multinucleated myofibers surrounded by laminin sheaths, a structural organization physiologically similar to individual native muscle fibers surrounded by basal lamin*a*.

Analysis of the IHC cross-sectional images showed significant difference in total SMU CSA between experimental groups ($p<0.001$, **Fig. 22A**). With an average of $1.80 \times 10^6 \pm 0.08 \times 10^6$ $\mu m^2$, P0 SMUs had total CSAs significantly larger than SMUs in all other experimental groups ($p=0.01$ for P1, $p<0.0001$ for both P2 and P3). Additionally, with an average of $1.36 \times 10^6 \pm 0.14 \times 10^6$ $\mu m^2$, P1 SMUs had significantly greater total CSA compared to P2 ($p=0.01$) and P3 ($p=0.002$) SMUs. P2 SMUs averaged a total CSA of $0.92 \times 10^6 \pm 0.05 \times 10^6$ $\mu m^2$, and P3 SMUs averaged a total CSA of $0.82 \times 10^6 \pm 0.06 \times 10^6$ $\mu m^2$ with no significant differences between the two groups.

Focusing on myosin-heavy chain content, a one-way ANOVA indicated significant differences in MF20-positive CSA between experimental groups ($p=0.0004$, **Fig. 22B**). With an average MF20-positive CSA of $1.06 \times 10^5 \pm 0.14 \times 10^5$ $\mu m^2$, P0 SMUs had significantly greater myosin heavy chain compared to P2 SMUs and P3 SMUs ($p=0.004$

for both). In a similar trend, P1 SMUs (average= $1.0 \times 10^5 \pm 0.11 \times 10^5$ $\mu m^2$) also had significantly greater myosin heavy chain compared to P2 SMUs and P3 SMUs (p=0.008 for both). P0 and P1 groups were not statistically significant from each other. Both P2 SMUs and P3 SMUs had average MF20-positive CSAs of $5.11 \times 10^4 \pm 0.61 \times 10^4$ $\mu m^2$, and the groups were not statistically significant from each other.

Analysis of laminin-positive CSA showed that there were significant differences in the amount of extracellular matrix between experiment groups (p<0.0001, **Fig. 22C**). With an average laminin-positive CSA of $1.29 \times 10^6 \pm 0.07 \times 10^6$ $\mu m^2$, P0 SMUs had significantly

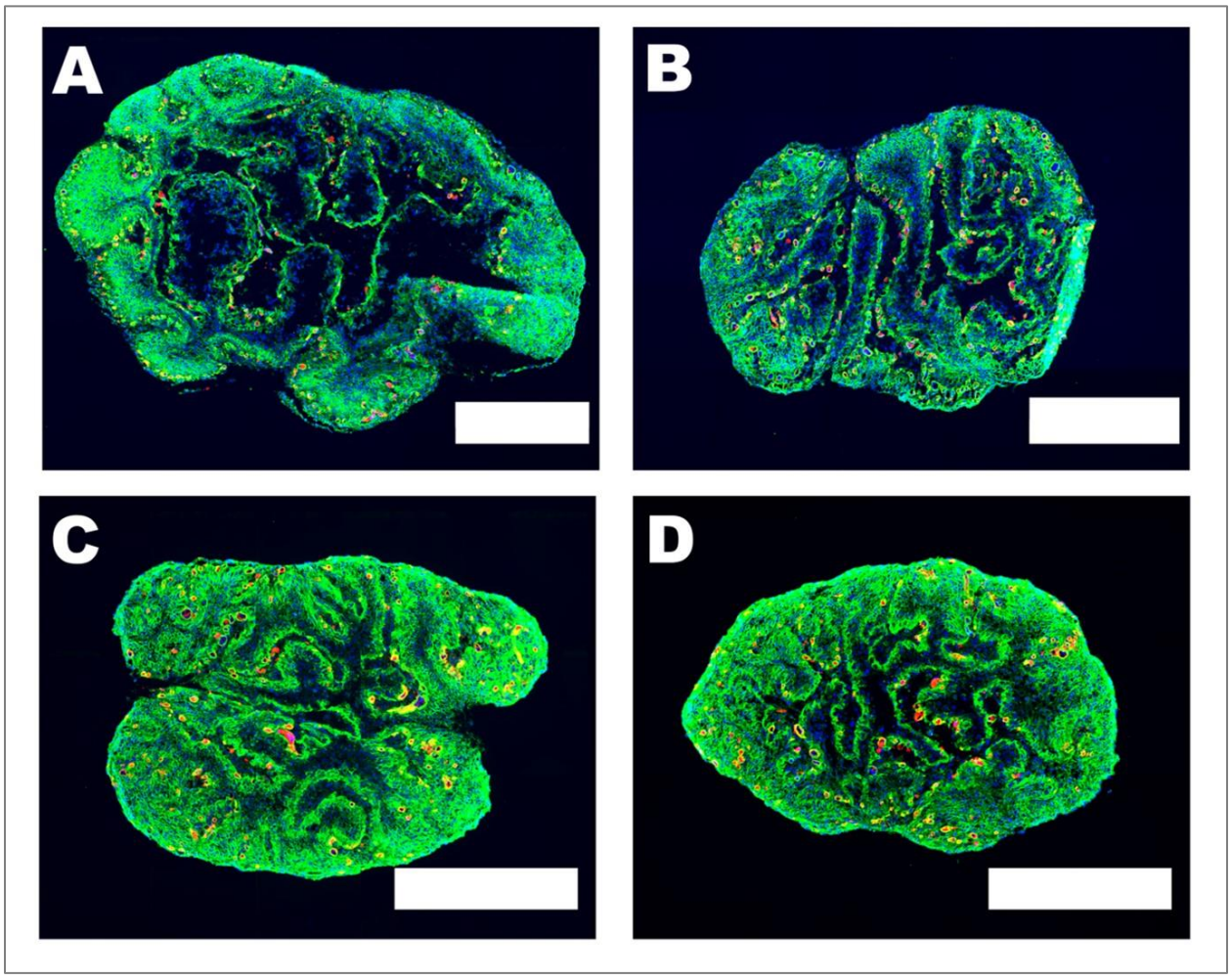


**Figure 21. Role of Cell Passaging on SMU Structure.** SMUs fabricated from P0 (**A**), P1 (**B**), P2 (**C**), and P3 (**D**) skeletal muscle cells underwent IHC staining for cell viability (DAPI, blue), myosin heavy chain (MF20, red), and extracellular matrix (laminin, green). Scale bars = 500 µm.

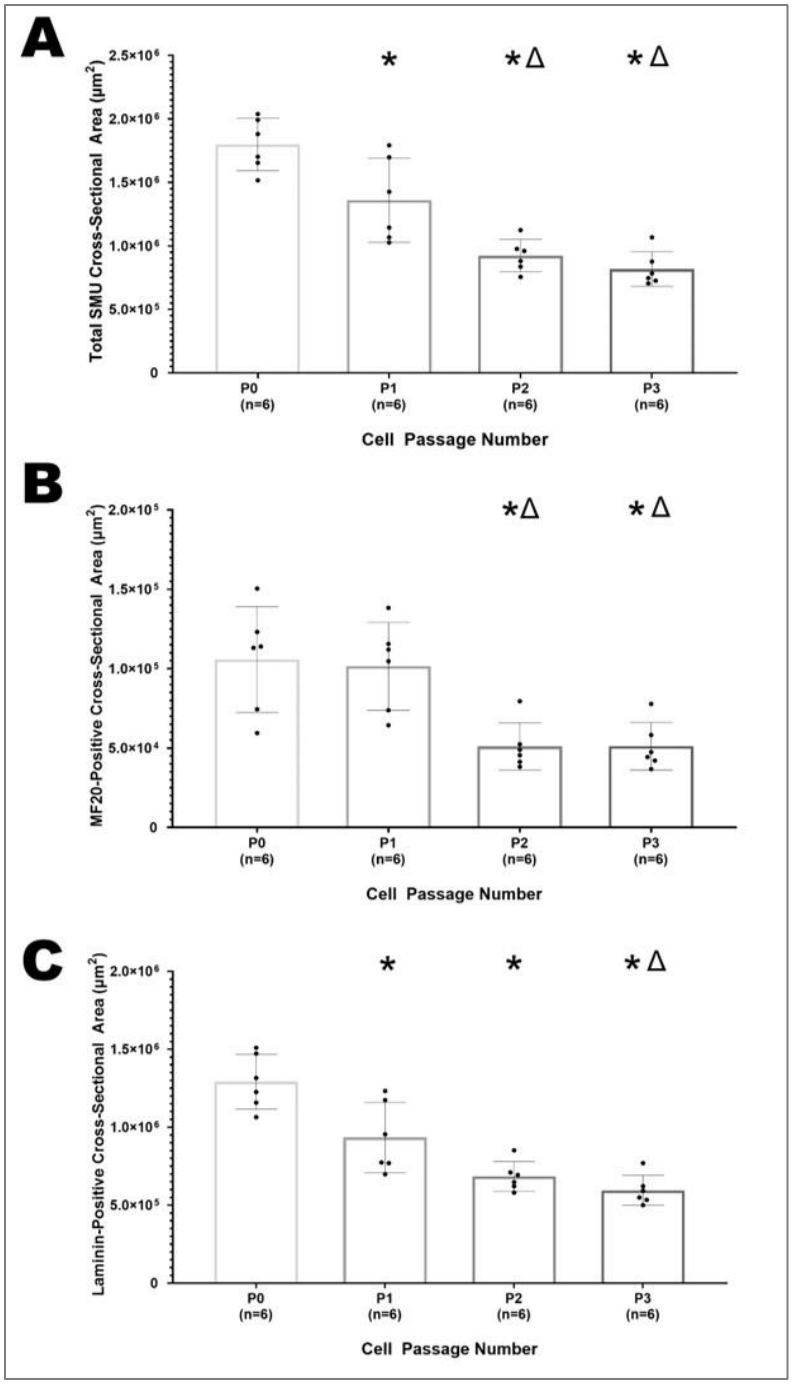


**Figure 22. Effect of cell passaging number on SMU total cross-sectional area (CSA) (A), MF20-positive CSA (B), and laminin-positive CSA (C).** Boxes and bars indicate mean ± standard error of the mean. Symbols above graphs indicate statistically significant differences: * from P0 (Control), and Δ from P1. A one-way ANOVA indicated that passage number has a statistically significant impact on total CSA ($p<0.001$), MF20-positive CSA ($p=0.0004$), and laminin-positive CSA ($p<0.0001$). P0 SMUs had significantly larger total CSAs than all other experimental groups ($p=0.01$ for P1, $p<0.0001$ for both P2 and P3). Additionally, P1 SMUs also had significantly greater total CSAs compared to P2 ($p=0.01$) and P3 ($p=0.002$) SMUs. Both P0 and P1 SMUs showed significantly greater myosin heavy chain content when compared to P2 ($p=0.004$ and $p=0.008$, respectively) and P3 SMUs ($p=0.004$ and $p=0.008$, respectively). P0 SMUs also had significantly greater extracellular matrix deposition compared to all other experimental groups ($p=0.004$ for P1, $p<0.0001$ for both P2 and P3). P1 SMUs were also found to have significantly greater laminin-positive CSA compared to P3 SMUs ($p=0.007$).

greater extracellular matrix deposition than all other experimental groups ($p=0.004$ for P1, $p<0.0001$ for both P2 and P3). With an average of $9.34 \times 10^5 \pm 0.92 \times 10^5$ $\mu m^2$ $um^2$, P1 SMUs were also found to have significantly greater laminin-positive CSA compared to P3 SMUs (average of $5.95 \times 10^5 \pm 0.39 \times 10^5$ $\mu m^2$, $p=0.007$). P2 SMUs were found to have a mean laminin-positive CSA of $6.84 \times 10^5 \pm 0.39 \times 10^5$ $\mu m^2$ and were not significantly different from P1 or P3 SMUs.

For each SMU, MF20-positive CSA and laminin-positive CSA were normalized by total CSA to determine the percentage of skeletal muscle and extracellular matrix in each SMU. SMUs consisted of 5.8±0.6%, 7.6±0.7%, 5.5±0.4%, and 6.2±0.4% MF20-positive content for P0, P1, P2, and P3 SMUs, respectively. Percentage of MF20-positive content was not significantly different between groups. SMUs consisted of 72±1%, 69±1%, 74±1%, and 73±1% laminin-positive content for P0, P1, P2, and P3 SMUs, respectively. P1 SMUs had significantly lower percentages of laminin-positive content compared to P2 ($p=0.002$) and P3 ($p=0.02$) SMUs.

### 4.4 Discussion

This study used the fabrication of scaffold-free skeletal muscle units to critically evaluate the impact of cell passaging of human primary skeletal muscle isolates in both 2D cell monolayers and 3D engineered skeletal muscle tissues. We aimed to determine the cell passaging parameters that could potentially enhance the use of human skeletal muscle cells for tissue engineering technologies. Specifically, we wanted to understand the number of times primary skeletal muscle cells obtained from human muscle biopsies could be passaged without negatively impacting 3-D SMU structure and contractile function.

Investigation into the 2D culture indicated a significant drop in cell population doubling-time. Cell isolations from skeletal muscle biopsies result in myogenic and non-myogenic cells, both of which impact the average cell population doubling-time. The main non-myogenic cells released from muscle biopsy specimens during enzymatic digestion are connective tissue fibroblasts, which are known to proliferate more rapidly than satellite cells [70, 78, 98, 99]. The main non-myogenic cells released from muscle biopsy specimens during enzymatic digestion are connective tissue fibroblasts, which are known to proliferate more rapidly than satellite cells [70, 78, 98, 99]. Our data suggests that, as passage number increased, the number of myogenic cells proliferating significantly decreased and the number of non-myogenic cells increased, decreasing the cell population doubling time. These changes in skeletal muscle cell isolate population are supported by our immunocytochemical results indicating a significant decrease in the total percentage of myogenic cells among the total cell population as passage number increased. This finding follows the same trend as previous work in a rat model, which showed a drop in myogenic cells from 90% to 55% of the total cell population by the third passage [103]. However, in the case of human cells, this drop was even greater with myogenic cell percentage dropping to below 30% by the first passage. Such a low percentage suggests limited myogenic cell expansion potential after the first passage, potentially because all available satellite cells have begun terminally differentiating into myoblasts. Coinciding with the decrease in myogenic cells, there was a significant increase in fibroblast cells in the total cell population within just one passage, as percentage vimentin-positive cells rose from 41% to 70% from P0 to P1. This transition in cell population appears to be detrimental to 2D SMU skeletal muscle structure as

monolayer analysis indicates a trend of decreasing myotube diameter starting at the second passage, potentially because the increased number of fibroblasts in cell culture decreased the amount of space available for myotubes to undergo hypertrophy Interesting, there was no impact on myotube density between experimental groups. This data suggests that, despite the low percentage of myogenic cells in highly passaged cell cultures, the SMU fabrication protocol can still promote the proliferation and differentiation of all available myogenic cells leading to robust monolayers with extensive myotube networking.

Analysis indicated that the alteration of cell populations due to passaging impacted the final structure of 3D SMUs. As noted in previous scaffold-free engineered tissue work, the presence of fibroblasts in monolayers create passive tension that promotes the roll-up and fusion of monolayers into cylindrical SMUs [106]. In this study, the increased number of fibroblasts in SMUs fabricated at higher cell passages could explain the greater SMU fusion and significant decrease in total SMU CSA as cell passage number increased. Changes in cell population due to extensive passaging also appeared to hinder extracellular matrix deposition, impacting the laminin-positive CSA of SMUs.

Interestingly, the content of muscle in the SMU only began decreasing at the second passage. Additionally, contractile function in SMUs peaked at P1 before beginning to decline at P3. Despite differences in the percentage of myogenic cells between P0 and P1, our SMU fabrication protocol results in SMUs with comparable amounts of mature skeletal muscle content. The increase in contractile function from P0 to P1 cells suggests that passaging altered the cell populations such that P1 SMUs had more organized myotubes, capable of producing greater forces.

Further passages prove detrimental to both SMU structure. However, despite a drop in MF20-content in P2 SMUs compared to P1 SMUs, SMU contractile function is maintained with no significant differences in maximum tetanic forces. The significant increase in P2 SMU specific force compared to other groups is due to P2 SMUs having no significant differences in maximum tetanic forces compared to P0 and P1 SMUs but containing around half of the myosin heavy chain content of P0 and P1 SMUs. These results suggest that SMU average maximum tetanic forces are not only correlated to the MF20-positive cross-sectional area, but additional factors such as the maturity and sarcomeric alignment of a SMU's skeletal muscle content. This finding aligns with previous investigations studying specific force in human SMUs [85].

Using our scaffold-free tissue engineering model, we demonstrated that human primary skeletal muscle cells can be passaged without negatively impacting the ability to engineered skeletal muscle with equivalent contractile function to freshly isolated cells. The ability to passage primary human skeletal muscle cells is critical to the advancement of engineered skeletal muscle tissue into clinically relevant grafts, because it addresses fabrication limitations due to inadequate numbers of cells. One passage significantly increases the total cell yield from a human skeletal muscle biopsy fifty times greater than the cells that would be harvested without a passage. Our scaled-up SMU studies have previously indicated that it would take about 20 million primary skeletal muscle cells to fabricate an SMU of a size capable of filling a 30% VML in a human tibialis anterior limb muscle (14 cm long, 2 cm diameter) [69]. Allowing for one passage of cells, this cell quota could be reached by harvesting and isolating a 40mg skeletal muscle biopsy, achieved from a sample size of around $4mm^3$ [101, 102]. A sample of such size could be collected

during a minimally-invasive procedure with minimal to no risk of donor-site morbidity [101, 102]. By significantly increasing the number of cells that can be harvested from a single minimally-invasive human skeletal muscle biopsy, these findings demonstrate a key advancement in the development of clinically-relevant engineered skeletal muscle from autologous muscle biopsies.

## Chapter 5 Conclusions

Acute VML necessitates medical intervention, but current surgical standards-of-care, autologous muscle flaps or grafts, are hindered by donor site skeletal muscle injury and morbidity. Such procedures have limited success in restoring contractile function. Scaffold-free tissue engineering approaches can address these limitations by using cells isolated from an autogenic skeletal muscle biopsy to grow exogenous skeletal muscle tissue that can promote muscle regeneration *in vivo*. The overall goal of my thesis was to advance our laboratory's engineered skeletal muscle units towards clinical use. Our SMUs have shown potential as engineered grafts partially repairing 30% VML in both rat and sheep animal models. However, prior to my thesis work, these methodologies had not been successfully translated to a human cell-sourced technology due to two key challenges:

(1) the lack of noteworthy contractile function in human cell-sourced SMUs (hSMU)

(2) the large number of satellite cells required for engineered tissue fabrication.

To address the lack of contractile function in hSMUs we investigated the literature for growth factors essential for the development of engineered skeletal muscle tissue. Human Epidermal Growth Factor (hEGF), a mitogenic polypeptide implicated in wound healing and tissue growth, was a growth factor of interest for our research because it had previously shown promise enhancing myobundle formation and contractile function in human myogenic cell cultures [37-39, 42, 43]. Additionally, the impact of hEGF treatment during the proliferation and differentiation phases of hSMU fabrication had yet to be

evaluated. Thus, the first aim of this dissertation evaluated the impact of a novel growth factor, hEGF, on SMU fabrication, structure, and biomechanical function (Chapter II). Our results indicated that the supplementation of hEGF to human primary myogenic cell cultures during myogenic cell proliferation, differentiation, and maturation phases improved tissue engineered skeletal muscle structure and function. Furthermore, hEGF was critical for the development of contractile function in hSMUs. The higher force produced by constructs formed in the presence of hEGF is predicted to be largely due to the higher concentration of myosin heavy chain and the enhanced organization of sarcomeric structures. The implications of these findings suggest that hEGF has a critical impact on myotube maturation. The design of this experiment did not allow us to determine the exact cellular pathways that are activated upon the presence of hEGF or the impact of hEGF on other key skeletal muscle proteins, such as myogenin, desmin, and titin. Further studies to continue to elucidate the role of hEGF *in vivo* and *in vitro* are warranted.

One of the greatest limitations preventing the scale-up of tissue-engineered constructs to clinically relevant sizes is the large numbers of satellite cell required for engineered tissue fabrication. While autologous cells could be used to grow human engineered skeletal muscle grafts, fabricating hSMUs using the large number of satellite cells required for successful rat and ovine SMUs would require large skeletal muscle biopsies from patients risking potential trauma at the donor site [78]. In the second aim of this dissertation, we sought to address this challenge by optimizing our methodologies so that fewer satellite cells and thus smaller muscle biopsies would be needed to fabricate hSMUs (Chapter III). Specifically, we tested the impact of cell seeding density on the

ability to fabricate functional hSMUs. Our results indicated that by altering the timing of our fabrication protocol and allowing cell cultures to reach >90% confluency in media that promotes proliferation, we could lower starting cell-seeding density by 90% compared to ovine models with no detrimental impact to monolayer development or hSMU function. This was somewhat surprising to us based on prior findings suggesting much larger numbers of satellite cells are required for the fabrication of contractile SMUs. Considering clinical translation, these findings imply that tissue engineered grafts large enough for the treatment of a 30% VML in a human extremity muscle can be fabricated from cells isolated from skeletal muscle harvested via a needle biopsy.

To further expand the capabilities of satellite cells from a single autogenic skeletal muscle biopsy, the third aim of this dissertation evaluated the impact of cell passaging on human primary skeletal muscle cells within an engineered skeletal muscle tissue environment (Chapter IV). The passaging of myoblasts is a common technique for engineered skeletal muscle systems in animal models [76, 79, 103]. However, prior to this work, the impact of the passaging of human primary skeletal muscle isolates on tissue engineered constructs intended for use as grafts for VML remained to be elucidated. By examining the cell culture, monolayer development, and hSMU fabrication from passaged human skeletal muscle primary cells, we were able to determine that cell passaging significantly decreased the percentage of myogenic cells in the total cell population. Despite this decrease, human primary skeletal muscle cells can be passaged up to two times without negatively impacting the contractile function of a SMU compared to one created with unpassaged cells. Even when passaging resulted in a drop from 32% to 10% MyoD-positive cells in the total cell population, our muscle growth media and muscle

differentiation media was capable of promoting satellite proliferation and differentiation to such a degree that SMU contractile function was not impacted. This finding is significant because, given a cell-seeding density of 1,000 cells/cm$^2$, a single passage can increase the total cell yield from a human skeletal muscle biopsy fiftyfold compared to cells harvested without a passage. Additionally, these findings indicate that our muscle growth media is capable of promoting satellite cell proliferation

These studies addressed two key limitations in human cell-sourced skeletal muscle tissue engineering by optimizing cell culture conditions to increase the cell yield from a single skeletal muscle biopsy while promoting SMU biomechanical function. Due to their significant impact on hSMU fabrication, hEGF-treated media and lower cell-seeding densities have been incorporated into our current hSMU fabrication protocol. Overall, this work was essential towards advancing hSMUs towards clinical use by enhancing fabrication methodologies to develop constructs of appropriate structure and function for human application. Ideally, similar techniques can be applied to other skeletal muscle tissue engineering modalities to promote the translation of engineered tissue from animal models to human cell-sources.

To continue advancing our engineered skeletal muscle towards clinical translation, several further studies need to be conducted. Through this thesis work, we have successfully developed small-scale hSMUs with *in vitro* contractile function. In order for hSMUs to potentially serve as grafts from VML treatment in human patients, a proof-of-concept study needs to be conducted to confirm that hSMUs can be scaled-up to clinically relevant sizes. . Importantly, such grafts need to be of dimensions appropriate for treating VML extremity injuries [46, 47, 50]. The Larkin laboratory's ovine SMU methodology and

lateral fusion techniques have resulted in SMUs of sizes capable of filling a 30% VML in an ovine peroneus tertius muscle (14 cm long, 2 cm diameter) [69]. An hSMU of such of size fabricated from human cells would be capable of filling a 30% VML in a human tibialis anterior muscle but proof-of-concept studies for hSMUs still need to be conducted. As determined by my Aim 2 and Aim 3 experiments, incorporating lower starting cell-seeding densities and passaging procedures in hSMU fabrication protocol would decrease the number of satellite cells that need to be isolated from a skeletal muscle biopsy. A scaled-up hSMU could potentially be fabricated from a minimally invasive autologous biopsy as small as 6mg [101, 102].

Another key step towards clinical translation is a thorough characterization of human-cell sourced SMUs in a long-term *in vivo* animal model. There are FDA approval concerns regarding the use of exogenous growth factors in tissue-engineered products intended for implantation [107, 108]. While growth factors are only provided to SMUs during fabrication and not upon or after implantation, they may potentially have an impact on the host's immune response, the health of the implant site's surrounding tissue, and the long-term biocompatibility of constructs [107, 108]. Additionally, key regulatory guidelines for cell-based therapies rely on cell phenotype stability upon implantation, emphasizing the importance of further investigating satellite cell, myoblast, and myotube *in vivo* behavior upon SMU implantation [109]. The fabrication of autologous tissue engineered grafts provides an opportunity for personalized medicine that address challenges with tissue rejection, immune reaction, donor tissue availability, and donor site morbidity in current standards-of-care [46, 49]. Given the variety of potential VML injuries and the large patient population, hSMUs would have to be fabricated from biopsies from

a variety of skeletal muscle sites and a wide range of donor ages for autologous engineered skeletal muscle grafts to be an accessible clinical therapy. While biopsies from both sexes and a range of ages have been used to create contractile hSMUs for this dissertation, further studies directly examining the impact of biopsy skeletal muscle site, donor age, and donor sex on hSMU fabrication need to be conducted to proceed with the optimization of hSMU methodologies from human cell sources. Our lab's previous work examining different ovine skeletal muscle as primary cell sources for SMUs indicated that biopsy muscle source significantly impacts satellite cell *in vitro* behavior and SMU contractile function [70]. Further investigation into cells isolated from multiple human hindlimb muscles would help determine the optimal, minimally-intrusive biopsy site. Due to higher satellite-cell density and myogenic potential in slow-twitch oxidative muscle fibers, it is theorized that muscles containing a higher percentage of Type I muscle fibers, such as the soleus muscle, will be the optimal biopsy locations. Furthermore, it is critical to examine to role of muscle biopsy donor age on SMU structure and contractile function. In human muscle, exact satellite cell number is dependent on age with an increase in age results in a decrease in the total number of satellite cells [18-21]. This suggests there could be an optimal patient age range for autologous tissue-engineered skeletal muscle graft. The hSMU fabrication protocol could have to be further optimized to create a more accessible therapy. However, as discussed in Chapter IV, our SMU fabrication protocol has been able to produce contractile hSMU constructs from cell cultures with less than 2% Pax7-positive satellite cells. These results suggest that our hSMU fabrication protocol is rigorous against variation in human satellite cell number.

In summary, my thesis work resulted in a hSMU fabrication methodology that optimizes the number of cells obtained in a human skeletal muscle biopsy and enhances the functional properties of the resultant muscle tissue. Such an advancement brings us one step closer to the clinical adoption of tissue-engineered based therapies for VML.

## Bibliography


1. Sherwood, L., *Human physiology : from cells to systems*. 2013: Eighth edition. Belmont, CA : Brooks/Cole, Cengage Learning, [2013] ©2013.
2. Sherman, J.H., D.S. Luciano, and A.J. Vander, *Human physiology : the mechanisms of body function*. 8th ed, ed. J.H. Sherman and D.S. Luciano. 2001, Boston: Boston : McGraw-Hill.
3. Cavagna, G., *Muscle, Locomotion and Heart*. 2019. p. 65-123.
4. Roy, R.R. and V.R. Edgerton, *Skeletal Muscle Architecture*, in *Encyclopedia of Neuroscience*, M.D. Binder, N. Hirokawa, and U. Windhorst, Editors. 2009, Springer Berlin Heidelberg: Berlin, Heidelberg. p. 3702-3707.
5. Frontera, W.R. and J. Ochala, *Skeletal muscle: a brief review of structure and function.* Calcif Tissue Int, 2015. **96**(3): p. 183-95.
6. Li, Y., et al., *Engineering cell alignment in vitro.* Biotechnol Adv, 2014. **32**(2): p. 347-65.
7. Folker, E. and M. Baylies, *Nuclear positioning in muscle development and disease.* Frontiers in Physiology, 2013. **4**(363).
8. Thomas, K., A.J. Engler, and G.A. Meyer, *Extracellular matrix regulation in the muscle satellite cell niche.* Connect Tissue Res, 2015. **56**(1): p. 1-8.
9. Grasman, J.M., et al., *Biomimetic scaffolds for regeneration of volumetric muscle loss in skeletal muscle injuries.* Acta Biomater, 2015. **25**: p. 2-15.
10. Boron, W.F. and E.L. Boulpaep, *Medical physiology : a cellular and molecular approach*. 2nd , updat ed. 2012, Philadelphia: Saunders/ Elsevier.
11. Burgoyne, T., E.P. Morris, and P.K. Luther, *Three-Dimensional Structure of Vertebrate Muscle Z-Band: The Small-Square Lattice Z-Band in Rat Cardiac Muscle.* Journal of molecular biology, 2015. **427**(22): p. 3527-3537.
12. Shiels, H.A., *DESIGN AND PHYSIOLOGY OF THE HEART | Cardiac Cellular Length–Tension Relationship*, in *Encyclopedia of Fish Physiology*, A.P. Farrell, Editor. 2011, Academic Press: San Diego. p. 1060-1066.
13. Lieber, R.L., *Skeletal muscle adaptability. I: Review of basic properties.* Dev Med Child Neurol, 1986. **28**(3): p. 390-7.
14. Widmaier, E.P., H. Raff, and K.T. Strang, *Muscle*, in *Vander's human physiology : the mechanisms of body function*. 2011, McGraw-Hill: New York.
15. Mertens, J.P., et al., *Engineering muscle constructs for the creation of functional engineered musculoskeletal tissue.* Regenerative medicine, 2014. **9**(1): p. 89-100.
16. Hawke, T.J. and D.J. Garry, *Myogenic satellite cells: physiology to molecular biology.* J Appl Physiol (1985), 2001. **91**(2): p. 534-51.
17. Halevy, O., et al., *Pattern of Pax7 expression during myogenesis in the posthatch chicken establishes a model for satellite cell differentiation and renewal.* Dev Dyn, 2004. **231**(3): p. 489-502.

18. Hawke, T.J. and D.J. Garry, *Myogenic satellite cells: physiology to molecular biology.* Journal of Applied Physiology, 2001. **91**(2): p. 534-551.
19. Hernandez, R.J. and L. Kravitz, *The Mystery of Skeletal Muscle Hypertrophy.* ACSM's Health & Fitness Journal, 2003. **7**(2).
20. Gibson, M.C. and E. Schultz, *Age-related differences in absolute numbers of skeletal muscle satellite cells.* Muscle Nerve, 1983. **6**(8): p. 574-80.
21. Schmalbruch, H. and U. Hellhammer, *The number of nuclei in adult rat muscles with special reference to satellite cells.* Anat Rec, 1977. **189**(2): p. 169-75.
22. Zammit, P.S., T.A. Partridge, and Z. Yablonka-Reuveni, *The skeletal muscle satellite cell: the stem cell that came in from the cold.* J Histochem Cytochem, 2006. **54**(11): p. 1177-91.
23. Yablonka-Reuveni, Z. and K. Day. *Skeletal Muscle Stem Cells in the Spotlight: The Satellite Cell*. 2011.
24. Scimè, A. and M.A. Rudnicki, *Anabolic potential and regulation of the skeletal muscle satellite cell populations.* Current Opinion in Clinical Nutrition & Metabolic Care, 2006. **9**(3).
25. Rodriguez, B.L. and L.M. Larkin, *12 - Functional three-dimensional scaffolds for skeletal muscle tissue engineering*, in *Functional 3D Tissue Engineering Scaffolds*, Y. Deng and J. Kuiper, Editors. 2018, Woodhead Publishing. p. 279-304.
26. Nguyen, J.H., et al., *The Microenvironment Is a Critical Regulator of Muscle Stem Cell Activation and Proliferation.* Front Cell Dev Biol, 2019. **7**: p. 254.
27. Chargé, S.B. and M.A. Rudnicki, *Cellular and molecular regulation of muscle regeneration.* Physiol Rev, 2004. **84**(1): p. 209-38.
28. Gopinath, S.D. and T.A. Rando, *Stem cell review series: aging of the skeletal muscle stem cell niche.* Aging Cell, 2008. **7**(4): p. 590-8.
29. Murphy, M.M., et al., *Satellite cells, connective tissue fibroblasts and their interactions are crucial for muscle regeneration.* Development, 2011. **138**(17): p. 3625-37.
30. Mathew, S.J., et al., *Connective tissue fibroblasts and Tcf4 regulate myogenesis.* Development, 2011. **138**(2): p. 371-84.
31. Zanou, N. and P. Gailly, *Skeletal muscle hypertrophy and regeneration: interplay between the myogenic regulatory factors (MRFs) and insulin-like growth factors (IGFs) pathways.* Cell Mol Life Sci, 2013. **70**(21): p. 4117-30.
32. Dhawan, J. and T.A. Rando, *Stem cells in postnatal myogenesis: molecular mechanisms of satellite cell quiescence, activation and replenishment.* Trends Cell Biol, 2005. **15**(12): p. 666-73.
33. Liao, I.C., et al., *Effect of Electromechanical Stimulation on the Maturation of Myotubes on Aligned Electrospun Fibers.* Cell Mol Bioeng, 2008. **1**(2-3): p. 133-145.
34. Schiaffino, S. and C. Mammucari, *Regulation of skeletal muscle growth by the IGF1-Akt/PKB pathway: insights from genetic models.* Skelet Muscle, 2011. **1**(1): p. 4.
35. Huard, J., Y. Li, and F.H. Fu, *Muscle injuries and repair: current trends in research.* J Bone Joint Surg Am, 2002. **84**(5): p. 822-32.

36. Husmann, I., et al., *Growth factors in skeletal muscle regeneration.* Cytokine Growth Factor Rev, 1996. **7**(3): p. 249-58.
37. Madden, L., et al., *Bioengineered human myobundles mimic clinical responses of skeletal muscle to drugs.* Elife, 2015. **4**: p. e04885.
38. Eberli, D., et al., *Optimization of human skeletal muscle precursor cell culture and myofiber formation in vitro.* Methods, 2009. **47**(2): p. 98-103.
39. St Clair, J.A., S.D. Meyer-Demarest, and R.G. Ham, *Improved medium with EGF and BSA for differentiated human skeletal muscle cells.* Muscle Nerve, 1992. **15**(7): p. 774-9.
40. Sicari, B.M., C.L. Dearth, and S.F. Badylak, *Tissue engineering and regenerative medicine approaches to enhance the functional response to skeletal muscle injury.* Anat Rec (Hoboken), 2014. **297**(1): p. 51-64.
41. Elder, J.B., et al., *Cellular localisation of human urogastrone/epidermal growth factor.* Nature, 1978. **271**(5644): p. 466-467.
42. Andree, C., et al., *In vivo transfer and expression of a human epidermal growth factor gene accelerates wound repair.* Proceedings of the National Academy of Sciences, 1994. **91**(25): p. 12188-12192.
43. Carpenter, G. and S. Cohen, *Epidermal growth factor.* J Biol Chem, 1990. **265**(14): p. 7709-12.
44. Wang, Y.X., et al., *EGFR-Aurka Signaling Rescues Polarity and Regeneration Defects in Dystrophin-Deficient Muscle Stem Cells by Increasing Asymmetric Divisions.* Cell Stem Cell, 2019. **24**(3): p. 419-432.e6.
45. Broholm, C. and B.K. Pedersen, *Leukaemia inhibitory factor--an exercise-induced myokine.* Exerc Immunol Rev, 2010. **16**: p. 77-85.
46. Corona, B., et al., *Volumetric muscle loss leads to permanent disability following extremity trauma.* The Journal of Rehabilitation Research and Development, 2015. **52**: p. 785-792.
47. Grogan, B.F. and J.R. Hsu, *Volumetric muscle loss.* J Am Acad Orthop Surg, 2011. **19 Suppl 1**: p. S35-7.
48. Corona, B.T., et al., *Autologous minced muscle grafts: a tissue engineering therapy for the volumetric loss of skeletal muscle.* Am J Physiol Cell Physiol, 2013. **305**(7): p. C761-75.
49. Corona, B.T., J.C. Wenke, and C.L. Ward, *Pathophysiology of Volumetric Muscle Loss Injury.* Cells Tissues Organs, 2016. **202**(3-4): p. 180-188.
50. Vogt, C., M. Tahtinen, and F. Zhao, *Engineering Approaches for Creating Skeletal Muscle.*, in *Tissue Engineering and Nanotheranostics*, D. Shi and Q. Liu, Editors. 2016, World Scientific.
51. *Web-based Injury Statistics Query and Reporting System (WISQARS)*. 2005, Centers for Disease Control and Prevention: National Centers for Injury Prevention and Control.
52. Owens, B.D., et al., *Characterization of extremity wounds in Operation Iraqi Freedom and Operation Enduring Freedom.* J Orthop Trauma, 2007. **21**(4): p. 254-7.
53. Belmont, P.J., et al., *The Nature and Incidence of Musculoskeletal Combat Wounds in Iraq and Afghanistan (200U 2009).* Journal of Orthopaedic Trauma, 2013. **27**: p. e107 e113.

54. Chuang, D.C., *Free tissue transfer for the treatment of facial paralysis.* Facial Plast Surg, 2008. **24**(2): p. 194-203.
55. Turner, N.J. and S.F. Badylak, *Regeneration of skeletal muscle.* Cell Tissue Res, 2012. **347**(3): p. 759-74.
56. Garg, K., et al., *Volumetric muscle loss: Persistent functional deficits beyond frank loss of tissue.* Journal of Orthopaedic Research, 2015. **33**(1): p. 40-46.
57. Mase, V.J., Jr., et al., *Clinical application of an acellular biologic scaffold for surgical repair of a large, traumatic quadriceps femoris muscle defect.* Orthopedics, 2010. **33**(7): p. 511.
58. Vandenburgh, H.H., P. Karlisch, and L. Farr, *Maintenance of highly contractile tissue-cultured avian skeletal myotubes in collagen gel.* In Vitro Cell Dev Biol, 1988. **24**(3): p. 166-74.
59. Larson, A.A., et al., *Effects of Dexamethasone Dose and Timing on Tissue-Engineered Skeletal Muscle Units.* Cells, tissues, organs, 2018. **205**(4): p. 197-207.
60. Vandenburgh, H.H., et al., *Mechanically induced alterations in cultured skeletal muscle growth.* J Biomech, 1991. **24 Suppl 1**: p. 91-9.
61. Juhas, M. and N. Bursac, *Engineering skeletal muscle repair.* Curr Opin Biotechnol, 2013. **24**(5): p. 880-6.
62. Rao, L., et al., *Engineering human pluripotent stem cells into a functional skeletal muscle tissue.* Nature Communications, 2018. **9**(1): p. 126.
63. Shah, R., et al., *Sequential identification of a degradable phosphate glass scaffold for skeletal muscle regeneration.* J Tissue Eng Regen Med, 2014. **8**(10): p. 801-10.
64. Wang, L., et al., *Nanofiber Yarn/Hydrogel Core-Shell Scaffolds Mimicking Native Skeletal Muscle Tissue for Guiding 3D Myoblast Alignment, Elongation, and Differentiation.* ACS Nano, 2015. **9**(9): p. 9167-79.
65. Kroehne, V., et al., *Use of a novel collagen matrix with oriented pore structure for muscle cell differentiation in cell culture and in grafts.* J Cell Mol Med, 2008. **12**(5a): p. 1640-8.
66. Zhang, M. and B. Guo, *Electroactive 3D Scaffolds Based on Silk Fibroin and Water-Borne Polyaniline for Skeletal Muscle Tissue Engineering.* Macromol Biosci, 2017. **17**(9).
67. VanDusen, K.W., et al., *Engineered skeletal muscle units for repair of volumetric muscle loss in the tibialis anterior muscle of a rat.* Tissue Eng Part A, 2014. **20**(21-22): p. 2920-30.
68. Syverud, B.C., K.W. VanDusen, and L.M. Larkin, *Effects of Dexamethasone on Satellite Cells and Tissue Engineered Skeletal Muscle Units.* Tissue engineering. Part A, 2016. **22**(5-6): p. 480-489.
69. Novakova, S.S., et al., *Repairing Volumetric Muscle Loss in the Ovine Peroneus Tertius Following a 3-Month Recovery.* Tissue Eng Part A, 2020. **26**(15-16): p. 837-851.
70. Rodriguez, B.L., et al., *A Comparison of Ovine Facial and Limb Muscle as a Primary Cell Source for Engineered Skeletal Muscle.* Tissue Eng Part A, 2020. **26**(3-4): p. 167-177.

71. Syverud, B.C., et al., *A Transgenic tdTomato Rat for Cell Migration and Tissue Engineering Applications.* Tissue Eng Part C Methods, 2018. **24**(5): p. 263-271.
72. Doumit, M.E. and R.A. Merkel, *Conditions for isolation and culture of porcine myogenic satellite cells.* Tissue Cell, 1992. **24**(2): p. 253-62.
73. Allen, R.E., et al., *Skeletal muscle satellite cell cultures.* Methods Cell Biol, 1997. **52**: p. 155-76.
74. Clegg, C.H., et al., *Growth factor control of skeletal muscle differentiation: commitment to terminal differentiation occurs in G1 phase and is repressed by fibroblast growth factor.* J Cell Biol, 1987. **105**(2): p. 949-56.
75. Cheng, C.S., et al., *Conditions that promote primary human skeletal myoblast culture and muscle differentiation in vitro.* Am J Physiol Cell Physiol, 2014. **306**(4): p. C385-95.
76. Mudera, V., et al., *The effect of cell density on the maturation and contractile ability of muscle derived cells in a 3D tissue-engineered skeletal muscle model and determination of the cellular and mechanical stimuli required for the synthesis of a postural phenotype.* J Cell Physiol, 2010. **225**(3): p. 646-53.
77. Gillies, A.R. and R.L. Lieber, *Structure and function of the skeletal muscle extracellular matrix.* Muscle Nerve, 2011. **44**(3): p. 318-31.
78. Machingal, M.A., et al., *A tissue-engineered muscle repair construct for functional restoration of an irrecoverable muscle injury in a murine model.* Tissue Eng Part A, 2011. **17**(17-18): p. 2291-303.
79. Syverud, B.C., et al., *Isolation and Purification of Satellite Cells for Skeletal Muscle Tissue Engineering.* J Regen Med, 2014. **3**(2).
80. Wroblewski, O.M., et al., *Impact of Human Epidermal Growth Factor on Tissue-Engineered Skeletal Muscle Structure and Function.* Tissue Eng Part A, 2021. **27**(17-18): p. 1151-1159.
81. Hirata, Y. and D.N. Orth, *Epidermal growth factor (urogastrone) in human tissues.* J Clin Endocrinol Metab, 1979. **48**(4): p. 667-72.
82. Kurek, J.B., et al., *The role of leukemia inhibitory factor in skeletal muscle regeneration.* Muscle Nerve, 1997. **20**(7): p. 815-22.
83. Boularaoui, S.M., et al., *Efficient transdifferentiation of human dermal fibroblasts into skeletal muscle.* J Tissue Eng Regen Med, 2018. **12**(2): p. e918-e936.
84. Barop, J., et al., *Differentiation-dependent PTPIP51 expression in human skeletal muscle cell culture.* J Histochem Cytochem, 2009. **57**(5): p. 425-35.
85. Wroblewski, O.M., et al., *Impact of Cell-Seeding Density and Cell Confluence on Human Tissue Engineered Skeletal Muscle.* Tissue Eng Part A, 2021.
86. Wu, X., et al., *A standardized rat model of volumetric muscle loss injury for the development of tissue engineering therapies.* Biores Open Access, 2012. **1**(6): p. 280-90.
87. Gilbert-Honick, J., et al., *Engineering functional and histological regeneration of vascularized skeletal muscle.* Biomaterials, 2018. **164**: p. 70-79.
88. Mintz, E.L., et al., *Long-Term Evaluation of Functional Outcomes Following Rat Volumetric Muscle Loss Injury and Repair.* Tissue Eng Part A, 2020. **26**(3-4): p. 140-156.
89. Fishman, J.M., et al., *Skeletal muscle tissue engineering: which cell to use?* Tissue Eng Part B Rev, 2013. **19**(6): p. 503-15.

90. Lepper, C., T.A. Partridge, and C.M. Fan, *An absolute requirement for Pax7-positive satellite cells in acute injury-induced skeletal muscle regeneration.* Development, 2011. **138**(17): p. 3639-46.
91. Rando, T.A. and H.M. Blau, *Primary mouse myoblast purification, characterization, and transplantation for cell-mediated gene therapy.* J Cell Biol, 1994. **125**(6): p. 1275-87.
92. Bischoff, R., *Enzymatic liberation of myogenic cells from adult rat muscle.* Anat Rec, 1974. **180**(4): p. 645-61.
93. Blau, H.M. and C. Webster, *Isolation and characterization of human muscle cells.* Proc Natl Acad Sci U S A, 1981. **78**(9): p. 5623-7.
94. Rosenblatt, J.D., et al., *Culturing satellite cells from living single muscle fiber explants.* In Vitro Cell Dev Biol Anim, 1995. **31**(10): p. 773-9.
95. Baltazar, T., et al., *Three Dimensional Bioprinting of a Vascularized and Perfusable Skin Graft Using Human Keratinocytes, Fibroblasts, Pericytes, and Endothelial Cells.* Tissue Eng Part A, 2020. **26**(5-6): p. 227-238.
96. Rudnicki, M.A., et al., *The molecular regulation of muscle stem cell function.* Cold Spring Harb Symp Quant Biol, 2008. **73**: p. 323-31.
97. Renault, V., et al., *Human skeletal muscle satellite cells: aging, oxidative stress and the mitotic clock.* Exp Gerontol, 2002. **37**(10-11): p. 1229-36.
98. Corona, B.T., et al., *Further development of a tissue engineered muscle repair construct in vitro for enhanced functional recovery following implantation in vivo in a murine model of volumetric muscle loss injury.* Tissue Eng Part A, 2012. **18**(11-12): p. 1213-28.
99. Gaster, M., H. Beck-Nielsen, and H.D. Schrøder, *Proliferation conditions for human satellite cells. The fractional content of satellite cells.* Apmis, 2001. **109**(11): p. 726-34.
100. Rodriguez, B.L., et al., *A tissue engineering approach for repairing craniofacial volumetric muscle loss in a sheep following a 2, 4, and 6-month recovery.* PLoS One, 2020. **15**(9): p. e0239152.
101. Shanely, R.A., et al., *Human skeletal muscle biopsy procedures using the modified Bergström technique.* J Vis Exp, 2014(91): p. 51812.
102. Spinazzola, J.M. and E. Gussoni, *Isolation of Primary Human Skeletal Muscle Cells.* Bio Protoc, 2017. **7**(21).
103. Machida, S., E.E. Spangenburg, and F.W. Booth, *Primary rat muscle progenitor cells have decreased proliferation and myotube formation during passages.* Cell Prolif, 2004. **37**(4): p. 267-77.
104. *Useful Terms for ATCC Microbiology*, in *American Type Culture Collection* American Type Culture Collection.
105. Vandermeer, J., *How Populations Grow: The Exponential and Logistic Equations.* Nature Education Knowledge, 2010. **3**(10): p. 15.
106. Baltich, J., et al., *Development of a scaffoldless three-dimensional engineered nerve using a nerve-fibroblast co-culture.* In Vitro Cell Dev Biol Anim, 2010. **46**(5): p. 438-44.
107. Webber, M.J., et al., *A perspective on the clinical translation of scaffolds for tissue engineering.* Ann Biomed Eng, 2015. **43**(3): p. 641-56.

108. Hoffman, T., A. Khademhosseini, and R. Langer, *Chasing the Paradigm: Clinical Translation of 25 Years of Tissue Engineering.* Tissue Eng Part A, 2019. **25**(9-10): p. 679-687.
109. Mount, N.M., et al., *Cell-based therapy technology classifications and translational challenges.* Philosophical transactions of the Royal Society of London. Series B, Biological sciences, 2015. **370**(1680): p. 20150017-20150017.